

CARBON CYCLING IN SUBTERRANEAN ESTUARIES AND IMPLICATIONS FOR
OCEANIC FLUXES

By

ANDREA J. PAIN

A DISSERTATION PRESENTED TO THE GRADUATE SCHOOL
OF THE UNIVERSITY OF FLORIDA IN PARTIAL FULFILLMENT
OF THE REQUIREMENTS FOR THE DEGREE OF
DOCTOR OF PHILOSOPHY

UNIVERSITY OF FLORIDA

2017

©2017 Andrea J. Pain

To my parents

ACKNOWLEDGMENTS

I thank my advisor, Jon Martin, for the support and enthusiasm for all things carbon, and my lab mates for assistance in the field, lab, and intellectual discussions. I acknowledge the Water Institute Graduate Fellowship cohort of 2013 for their thoughtful contributions, discussions, and shared love of cochinita, to the Dixie Motel in Cocoa, FL for their hospitality and for never failing to provide colorful field experiences. I would also like thank my family for their continued support throughout this process. This research was supported by funding provided by the National Science Foundation and the St. John's River Water Management District.

TABLE OF CONTENTS

	<u>page</u>
ACKNOWLEDGMENTS.....	4
LIST OF TABLES.....	8
LIST OF FIGURES.....	9
ABSTRACT.....	11
CHAPTER	
1 BIOGEOCHEMISTRY OF CARBONATE VERSUS SILICICLASTIC SUBTERRANEAN ESTUARIES AND IMPLICATIONS FOR CARBON CYCLING: A REVIEW	13
Role of Submarine Groundwater Discharge in Coastal Carbon Cycle.....	13
Carbonate Versus Siliciclastic STEs.....	14
Hydrological Impact on Biogeochemical Reactions.....	15
Mineralogical Impact on Carbon Cycling	18
Feedbacks with Biogeochemical Cycling of Nutrients and Metals.....	19
Summary and Implications.....	23
2 ORGANIC CARBON QUANTITY AND QUALITY ACROSS SALINITY GRADIENTS IN CONDUIT- VERSUS DIFFUSE FLOW-DOMINATED SUBTERRANEAN ESTUARIES	31
Introduction.....	31
Methods.....	35
Study Locations.....	35
Sample Collection	36
Laboratory Methods	38
Modeling.....	38
Results.....	41
PARAFAC Results	41
Organic Carbon Concentrations and Conservative Mixing Model Results	41
PARAFAC Component Abundance with Salinity	43
Discussion	44
Organic Carbon Dynamics and Sources	45
Organic Carbon Quality Across Salinity Gradients	46
Distribution of Residuals and Implications for Controls of Biogeochemical Reactions	47
Conclusions	50
3 ORGANIC-INORGANIC CARBON FEEDBACKS IN A CARBONATE KARST AQUIFER AND IMPLICATIONS FOR NUTRIENT AVAILABILITY	58

Introduction	58
Study Location	60
Methods	63
Field Methods.....	63
Laboratory Methods	64
Modeling.....	65
STE conservative mixing models.....	65
Surface water organic carbon mass balance	66
Results.....	67
Salinity and Biogeochemical Parameters	67
Organic Carbon Character and Distribution.....	69
Discussion	70
Terrestrial Sources and Processing of Organic Carbon	71
Biogeochemical processing in the STE	73
Implications for STE Nutrient Sources and Sinks	76
Impact on Surface Water Carbon Cycling	78
Conclusions	81
4 BIOGEOCHEMICAL CONTROLS OF GREENHOUSE GAS PRODUCTION AND SEQUESTRATION IN SILICICLASTIC SUBTERRANEAN ESTUARIES	91
Introduction	91
Carbon Dioxide and Carbonate Equilibria	92
Methanogenesis and Carbonate Equilibria.....	95
Methods.....	97
Sample Collection	98
Laboratory Methods	99
Data Processing.....	100
Dissolved gas concentrations	100
Modeling	102
Results.....	102
Dissolved Gas Concentrations and Carbonate Chemistry.....	102
Distribution of Redox Reactions	103
CH ₄ Concentrations and Oxidation.....	104
Δ Alk: Δ DIC Ratios Compared to Reaction Stoichiometries	105
Discussion	105
Impacts on CO ₂ Concentrations and DIC speciation	106
Lower salinity portions of STEs (salinity < 15)	106
Higher salinity portions of STEs (salinity > 15).....	109
Δ Alk: Δ DIC ratios.....	109
Redox and Mineralogical Controls of Dissolved Gas Concentrations.....	111
Implications for CO ₂ and CH ₄ Fluxes.....	113
Conclusions	114
5 SUMMARY AND CONCLUDING REMARKS	131
Impacts Due to Flow	131

Impacts Due to Aquifer Solid Material.....	133
Concluding Remarks.....	134
APPENDIX	
A PARAFAC MODEL.....	136
B YUCATAN WATER CHEMISTRY DATA.....	147
C INDIAN RIVER LAGOON WATER CHEMISTRY DATA.....	149
LIST OF REFERENCES.....	152
BIOGRAPHICAL SKETCH.....	166

LIST OF TABLES

<u>Table</u>	<u>page</u>
1-1 Hydrologic properties of carbonate and siliciclastic subterranean estuaries.....	26
1-2 Reduction half reactions coupled with oxidation of organic matter.....	26
2-1 PARAFAC component matches as identified via OpenFluor.....	52
2-2 R ² and p-value for correlations between PARAFAC components in PARAFAC model.....	52
3-1 Chemical characterization of conservative mixing model end members	82
3-2 Water chemistry parameters of terrestrial water, near-shore springs, and seawater.....	83
3-3 R ² between PARAFAC components in Yucatan samples.....	84
3-4 Mass balance of terrestrial PARAFAC components based on salinity.....	84
4-1 Impact of redox pathways and biogeochemical reactions on alkalinity and DIC.....	116
4-2 ΔDIC concentrations compared to concentrations produced from reactions. ...	117
4-3 ΔAlk concentrations compared to concentrations produced from reactions	120
A-1 Complete list of samples included in PARAFAC model.....	137
B-1 Yucatan water chemistry parameters for geochemical modeling in PHREEQc	148
C-1 Indian River Lagoon water chemistry input parameters for geochemical modeling in PHREEQc.....	150

LIST OF FIGURES

<u>Figure</u>	<u>page</u>
1-1 Ghyben-Herzberg relationship demonstrating the depth of a freshwater lens overlying saline groundwater.....	27
1-2 Conceptual models of subterranean estuaries.	28
1-3 Map of locations of piezometer transects at Indian River Lagoon Florida.	29
1-4 Maps of Yucatan study site and sampling locations.	30
2-1 Five-component PARAFAC model for subterranean estuary samples.	53
2-2 Cross plots of salinity versus DOC, total CDOM, and ORP.....	54
2-3 Residuals of salinity-based conservative mixing models for DOC and total CDOM..	55
2-4 Relative PARAFAC component abundance versus salinity.....	56
2-5 Conceptual model of CDOM concentrations versus salinity in STEs.....	57
3-1 Conceptual model of organic matter sources to Yucatan STE	85
3-2 Salinity versus solute concentration in Yucatan STE.....	86
3-3 Salinity versus CDOM and PARAFAC component abundance in Yucatan STE..	87
3-4 Cross plot of Ca versus DIC residuals in Yucatan STE water samples.....	88
3-5 Cross plots of salinity versus N:P and Ca:P molar ratios in Yucatan STE.....	89
3-6 Conceptual model of biogeochemistry within Yucatan STE.	90
4-1 Relationship between dissolved gas concentrations and salinity STE sites.	123
4-2 Carbonate chemistry versus salinity at Indian River Lagoon STEs.	124
4-3 Contour plots of salinity, DOC, redox species, and dissolved gases at Indian River Lagoon STEs..	125
4-4 Distribution of salinity Δ DIC, Δ Alk, and Δ Ca between seepage faces.....	126
4-5 CH ₄ concentrations versus $\delta^{13}\text{C}$ -CH ₄ signatures and CH ₄ oxidation.	127
4-6 Δ Alk and Δ DIC compared to Δ Alk: Δ DIC ratios produced by reactions.....	128

4-7	Alk:DIC ratios modeled by conservative mixing model compared to measured values.	129
4-8	Relationships between Δ DIC and Δ Alk estimated via salinity-based conservative mixing models.....	130

Abstract of Dissertation Presented to the Graduate School
of the University of Florida in Partial Fulfillment of the
Requirements for the Degree of Doctor of Philosophy

CARBON CYCLING IN SUBTERRANEAN ESTUARIES AND IMPLICATIONS FOR
OCEANIC FLUXES

By

Andrea J. Pain

December 2017

Chair: Jonathan Martin

Major: Geology

Subterranean estuaries (STEs) are biogeochemically active zones where fresh groundwater and saline pore water mix. Biogeochemical reactions are fueled by organic carbon (OC), and produce the greenhouse gases carbon dioxide (CO₂), methane (CH₄), and remineralized nutrients. Reactions modify the chemical composition of submarine groundwater discharge (SGD), which alters coastal ocean chemical compositions through delivery of solutes. The extent of reactions should depend on STE hydrogeology, which regulates groundwater flow and provides solid phase reactants for biogeochemical reactions. To constrain the impacts of SGD on coastal C cycling, I characterize STEs representing two hydrogeologic end members: a carbonate karst STE, located in Puerto Morelos, Quintana Roo, Mexico, where numerous submarine springs act as point sources for SGD, and a siliciclastic STE located in Indian River Lagoon, FL, which is the site of widely distributed groundwater seepage. Yucatan hydrogeology leads to rapid groundwater flow rates relative to reaction kinetics and near conservative mixing of OC. In contrast, Florida STEs have long groundwater residence times and microbial activity causes colored dissolved organic matter (CDOM)

concentrations to increase to several times the concentration of background values. OC characterization via fluorescence and PARAFAC modeling reveals increases in the proportion of labile protein-like OC with salinity at both sites, reflecting mixing of terrestrial organic matter with fresh marine OC. At both sites, remineralization of OC modifies SGD composition and produces CO₂. The Yucatan calcium carbonate (CaCO₃) aquifer dissolves and partially buffers excess CO₂, but buffering may be limited by dissolution kinetics. Indian River Lagoon STEs produce both CO₂ and CH₄ but limited amounts of CaCO₃ in sediment reduces CO₂ buffering. Differences between Yucatan and Florida STEs suggest that more organic carbon and CO₂ discharges from siliciclastic than carbonate STEs, and SGD from these systems may impact coastal carbon cycling differently. These results highlight the role of STE hydrogeology for carbon and nutrient cycling, altering SGD composition. Although STEs appear important to coastal C and nutrient budgets, heterogeneity in STE hydrogeology complicates estimates of global fluxes.

CHAPTER 1
BIOGEOCHEMISTRY OF CARBONATE VERSUS SILICICLASTIC SUBTERRANEAN
ESTUARIES AND IMPLICATIONS FOR CARBON CYCLING: A REVIEW

Role of Submarine Groundwater Discharge in Coastal Carbon Cycle

The coastal ocean is a dynamic component of the global carbon cycle, and may serve as a significant CO₂ source or sink depending on the relative magnitudes of carbon fixation via primary productivity versus organic carbon remineralization (Cai, 2011). Coastal carbon cycling is magnified in surface estuaries where fresh and saltwater mix and enhance organic carbon remineralization reactions. Reactions are enhanced due to delivery of suspended matter from riverine input, which increases organic carbon remineralization rates, while associated light attenuation decreases primary productivity (Abril and Borges, 2004). In the marine C cycle, only estuaries are typically net sources of CO₂, while continental shelves and the open ocean are net CO₂ sinks (Cai, 2011). On a global scale, estuaries comprise only 0.3% of ocean surface area but contribute more CO₂ to the atmosphere than is fixed by continental shelves (7.3% of ocean surface area), and one third the amount that is fixed in the open ocean (92.5% of ocean surface area; Cai, 2011).

A freshwater-saltwater mixing zone, analogous to surface water estuaries, occurs where freshwater in coastal aquifers mixes with marine pore water. This zone, known as the subterranean estuary (STE; Moore, 1999), contributes freshwater and terrestrial solutes to the coastal zone via submarine groundwater discharge (SGD; Lambert and Burnett, 2003). SGD is comprised of both fresh and saline components, similar to surface estuaries, and the composition of SGD depends on the composition of fresh and saltwater end members but may be strongly modified by biogeochemical reactions within the STE (Moore, 1999). While groundwater input volumes are typically more

poorly constrained than those from riverine discharge or surface water runoff, combined fresh and marine SGD fluxes may be equivalent to or greater than riverine input in some regions, and are therefore critical to coastal biogeochemical budgets (Burnett et al., 2006; McCoy and Corbett, 2009). Similar to surface estuaries, biogeochemical processing occurs in STEs, which is enhanced by their low water:rock ratio. These low ratios result in enhanced availability of reactive solid phase material such as organic matter and mineral phases, and terminal electron acceptors, such as Fe and Mn oxides, which may be used to remineralize organic carbon. While most studies quantifying SGD fluxes have focused on nutrients and metals (Slomp and Van Cappellen, 2004; Roy et al., 2013a; Null et al., 2014), estimates of carbon fluxes indicate that SGD may be a source of CO₂ (Sadat-noori et al., 2016; Liu et al., 2017), dissolved inorganic carbon (Dorsett et al., 2011; Szymczycha et al., 2013), methane (CH₄; Bugna et al., 1996; Dulaiova et al., 2010; Lecher et al., 2015), and organic carbon (Suryaputra et al., 2015; Yang et al., 2015). SGD may therefore be an important source of carbon and reaction products of organic carbon remineralization, which include greenhouse gases (CO₂ and CH₄), and nutrients. These fluxes, however, should depend on biogeochemical processing of carbon in in subterranean estuaries prior to discharge.

Carbonate Versus Siliciclastic STEs

While subterranean estuaries are active sites of biogeochemical reactions, variability in mineralogical and hydrogeological properties impact the range and magnitude of reactions that can be expected to occur, and may determine the net impact of reactions on carbon cycling. Subterranean estuaries may be broadly separated into two hydrological end members: those dominated by widely distributed diffuse flow, as is typical where groundwater flows through siliciclastic sediments (Martin

et al., 2007; Spiteri et al., 2008a), versus conduit-flow, which is typical of karstic carbonate aquifers (Null et al., 2014).

Most studies to date have focused on fluxes from siliciclastic STEs because of their predominance in heavily populated regions of the U.S. East Coast (Cai et al., 2003; Michael et al., 2005; Spiteri et al., 2008a; Gonnee and Charette, 2014), and Europe (Jankowska et al., 1994; Szymczycha et al., 2012). In karstic groundwater systems, most freshwater input to the coast occurs as SGD because high hydraulic conductivity leads to rapid infiltration of precipitation which limits surface water sources and runoff (Fleury et al., 2007). Carbonate karst coastlines are found throughout the Caribbean (Hernández-Terrones et al., 2011; Null et al., 2014; Young et al., 2017) Gulf Coast of Florida (Brooks, 1961; Corbett et al., 1999; Swarzenski et al., 2001) and Mediterranean regions (Fleury et al., 2007), but have received relatively less attention than siliciclastic systems. While both types of STEs provide important solute fluxes to coastal oceans, there are distinct differences between the hydrological properties of siliciclastic versus carbonate STEs that determine groundwater flow rates and residence time, while mineralogical differences impact biogeochemical feedbacks in carbon cycling.

Hydrological Impact on Biogeochemical Reactions

The location of the freshwater-saltwater interface in coastal systems can be described by the Ghyben-Herzberg relationship (Verruijt, 1968). This relationship describes the hydrostatic balance of a freshwater lens floating on denser saltwater, which is maintained through freshwater recharge (Fig. 1-1),

$$z = \frac{\rho_f}{\rho_s - \rho_f} h \quad (1-1)$$

where z is the depth of the freshwater lens below sea level, h is the height of the water table above sea level, and ρ_f and ρ_s represent the density of fresh and saltwater, respectively (Eq. 1-1). The depth of the base of the freshwater lens can be estimated as the ratio of the density of freshwater over the difference in densities between salt and freshwater (approximately ~40 for fresh water ($S=0$) and average ocean water ($S = 35$)) multiplied by the elevation of the water table above sea level (Eq. 1-1, Fig. 1-1). The position of the freshwater-saltwater interface is controlled by hydrologic factors including groundwater recharge rates, which increases hydraulic head, as well as hydraulic conductivity, which regulates groundwater flow.

Siliciclastic and karst carbonate aquifers possess different hydrological properties that impact their flow dynamics (Fig. 1-2). Differences in hydrologic properties should affect biogeochemical reactions because of their control on residence time as well as delivery of solutes and removal of reaction products. For instance, compared to siliciclastic aquifers (Fig. 1-2a), carbonate aquifers may have orders of magnitude higher hydraulic conductivity (Fig. 1-2b; Table 1-1), which prevents the development of high hydraulic gradients and leads to lower residence time of groundwater in karst aquifers, particularly in conduits. When hydraulic head decreases relative to sea level, high hydraulic conductivity of karst aquifers allows surface seawater to intrude into conduits for meters to kilometers inland (Fig. 1-2b; Beddows et al., 2007). In contrast, lower hydraulic conductivity and slower groundwater flow in siliciclastic systems leads to higher groundwater residence times (Michael et al., 2005). Because of the differences in water residence time in siliciclastic versus carbonate aquifers, reaction dynamics should

vary between these aquifer end members, and may lead to systematic variations in the chemical composition of SGD. Relationships between reaction kinetics and transport rates are expressed through the Damkohler number, Da , which is the ratio of the reaction rate to the transport rate:

$$Da = \frac{\text{Reaction rate}}{\text{Transport rate}} \quad (1-2)$$

Where Da is high, reactions may be expected to approach thermodynamic equilibrium because the reaction occurs quickly relative to transport. The differences in transport rates between carbonate and siliciclastic aquifers may impact biogeochemical reactions by altering Da .

An important chemical parameter that regulates the type and kinetics of biogeochemical reactions in groundwater systems is the redox potential of pore waters. Redox potential is related to the availability of terminal electron acceptors (TEAs) used by microbial communities to remineralize organic carbon, and in marine systems predominantly include oxygen, nitrate, manganese, iron, and sulfate (Froelich et al., 1979). The relative energy yield of reactions declines along the redox ladder, represented sequentially in Table 1-2. For instance, oxic respiration yields more energy than any of the other TEAs and thus occurs preferentially. Once oxygen is depleted, less energetically favorable reactions will occur, in the order of nitrate reduction, iron reduction, sulfate reduction, and methanogenesis, though redox zones may overlap.

Because the suite of redox reactions occurs sequentially according to the energy yield of reactions, redox potential predominantly depends on the rate of replenishment of TEAs compared to the rate of organic carbon remineralization, and thus should depend on groundwater residence time (Spiteri et al., 2008b). For instance, Slomp and

Van Cappellen (2004) suggested that, given equivalent inputs of organic carbon and terminal electron acceptors, aquifers with hydrological parameters that reduce groundwater residence time (e.g. high recharge and flow rates) are more likely to maintain oxic conditions than aquifers with low recharge and flow rates. Redox potential affects microbial N cycling (Santoro, 2009; Gonneea and Charette, 2014) as well as phosphorus mobilization (Slomp and Van Cappellen, 2004) because of NO₃'s role as a TEA and from the production of NH₄ and PO₄ during organic carbon remineralization.

Mineralogical Impact on Carbon Cycling

Apart from differences in hydrologic characteristics, and their control on biogeochemical reactions, siliciclastic and carbonate STEs impact carbon cycling differently because of feedbacks from reactions with the different aquifer solids. In particular, CO₂ concentrations are altered by feedbacks between organic carbon remineralization and carbonate mineral dissolution. These feedbacks are initiated when remineralization of organic matter generates carbonic acid (H₂CO₃),



which decreases the pH of pore waters:



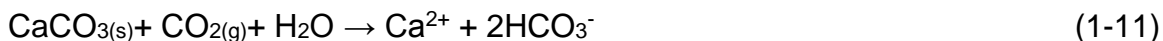
The dissociation of carbonic acid (H₂CO₃) into HCO₃⁻ and CO₃²⁻ depends predominantly on ambient pH. At standard oceanic pH (8.2), about 88% of dissolved inorganic carbon is present as HCO₃⁻, while 11% is CO₃²⁻ and 1% is dissolved CO₂ and H₂CO₃ (Sarmiento and Gruber, 2006).

When contributions of CO₂ via Eq. 1-8 cause dissolved CO₂ concentrations to increase beyond the partial pressure of atmospheric CO₂, currently at approximately 400 ppm, outgassing can occur and water will become a source of atmospheric CO₂.

However, increased acidity in water drives Eq. 1-8 to the left, reducing the concentration of CO_3^{2-} ions and causing undersaturation of CaCO_3 minerals, which dissolve according to:



However, because this reaction impacts the speciation of C in Eq. 1-9, it is often represented as:



This reaction illustrates that the dissolution of CaCO_3 consumes one molecule of atmospheric CO_2 and produces 2 moles of HCO_3^- , and is therefore a net sink of atmospheric CO_2 , and the combined effects of aerobic respiration and carbonate dissolution lead to no net change in atmospheric C concentrations. Therefore, the presence of carbonate minerals may limit increases in partial pressure of CO_2 dissolved in the water (P_{CO_2}) derived from organic carbon remineralization. This buffering represents a negative feedback between C released via organic matter remineralization and P_{CO_2} of pore waters, thus impacting the status of waters as either CO_2 sources or CO_2 sinks.

Feedbacks with Biogeochemical Cycling of Nutrients and Metals

In surface waters, carbon cycling depends on the availability of macronutrients such as nitrogen (N), phosphorus (P) and micronutrients such as iron (Fe) due to nutrient requirements of primary producers. Marine primary producers typically fix carbon and nutrients at an average C:N:P ratio of 106:16:1 (Redfield, 1934). Carbon and nutrient cycling in STEs may therefore impact carbon fixation in surface waters when SGD contains elevated concentrations of nutrients. For instance, phosphorus

delivery via SGD has been linked to increased primary productivity near submarine springs in the Yucatan (Carruthers et al., 2005), while enhanced SGD-derived nutrient fluxes to the Gulf of Mexico have been linked to red tides and harmful algal blooms (Hu et al., 2006). These local observations suggest that nutrient-enriched SGD may trigger large-scale shifts in ecological structures and significantly impact net primary productivity (Lyons et al., 2014).

Compared to nitrogen, which has few significant mineral reservoirs (Holloway and Dahlgren, 2002), multiple feedbacks between phosphorus concentrations and mineral stability in siliciclastic and carbonate STEs suggest that it could be coupled to carbon cycling. Phosphorus is often the limiting nutrient for primary productivity in coastal marine environments, and has been cited as the ultimate limiting nutrient for primary productivity in marine ecosystems over geologic timescales (Toggweiler, 1999; Tyrrell, 1999). In the ocean, the largest source of P is riverine input of particulate matter and dissolved P species, and up to 99% of particulate P and 25% of dissolved phosphate delivered by rivers are buried in deltas and continental shelves (Paytan and McLaughlin, 2007). As the main repository of oceanic P, sediment P cycling often plays an important role in controlling the concentration of P in overlying waters. Dominant forms of P in sediment include organic P, phosphate adsorbed to Fe-oxide or carbonate minerals, and P stored in apatite minerals. Diagenetic interactions between these reservoirs affect the rate and extent by which P can be remobilized and returned to the water column (Ruttenberg and Berner, 1993; Koch et al., 2001). Depending on these interactions, sediment can be a net source if reactions lead to net liberation of P from sedimentary reservoirs so that it can be transported from STEs to surface waters, but

may also be P sinks if reactions lead to net decreases in dissolved P concentration due to precipitation or adsorption to minerals (Short et al., 1990; Jensen et al., 1998).

In siliciclastic sediments, cycling of organic carbon, iron, and phosphorus are coupled due to the impact of redox status on the stability of Fe oxide minerals, which form sorption interactions with dissolved phosphate (PO_4^{3-}). Fe oxide minerals may be reduced under anoxic conditions during microbial remineralization of organic matter (Table 1-2; Eq. 1-5). Reduction of iron from Fe(III) to Fe(II) strongly increases its solubility and results in the dissolution of solid Fe-oxyhydroxides and the liberation of sorbed P (Caraco et al., 1989; Blomqvist et al., 2004; Roy et al., 2012). Once liberated, dissolved Fe and P are mobile and may be transported through sediment and to surface waters via advective or diffusive transport processes, where they can be consumed by primary producers. Re-precipitation of iron oxide or iron sulfide minerals may occur, however, depending on the saturation state of these minerals in pore waters. When iron oxides re-precipitate near the sediment-water interface, they may re-sorb phosphorus and strongly reduce fluxes, forming what is referred to as an “iron curtain” (Chambers et al., 1990; Linkhorst et al., 2017). However, in marine systems where sulfate reduction generates sulfide, iron sulfide minerals may precipitate. These minerals have very low sorption potential for phosphorus, and their precipitation will not impact P fluxes from sediment. The conversion of Fe oxides to Fe sulfides is noted to increase P fluxes from sediment in marine systems, and has been proposed as a mechanism to explain the predominance of N limitation in marine environments as a consequence of greater P inputs (Blomqvist et al., 2004).

In sediments predominantly composed of carbonate minerals, strong associations between P and CaCO₃ minerals and subsequent conversion into more stable apatite phases cause it to become a limiting nutrient for primary productivity (DeKanel and Morse; 1978; Rosenfeld, 1979; Short, 1985; Millero, 2001). The high affinity of PO₄ for carbonate mineral surfaces is evident in the distribution of dissolved PO₄ and N:P ratios in carbonate versus siliciclastic systems. For instance, pore waters in low-CaCO₃ sediments along temperate coasts typically have higher PO₄ concentrations and lower N:P ratios than shallow marine CaCO₃-dominated sediments, which have lower PO₄ concentrations and higher N:P ratios (Lapointe et al., 1992). Because organic carbon remineralization is coupled with CaCO₃ dissolution in carbonate systems, sorbed P may be liberated and transported to surface waters. Enhanced delivery of P due to CaCO₃ dissolution may lead to enhanced primary productivity where P is limiting (Carruthers et al., 2005).

The coupling of the above reactions in both siliciclastic and carbonate STEs depends on the kinetics of reactions relative to transport rate. For instance, while organic carbon remineralization kinetics largely depend on the quality of organic substrates and availability of terminal electron acceptors (Arndt et al., 2013), dissolution and precipitation kinetics of CaCO₃ minerals depend on the degree of over- or under-saturation and reactions are slow when waters are close to saturation (Morse and Arvidson, 2002). Therefore, where Da is small (reaction rate is slow relative to transport rate), reactions may not reach thermodynamic equilibrium. In the case of carbonate STEs where CO₂ generation may be buffered by CaCO₃ dissolution, a low Da number

may reduce the extent of buffering and water may still serve as a source of atmospheric CO₂ from organic C remineralization.

Summary and Implications

Hydrological and mineralogical differences between siliciclastic and carbonate STEs may lead to significant variations in biogeochemical reactions involving carbon and nutrients, and may therefore systematically differ in the impact of SGD on surface water carbon budgets. While organic carbon remineralization generates carbonic acid (Eq. 1-8), only sediments with carbonate minerals may buffer pore waters through CaCO₃ dissolution and cause CO₂ to be sequestered as HCO₃⁻ or CO₃²⁻. Moreover, feedbacks between carbon and phosphorus cycling are likely to be more important in carbonate systems versus siliciclastic due to the affinity of P for CaCO₃ minerals and the increased likelihood of P limitation in carbonate systems. While sediment mineralogy may control the extent of biogeochemical feedbacks impacting the C cycle, systems may only be expected to reach chemical equilibrium when the rate of water transport is slow compared to reaction kinetics. Since carbonate and siliciclastic systems have widely variable hydrological properties (Fig. 1-2), with higher hydraulic conductivity and flow rates in carbonate systems, the hydrological characteristics of STEs may control the impact of biogeochemical processing on SGD composition by impacting the redox potential of water as well as the dissolution of CaCO₃ minerals following organic carbon remineralization.

I address the impacts of biogeochemical reactions on carbon processing in carbonate versus siliciclastic STEs by comparing two STEs representing hydrogeologic end members. The siliciclastic end member is represented by Indian River Lagoon on the east coast of Florida (Fig. 1-3), where groundwater flows through siliciclastic

sediments as diffuse discharge (Martin et al., 2007; Smith et al., 2008; Dorsett et al., 2011; Roy et al., 2013a). The carbonate end member is represented by submarine springs offshore of the Yucatan peninsula (Fig. 1-4), Mexico, where groundwater discharges to the coast through conduits in the carbonate karst aquifer (Valle-Levinson et al., 2011; Parra et al., 2014; Parra et al., 2015; Young et al., 2017). Hydrological properties and magnitudes of SGD between field sites are given in Table 1-1. I address variations in carbon processing by first evaluating organic carbon sources and processing with respect to the impact on redox potential across salinity gradients in both types of STEs (Ch. 2). I then explore relationships between organic carbon remineralization, carbonate mineral dissolution, and phosphorus dynamics at the Yucatan field site (Ch. 3), and discuss greenhouse gas (CO₂ and CH₄) production and sequestration in siliciclastic systems as represented by the Indian River Lagoon field site (Ch. 4).

In order to assess the change in the chemical composition of submarine groundwater discharge due to reactions that occur in the freshwater-saltwater mixing zone, I employ salinity-based conservative mixing models. These mixing models assume deviations from a line drawn between these two points reflect changes in composition due to reactions. Deviations depend on the position of the line and thus on the definition of fresh and saltwater end members. This approach is frequently employed in environments where water sources with distinct chemistries mix, including surface water (Guo et al., 2007; Spencer et al., 2007; Markager et al., 2011) and subterranean estuaries (Beck et al., 2007; Sanders et al., 2012; Gonnee et al., 2014). However, uncertainty in end member selection results in mixing models that may over-

or under-estimate the magnitudes of reactions. In mixing models employed throughout this dissertation, I define the fresh end member as the freshest subterranean estuary sample collected at each sampling location and during each sampling time, and use compositions of surface lagoon water as the saltwater end member. This approach is taken to assess biogeochemical changes that occur where freshwater and salt mix and assumes that the freshest subterranean estuary sample is representative of the freshwater flowing to the subterranean estuary. However, while composition of surface seawater is approximately constant over the width of seepage faces, chemical gradients may develop in fresh groundwater that result in a high degree of variability in water samples of similar salinity. Where this is the case (e.g. Fig. 4-2), results of mixing models are sensitive to end member selection. While I am aware of the impact that end member values have on determining residual values, my general interest is in looking at overall trends in a qualitative way to determine the sign and not necessarily the absolute magnitude of processes. Use of conservative mixing models for quantitative assessments such as mass balance would require more rigorous determination of the uncertainty of end members.

Table 1-1. Hydrologic properties of carbonate and siliciclastic subterranean estuaries in this study.

Location	Type	Fresh SGD (m ³ km ⁻¹ yr ⁻¹)	Marine SGD (m ³ km ⁻¹ yr ⁻¹)	Total SGD (m ³ km ⁻¹ yr ⁻¹)	Hydraulic Conductivity (m/s)
Yucatan Peninsula	Carbonate karst	8.6 ⁽¹⁾	--	--	1x10 ⁰ to 1x10 ⁻¹ ⁽²⁾
		0.7–3.9 ⁽³⁾	--	--	
		0.5 ⁽⁴⁾	--	--	
		--	--	112 ⁽⁵⁾	
Indian River Lagoon	Siliciclastic	0.05-2.5 ⁽⁶⁾	320 ⁽⁶⁾		1x10 ⁻⁶ ⁽⁷⁾

⁽¹⁾Hanshaw and Back (1980)

⁽²⁾González-Herrera et al. (2002)

⁽³⁾ Smith et al. (1999)

⁽⁴⁾ Hernández-Terrones et al. (2011)

⁽⁵⁾ Null et al. (2014)

⁽⁶⁾ Martin et al. (2007)

⁽⁷⁾ Zimmermann et al. (1985)

Table 1-2. Reduction half reactions coupled with oxidation of organic matter (CH₂O + H₂O → CO₂ + 4H⁺ + 4e⁻). Relative energy yield is reported with respect to aerobic respiration and is taken from Lovley and Chapelle (1995). Reactions modified from Stumm and Morgan (1996).

Equation	Reduction reaction	Relative energy yield
1-3	Aerobic respiration $O_{2(g)} + 4H^+ + e^- \rightarrow 2H_2O$	100
1-4	Nitrate reduction $NO_3^- + 10H^+ + 8e^- \rightarrow NH_4^+ + 3H_2O$	93
1-5	Iron reduction $FeOOH_{(s)} + HCO_3^- + 2H^+ + e^- \rightarrow FeCO_{3(s)} + 2H_2O$	84
1-6	Sulfate reduction $SO_4^{2-} + 9H^+ + 8e^- \rightarrow HS^- + 4H_2O$	6
1-7	Methanogenesis $CO_{2(g)} + 8H^+ + 8e^- \rightarrow CH_{4(g)} + 2H_2O$	3

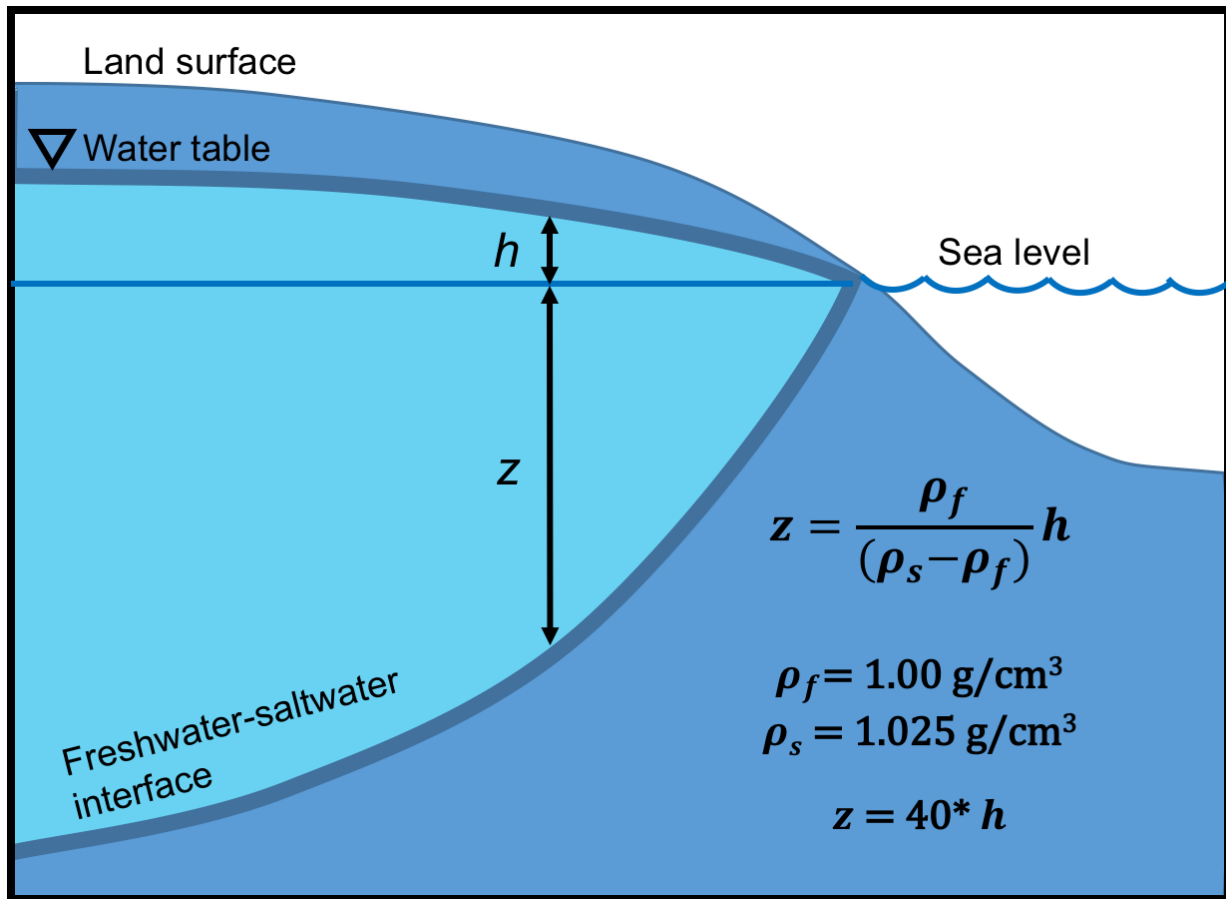


Figure 1-1. Ghyben-Herzberg relationship demonstrating the depth of a freshwater lens overlying saline groundwater. The border between fresh and saltwater is represented as a sharp interface over which no mixing occurs. This schematic assumes static conditions (no flow), but flow is required to maintain the position of the freshwater lens and necessitates the development of submarine groundwater discharge at a seepage face. Modified from Verruijt (1968).

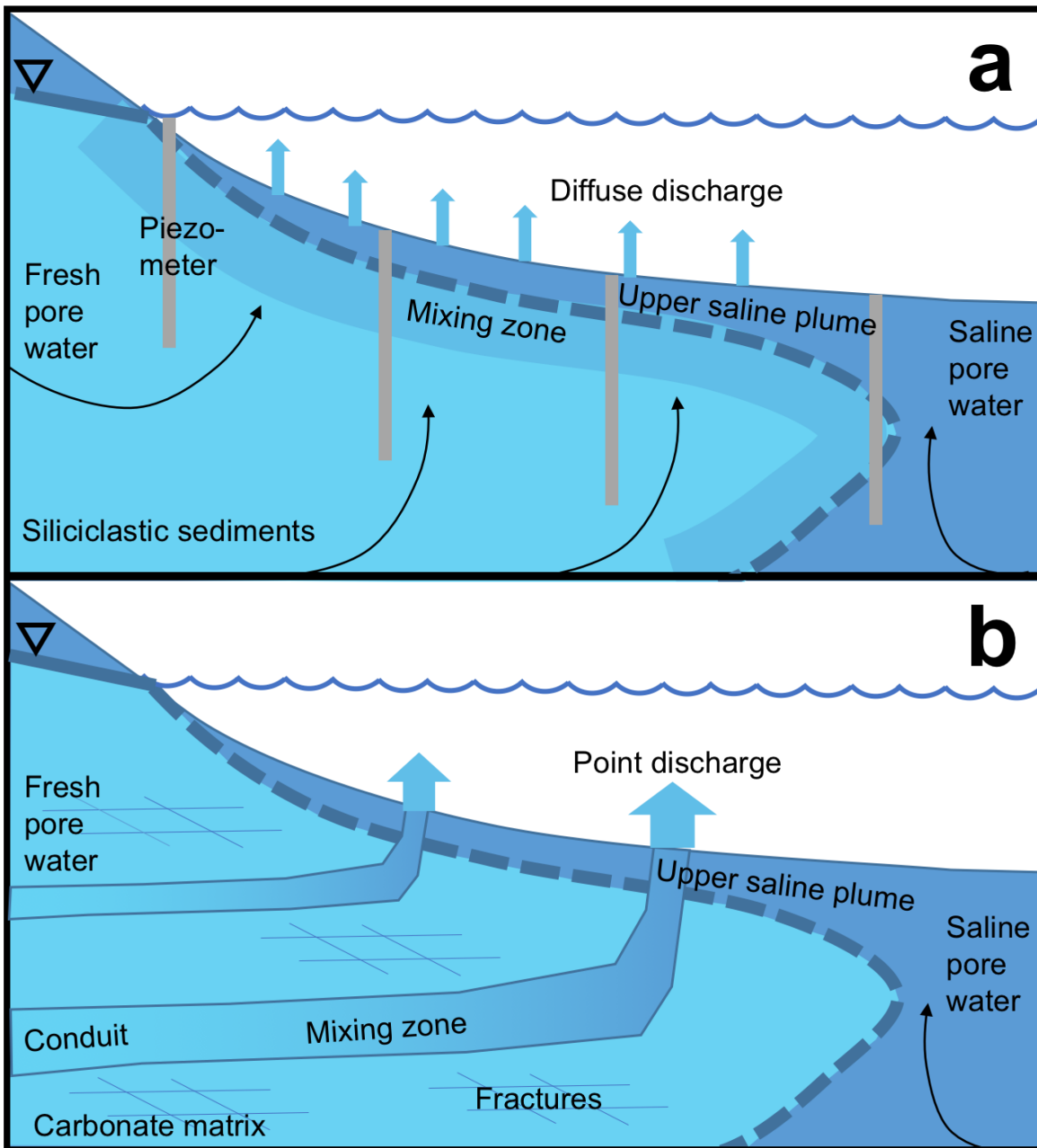


Figure 1-2. Conceptual models of subterranean estuaries. (a) Siliciclastic STEs with diffuse flow through porous sediments. The subterranean estuary, or mixing zone between fresh and saltwater end members, occurs across the entire freshwater-saltwater interface. Because it is not a sharp interface, it is represented as a dashed line. Permanent piezometers installed in sediment are used to sample across the seepage face. Modified from Martin et al. (2007). (b) Carbonate karst STE with point discharge through conduits. Mixing occurs within conduits that have much higher hydraulic conductivity than the carbonate matrix.

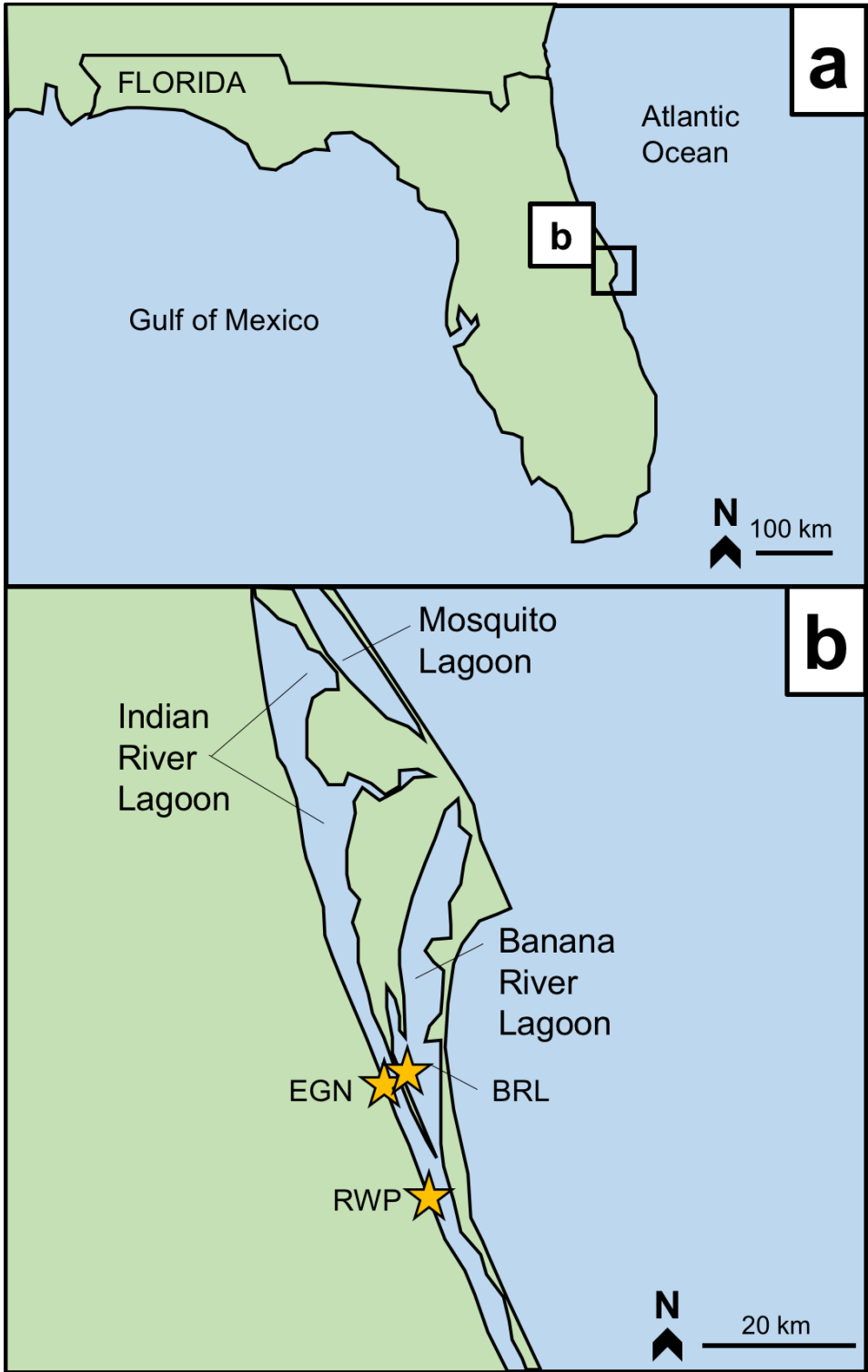


Figure 1-3. Map of locations of piezometer transects at Indian River Lagoon Florida. (a) Indian River Lagoon is situated on the east coast of Florida. (b) Transects are located in the central portions of Indian River Lagoon (EGN and RWP) and Banana River Lagoon (BRL).

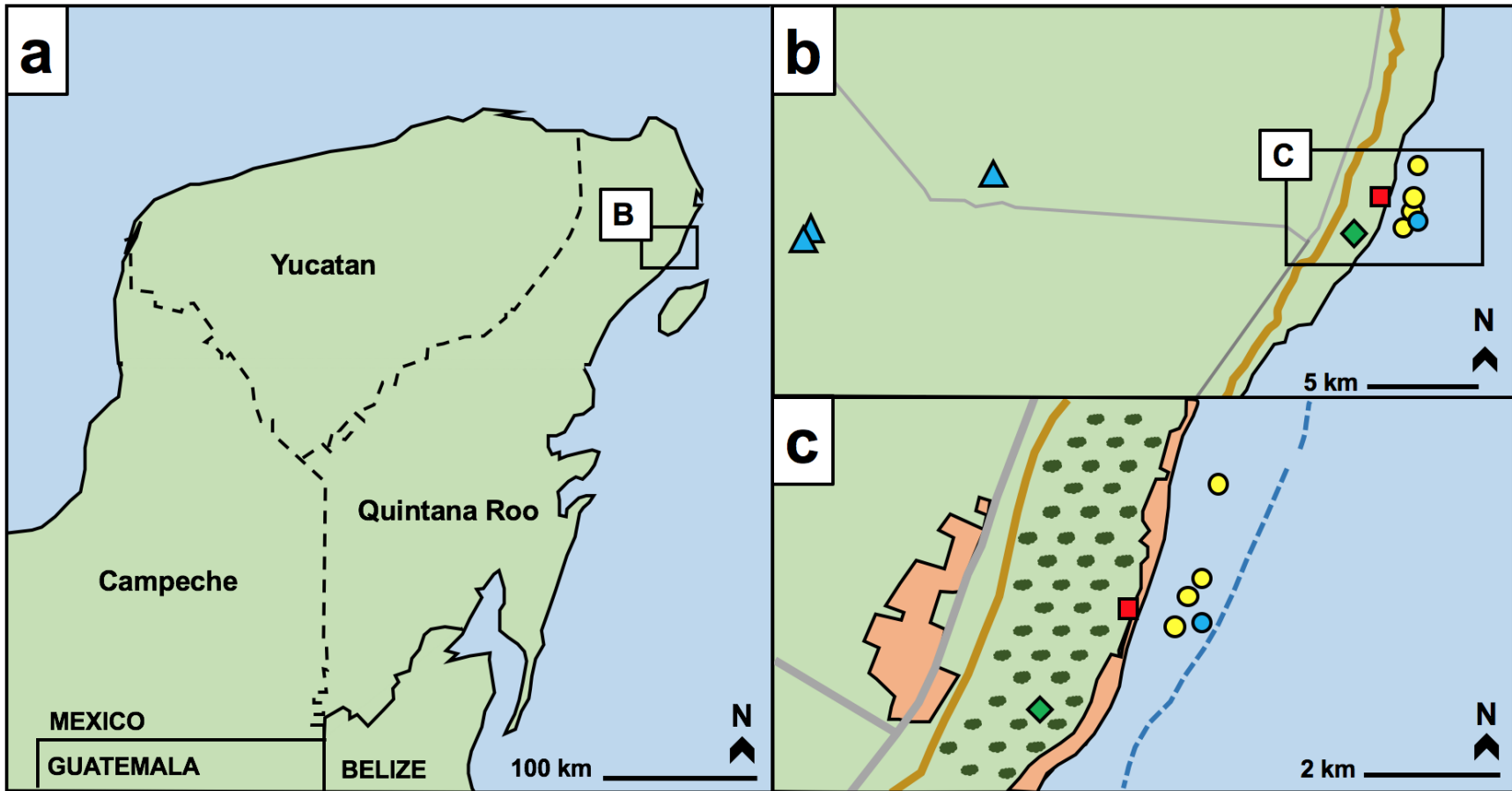


Figure 1-4. Maps of Yucatan study site and sampling locations. (a) Location of study site on Yucatan peninsula. (b) Location of sampling points including inland cenotes. (c) Nearshore sampling sites and extent of lagoon bounded by reef crest.

CHAPTER 2 ORGANIC CARBON QUANTITY AND QUALITY ACROSS SALINITY GRADIENTS IN CONDUIT- VERSUS DIFFUSE FLOW-DOMINATED SUBTERRANEAN ESTUARIES

Introduction

Subterranean estuaries (STEs) occur where fresh groundwater and saline pore water mix in coastal aquifers and are zones of active biogeochemical transformation of ecologically relevant solutes such as nutrients, metals, and carbon (Moore, 1999). While STEs are analogous to surface estuaries, longer residence times in STEs and lower water:rock ratios should allow for a greater range of biogeochemical reactions to occur, in part due to the remineralization of organic carbon, which depletes terminal electron acceptors and lowers redox potential (Slomp and Van Cappellen, 2004). These transformations could alter fluxes of terrestrial solutes in submarine groundwater discharge (SGD) when delivered to the coastal ocean. SGD has long been recognized as a source of freshwater and terrestrial solutes to the coastal zone (Slomp and Van Cappellen, 2004; Windom et al., 2006; Martin et al., 2007; Roy et al., 2013b; Kwon et al., 2014), but the link between biogeochemical processing in STEs, variations in hydrogeology, and fluxes from SGD is poorly known.

The distribution of redox reactions in STEs are driven by the distributions of terminal electron acceptors (TEAs) that microbes use to remineralize organic carbon (Slomp and Van Cappellen, 2004). In STEs, intensity of organic carbon processing should vary with salinity, which may be regarded as a tracer for the proportion of fresh and saltwater sources in the mixing zone. This co-variance would result from two processes in STEs, specifically changes in the relative proportion of terrestrial versus marine organic matter, and changes in the concentrations of terminal electron acceptors available to remineralize organic carbon. In addition to the biogeochemical control,

physical controls related to flow rates through the STEs should also impact distribution of redox reactions and resulting changes in pore water compositions in and fluxes of solutes from STEs. This chapter evaluates the relative effect of these three processes on potential solute fluxes from STEs.

The kinetics of organic carbon remineralization are impacted by its reactivity, which relates to the ease with which microbes can metabolize organic compounds. In nature, organic carbon reactivity lies along a spectrum from highly reactive to virtually inert under ambient environmental conditions. The distribution of organic carbon along this reactivity spectrum is thus more important to its remineralization dynamics than its bulk quantity (Berner, 1980; Arndt et al., 2013). Terrestrial organic carbon is typically less reactive than marine organic carbon, in part because of higher proportion of vascular plant material that is comprised of structural biomolecules such as lignin and cutin. These compounds are typically less readily degraded than proteins and carbohydrates, which are characterized by weaker peptide bonds and greater nutrient (nitrogen and phosphorus, N and P) content (Arndt et al., 2013). Moreover, labile fractions of terrestrial organic carbon may be degraded during delivery to the STEs through long flow paths within coastal aquifers, resulting in a residual organic carbon fraction that is more recalcitrant than fresh terrestrial organic carbon (Hopkinson et al., 1998). On the other hand, marine organic matter contains a greater proportion of relatively more reactive compounds such as carbohydrates and proteins (Schwarzenbach et al., 2003). Marine organic carbon is also produced closer to the STE than terrestrial organic carbon and can be rapidly transported into the STE through mixing with saline water (Martin et al., 2006; Young et al., 2017). The relative freshness

of marine organic matter in STEs may therefore be greater, and hence more reactive, than terrestrial organic carbon in fresh groundwater and may affect the magnitude and rates of biogeochemical reactions in mixed marine and terrestrial water of STEs.

Remineralization dynamics in STEs may also be a function of changes in terminal electron acceptor availability. For example, surface saltwater contains high concentrations of oxygen (Young et al., 2017) and sulfate, while fresh water may contain high concentrations of nitrate (Kroeger et al., 2007; Kroeger and Charette, 2008) that may be used to remineralize organic carbon (Froelich et al., 1979). In freshwater with sufficient reactive organic carbon, organic carbon remineralization can commonly progress to methanogenesis because of low availability of other terminal electron acceptors, such as sulfate. Because seawater is a major source of sulfate, increased sulfate availability due to increases in salinity should enhance organic carbon remineralization rates in methanogenic freshwater. These effects have been observed in saltwater intrusion experiments on methanogenic freshwater sediments, which demonstrated that organic carbon remineralization rates increase with the addition of sulfate (Weston et al., 2011). Similarly, oxygen contained in surface seawater may increase remineralization rates in anoxic freshwater, though the extent of this increase depends on saltwater transport rates. For instance, rapid aerobic remineralization rates lead to the consumption of oxygen within the first few millimeters of typical marine sediments when transport occurs via diffusion (Megonigal et al., 2005). Because it is consumed rapidly, enhanced remineralization from oxygen would require rapid transport of surface seawater to deep portions of STEs via advection.

Hydrogeological characteristics of STEs could also affect organic carbon processes in STEs. Two distinct end member hydrologic settings occur in STEs and include diffuse seepage from porous media, for example in sand and gravel aquifers (Martin et al., 2007; Spiteri et al., 2008a) and point discharge from karstic conduit systems (Swarzenski et al., 2001; Null et al., 2014; Young et al., 2017). These two end-member settings are characterized by different flow rates and thus residence time of water and reactants in the mixing zone and with aquifer solid materials.

Here, I characterize changes in the quantity and quality of DOC along salinity gradients in two STEs that represent these hydrogeologic end members. One represents diffuse seepage from siliciclastic sediments (Indian River Lagoon, FL; Martin et al., 2007) and the other represents conduit flow through a carbonate karst aquifer (Yucatan Peninsula, Mexico; Null et al., 2014; Parra et al., 2014; Parra et al., 2015). I evaluate non-conservative mixing behavior of organic carbon using dissolved organic carbon (DOC) concentrations and characterization of colored dissolved organic matter (CDOM) via fluorescence spectroscopy and PARAFAC analysis (Murphy et al., 2013). DOC includes all organic molecules, while CDOM includes the fraction of total DOC that exhibits chromophoric properties, and CDOM is therefore a subset of total DOC although the two are often collinear in coastal systems (Del Castillo, 2005). I link organic carbon processing with biogeochemical reactions via oxidation-reduction potential (ORP), which is a measure of the availability of terminal electron acceptors (TEAs) to respire organic carbon. Elevated ORP values indicate that fewer redox reactions have occurred, or more oxidized species have been delivered to the STE. Because organic carbon is consumed in most microbially-mediated redox reactions, I use the distribution

of organic carbon with salinity to depict the general controls of biogeochemical reactions within STEs and propose a conceptual model that describes reactive zones in STEs due to fresh and saltwater mixing.

Methods

Study Locations

Indian River Lagoon is located on the east coast of Florida (Fig. 1-3) and the Yucatan field site is located in a reef lagoon offshore of Puerto Morelos approximately 40 km south of Cancun in the state of Quintana Roo, Mexico (Fig. 1-4). These two sites are separated by only a few hundred kilometers and thus have similar climate regimes, including cool dry winter months with warm humid summer months and periodic impacts from tropical storms. Both sites are microtidal and have low wave energy as a result of barriers separating them from the ocean.

However, the geological and hydrogeologic characteristics of sites settings differ. The Yucatan Peninsula is a karstic carbonate platform of Triassic to Holocene age, and is characterized by dissolutional secondary porosity. This secondary porosity generates high aquifer permeability and hydraulic conductivity, which limits surface water on the terrestrial portion of the peninsula and causes precipitation to recharge the aquifer through thin soil layers overlying the carbonate matrix. The aquifer discharges at the coast as SGD from submarine springs (~ 78.5% of the discharge at the Puerto Morelos lagoon) with the remainder from diffuse seepage from the beach shore face (Beddows et al., 2007; Null et al., 2014). The springs can reverse flow during extreme high tides, storm surges, and wind set-up, allowing surface seawater to intrude into conduits (Parra et al., 2015; Young et al., 2017) and create a brackish mixing zone between fresh and saltwater that extends approximately 1-4 km inland (Beddows et al., 2007).

Indian River Lagoon is located on the Atlantic coast of central Florida and spans approximately 250 km of coastline in three hydrological subunits: Mosquito Lagoon, Indian River Lagoon, and Banana River Lagoon (Fig. 1-3). Three STEs in the Indian River and Banana River lagoon were included in this study, Eau Gallie North (EGN), Banana River Lagoon (BRL) and Riverwalk Park (RWP). Sediments in these STEs are siliciclastic ranging from fine sand to clays, which allow groundwater seepage to occur at rates ranging from 0.02 to 0.9 m³/d per meter of shoreline at EGN (Martin et al., 2007). This slow seepage makes STE salinity gradients static over timescales of days to weeks in contrast to the rapid exchange of the Yucatan aquifer. However, seasonal variation in lagoon water salinity and fresh groundwater head are known to cause fluctuations in seepage face width (Roy et al., 2013) and storm-driven saltwater intrusion events can alter seepage face salinity for several months (Smith et al., 2008).

Sample Collection

At the Yucatan site, water was sampled over a two-week period in September 2014 from four submarine springs (Hol Kokol, Gorgos, Laja, and Pargos) that are distributed along ~5 km of shoreline in Puerto Morelos (Fig.1-4). During the sampling periods, surface lagoon water periodically intruded into springs and caused variable salinity of vent discharge that serves as a conservative tracer to assess mixing, from which biogeochemical processing in the STE may be evaluated (Young et al., 2017). All spring samples were collected during spring discharge periods. To characterize freshwater inputs to the coastal zone, water samples were also collected from inland cenotes (water-filled sinkholes), mangrove surface water, and an inland well (Fig. 1-3).

Indian River Lagoon samples were collected four times during fall (September-October) and spring (May), starting in fall 2014 and ending spring 2016, at all three

seepage faces (locations of fresh water discharge) (Fig. 1-3). Seepage face widths varied between sites and extended about 20 m offshore at EGN, 35 m offshore at RWP, and 50 m offshore at BRL. Permanent multilevel piezometers (multisamplers; Martin et al., 2003) were installed at increasing distances offshore to permit recurring sampling at fixed sediment depths across the seepage faces (Fig. 1-3). Piezometers were installed in 2004 at EGN and between May 2014-September 2015 at RWP and BRL. Sampled piezometers were located 0, 10, 20 and 22.5 m offshore at EGN (EGN-X), 10, 20, and 35 m offshore at RWP (RWP-X) and 1, 11, 21, and 45 m offshore at BRL (BRL-X; Fig. 1-4), where the value of X represents the distance offshore in meters.

Samples were collected by pumping water to the surface through 0.5 cm diameter flexible PVC tubing. In the Yucatan, tubes were installed at the spring openings by SCUBA diving, and by lowering the tubing from the surface to measured depths within the cenotes and well. At Indian River Lagoon, the tubing was connected to multisampler piezometer ports (Fig. 1-2a; Martin et al., 2003). A YSI Pro-Plus sensor was installed in an overflow cup in-line with the tubing to measure salinity, temperature, pH, dissolved oxygen, and oxidation-reduction potential (ORP) while pumping water. Once these parameters were stable, water samples were filtered through 0.45 μm trace-metal grade Geotech medium capacity disposable canister filters and collected and preserved in the field according to the specific solute. Samples for dissolved organic carbon (DOC) concentration and CDOM analysis were collected in amber borosilicate vials that were combusted at 550°C prior to use. Although the < 0.45 μm fraction also includes colloids, I refer to this size fraction as dissolved because both dissolved and colloidal organic carbon fractions are mobile in groundwater. Changes in the abundance

and quality of the $<0.45 \mu\text{M}$ fraction should reflect changes in organic carbon processing due to end-member mixing and in situ reactions such as remineralization (consumption) or production from other organic carbon pools (e.g. particulate or sedimentary organic carbon). DOC concentration samples were acidified with hydrochloric acid to $\text{pH}<2$. Fluorescent DOC samples were not acidified and kept frozen until analysis within one month of collection.

Laboratory Methods

DOC concentrations were analyzed on a Shimadzu TOC-VCSN total organic carbon analyzer, and the coefficient of variance for check standards was less than 2%. Spectroscopic and fluorescence techniques were used to assess organic carbon quality. Fluorescence measurements were collected on a Hitachi F-7000 Fluorescence Spectrophotometer to generate 3D Excitation-Emission Matrices (EEMs). Scans were collected at 700 V and at excitation wavelengths ranging from 240-450 nm at 5-nm intervals, and emission wavelengths ranging from 250-550 nm at 2-nm intervals. Instrument-specific effects were corrected from data utilizing a correction that accounts for difference in lamp intensity across the excitation-emission wavelength range. Inner filter effects due to organic carbon content were corrected with UV spectra according to methods outlined in Ohno (2002). An aliquot of the fluorescence sample was used to measure UV absorption on a Shimadzu 1800 UV Spectrophotometer, and UV absorption data were collected at 1 nm intervals from 240-550 nm.

Modeling

Sufficiently large sets of EEMs can be deconvolved using Parallel Factor Analysis (PARAFAC) into statistically significant fluorophores that comprise colored dissolved organic matter (CDOM). Fluorophores represent distinct structural groups of

organic matter that have fluorescent properties, and principally include humic acids, fulvic acids, and proteins (Murphy et al., 2013). The absolute and relative abundances of these organic compounds are often utilized as “fingerprints” for organic carbon sources, but also provide an indication of the quality of organic matter because proteins are typically more labile than humic or fulvic acids. Processing of EEMs for modeling with PARAFAC included pre-processing of raw data and corrections for instrument-specific effects, inner-filter effects, masking to eliminate signals from first and second order Rayleigh scattering, and conversion to Raman Units. PARAFAC modeling was achieved using the drEEM toolbox in Matlab version 2015b (MathWorks, 2015; Murphy et al. 2013b). To reduce collinearity between samples due to dilution effects and to better model low-concentration samples, EEMs were normalized to total sample fluorescence intensity before modeling with PARAFAC. A total of 322 samples were included in the PARAFAC model (Appendix A lists full descriptions). The PARAFAC model was run with non-negativity constraints and was split-half validated, and model results were reverse-normalized before being exported. The abundances of PARAFAC components are reported in Raman Units (R.U.) that are normalized to the fluorescence intensity of water to remove variability due to instrument drift. While Raman units are quantitative, they cannot be converted to molar units as the relationships between concentration and fluorescence intensity for each PARAFAC component is unknown. Knowledge of these relationships would require an instrument-specific calibration for each component. As components may not be physically or chemically separated from one another, molar conversion is not possible and therefore component abundance is discussed in terms of their relative concentrations. I report PARAFAC component

abundances in both Raman Units and proportional to total fluorescence (Eq. 2-1; %C1, %C2, etc.), calculated as component abundance (R.U.) divided by total CDOM (Eq. 2-2)

$$\%C_n = \frac{C_n \text{ (R. U.)}}{\text{Total CDOM}} \quad (2-1)$$

$$\text{Total CDOM} = \sum C_1 - C_i \quad (2-2)$$

for a PARAFAC model of i components, where C_n represents one of the identified components.

To separate changes in organic carbon concentration due to end member mixing from changes due to reactions involving organic carbon, I construct salinity-based conservative mixing models for DOC and total CDOM. I define the fresh end member of conservative mixing models as the freshest groundwater sample for each STE location at each sampling time, and the saline end member as the surface saltwater sample for each location at each sampling time. In most cases, the surface saltwater sample has the highest salinity in the dataset, however some pore water samples at EGN have higher salinity than surface water during each sampling time. While sediment salinity fluctuates with surface water salinity, a time lag is induced as salt diffuses into the STE from the lagoon that can induce short-term salinity inversions in sediment (Martin et al., 2006).

I quantify changes in concentration due to reactions by comparing measured concentrations to those predicted by two end-member mixing, and assume deviations from conservative mixing represent biogeochemical alteration.

$$\text{Percent (\%) deviation} = \frac{[\text{Measured}] - [\text{Mixing model}]}{[\text{Mixing model}]} \quad (2-3)$$

When the measured concentration ([Measured]) is greater than the concentration predicted by conservative mixing model ([Mixing model]), reactions resulted in a net gain of the solute, while lower measured concentrations than mixing model concentrations indicate that reactions resulted in a net loss of the solute. I report deviations from conservative mixing in concentration units (mg/L for DOC and R.U. for CDOM), as well as the percent deviation from the conservative mixing line (Eq. 2-3).

Results

PARAFAC Results

PARAFAC modeling results in a 5-component model that explains >99% of the variability (Fig. 2-1). Model components are compared to those previously identified in the literature via OpenFluor (<http://www.openfluor.org/>), where components are considered matches when a comparison of the excitation-emission spectra between components yields an $R^2 > 0.95$ (Table 2-1). Components C1, C2, and C4 are characterized as terrestrial humic-like, while C3 is microbial humic-like and C5 is protein-like. All components are significantly positively correlated, but the strengths of correlations vary. The strongest relationships are between component C1 and C3 ($R^2=0.88$) as well as between C1 and C5 ($R^2 = 0.84$), and between C2 and C4 ($R^2 = 0.95$; Table 2-2).

Organic Carbon Concentrations and Conservative Mixing Model Results

Concentrations of organic carbon (both DOC and CDOM) are lower in the Yucatan than the Indian River Lagoon sites. Yucatan samples exhibit significant negative correlations between DOC and CDOM with salinity (DOC: $r^2 = 0.92$; $p < 0.0001$; CDOM: $r^2 = 0.96$; $p < 0.0001$), but ORP values display no significant correlation to salinity Fig. 2-2a). The greatest DOC concentration in Yucatan water measures 3.5

mg/L and occurs in the freshest sample (salinity=9.7), decreasing to between 0.5-1 mg/L at seawater salinity. CDOM follows a similar trend with the greatest value in the freshest sample, ~4 R.U. that decreases to ~0.5 R.U. in the surface seawater sample.

In Indian River Lagoon at BRL, no significant relationship exists between salinity and DOC or total CDOM, but the maximum DOC concentration of 60 mg/L and highest CDOM abundance of 64 R.U. occur in samples with salinity < 5 (Fig. 2-2b), though one outlier exists with a DOC concentration of 85 mg/L at a salinity of 10 (Fig. 2-2b). Surface lagoon water contains from 10-24 mg/L DOC and 2.5-4.0 R.U. CDOM. At EGN, both total DOC and CDOM exhibit a significant positive correlation with salinity (DOC: $r^2 = 0.47$; $p < 0.0001$; CDOM: $r^2 = 0.49$; $p < 0.0001$) (Fig. 2-2c). Freshwater (salinity <5) at EGN has lower DOC and CDOM content than surface saltwater, and ranges from 1.3-4.4 mg/L and 0.5-1.8 R.U., respectively. Surface saltwater ranges from 7.0-12.7 mg/L DOC and 2.8-4.1 R.U. CDOM. At RWP, DOC concentrations exhibit a significant ($r^2 = 0.52$; $p < 0.0001$) positive correlation with salinity while CDOM exhibits a significant negative correlation ($r^2 = 0.38$; $p < 0.0001$; Fig. 2-2d). Freshwater (salinity<5) has DOC concentrations from 7.3-10.0 mg/L DOC and 3.2-8.2 R.U. CDOM. Saltwater ranges from 10.8-12.9 mg/L DOC and 2.3-2.8 R.U. CDOM. At all Indian River Lagoon sites, all pore water ORP values decrease with salinity and all are lower than surface water samples, which have values near zero. These correlations are significant at EGN ($r^2 = 0.50$, $p < 0.0001$) and RWP ($r^2 = 0.75$, $p < 0.0001$) but not at BRL. Pore water and surface water samples display similar salinity-organic carbon relationships over time.

Differences between measured and modeled DOC and CDOM concentrations as estimated with conservative mixing models are smaller in the Yucatan than the Indian

River Lagoon samples (Fig. 2-3). The Yucatan samples show a net loss of up to 0.75 mg/L DOC (40%) across the freshwater-saltwater mixing zone compared to the concentration expected from conservative mixing (Fig. 2-3a). This loss coincides with a gain of 0.9 R.U. (45%) of CDOM. The highest deviations from conservative mixing occur at intermediate salinity of approximately 20.

For Indian River Lagoon sites, measured CDOM and DOC concentrations are both greater and less than those predicted by conservative mixing. At BRL, a maximum enrichment of 65 mg/L DOC (350%) occurs, as well as 55 R.U. (550%) CDOM at salinities less than 10 (Fig. 2-3b). At EGN, measured DOC concentrations are both higher and lower than those predicted by conservative mixing: measured DOC concentrations range between 8 mg/L (60%) lower and up to 5 mg/L 90% greater than expected conservative mixing values (Fig. 2-3c). These deviations occur both in fresh as well as in more saline portions of the salinity gradient. At RWP, measured DOC concentrations are generally higher than conservative mixing line in the fresher portion of the salinity gradient, and reach concentrations up 1.5 mg/L (20%) higher than expected from conservative mixing. Measured DOC concentrations are lower than expected from conservative mixing in the saltier portion of the salinity gradient, and are up to 1 mg/L (10%) lower than conservative mixing concentrations (Fig. 2-3d). Measured CDOM concentrations are generally higher than conservative mixing values, and reach up to 4 R.U. (70%) greater than expected from conservative mixing at salinities less than 10.

PARAFAC Component Abundance with Salinity

PARAFAC components display similar quantitative relationships to salinity as those observed for total CDOM; however, the relative abundance of PARAFAC

components differ with salinity (Fig. 2-4). At all locations, the C2 component exhibits significant negative correlations with salinity (Yucatan $r^2=0.57$, $p<0.0001$; BRL $r^2=0.08$, $p<0.05$; EGN $r^2=0.32$, $p<0.0001$; RWP $r^2=0.77$, $p<0.0001$), although the correlations are weak at BRL and EGN. In contrast, the C5 component exhibits significant positive correlations with salinity (Yucatan $R^2=0.49$, $p<0.001$; BRL $r^2=0.54$, $p<0.0001$; EGN $r^2=0.32$, $p<0.0001$; RWP $r^2=0.44$, $p<0.0001$). Except for the Yucatan site, the C3 component exhibits a weak but significant positive correlation with salinity (Yucatan $R^2=0.03$; BRL $R^2=0.19$, $p<0.001$; EGN $R^2=0.32$, $p<0.0001$; RWP $R^2=0.16$, $p<0.01$). The other components have little consistent variations with salinity between sites. The C1 component decreases in relative abundance with salinity, though this relationship is only significant at Yucatan and EGN sites and is poor at all sites. The C4 component shows little correlation with salinity at all sites except for EGN which exhibits a significant ($R^2 = 0.33$; $p<0.0001$) positive correlation with salinity.

Discussion

Concentrations of DOC and CDOM vary by an order of magnitude between sites, with lowest concentrations in the Yucatan and EGN, followed by RWP and BRL (Fig.2-2). Because organic carbon remineralization drives many biogeochemical reactions, these concentration differences may affect the magnitude of biogeochemical reactions in the STEs. The extent of reactions between STEs should also be impacted in a variety of ways due to their distinct flow regimes (Yucatan = conduit flow; Indian River Lagoon = widely distributed seepage). First, mixing occurs rapidly in the conduits in the Yucatan, which could limit biogeochemical processing if mixing rates are faster than reaction rates. Second, karstic conduits have a lower rock:water ratio than the primary (i.e., intergranular) porosity in karst terrains or porous media. Aquifer solid materials are

important sites of sedimentary organic carbon storage as well as mineral phases used by microbial communities to remineralize organic carbon (e.g. iron oxide minerals), and provide a substrate for microbial communities to grow and catalyze biogeochemical reactions.

To depict differences in organic carbon processing between STEs, I first discuss the distribution of DOC, CDOM, and deviations from values expected from conservative mixing based on variation in salinity. I then assess general trends in the quality of organic carbon between sites as indicated from the PARAFAC modeling. These results inform a conceptual model that outlines zones of enhanced biogeochemical activity in STEs as inferred by changes to organic carbon concentrations, and by analogy, products of biogeochemical reactions in STEs (Fig. 2-5).

Organic Carbon Dynamics and Sources

In the Yucatan, the near linear relationship between salinity and DOC ($r^2=0.90$) and total CDOM ($r^2>0.95$; Fig. 2-2a) suggests that salt and fresh water mixing rate is high relative to reaction rates, and that dilution of OC-rich groundwater with OC-poor seawater is the primary control of the DOC and total CDOM concentrations. This result contrasts with the distribution of DOC and CDOM at Indian River Lagoon sites, where weak correlations between salinity and DOC and CDOM (Fig. 2-2b-d) reflect non-conservative relationships. A greater degree of non-conservative behavior at Indian River Lagoon sites is further indicated by greater residuals conservative mixing models than at the Yucatan site. Residuals are greater at Indian River Lagoon in absolute concentration as well as relative change (% deviation, Eq. 2-3). For instance, the maximum deviation of DOC concentrations from the conservative mixing line for the Yucatan is a 0.7 mg/L loss (40%), compared to gains of 65 mg/L (>350%) at BRL, 5

mg/L (100%) at EGN, and 2 mg/L (20%) at RWP (Fig. 2-3a-d). Similar trends are observed for CDOM. The maximum deviation of CDOM abundance from the conservative mixing line for the Yucatan is a gain of approximately 1 R.U. (40%), compared to 55 R.U. (600%) at BRL, 4 R.U. (300%) at EGN, and 4 R.U. (90%) at RWP. These changes reflect more organic carbon processing in Indian River Lagoon than Yucatan STEs, and is likely a result of the differences in flow rates and water-rock ratios. Because organic carbon drives redox reactions, which consume terminal electron acceptors (e.g. oxygen and nitrate, Table 1-2) and produce remineralized carbon (CO₂, CH₄) and nutrients (nitrogen and phosphorus, N and P), the greater degree of organic carbon processing at Indian River Lagoon compared to Yucatan sites implies greater consumption of terminal electron acceptors as well as production of reaction products. The extent of these reactions may therefore be critical in determining the chemical composition of SGD.

Organic Carbon Quality Across Salinity Gradients

Despite differences in DOC concentrations among sites, similarities in the relative abundance of PARAFAC components as a function of salinity reveal systematic variations in organic carbon quality (Fig. 2-4). In particular, the relative abundance of C2, characterized as terrestrial humic-like, decreases with salinity, while the relative abundances of C3 (microbial humic-like) and C5 (protein-like) increase with salinity at all sites (Fig. 2-4). Decreasing terrestrial humic-like organic matter with salinity would be expected from dilution of terrestrial groundwater through mixing with marine water. Additionally, marine water appears to serve as a source of reactive proteins, as demonstrated by the relative increase of C5 with salinity. Proteins may be produced through primary productivity in seawater or alternatively, through in situ microbial cell

turnover or degradation of particulate or solid-phase organic carbon within the STE (Blough and Del Vecchio, 2002). Because C3 is microbial humic in nature, it may more likely be derived from in situ production, while C5 may be derived from either surface water primary production or in situ STE reactions.

Although the exact origins and reactivity of C3 and C5 cannot be determined from these data, their relative abundances have implications distribution of biogeochemical reactions within the STE. The increase in labile protein-like C5 with salinity suggests that biogeochemical reactions may be intensified on the saline side of STEs, particularly if organic carbon availability limits reactions. However, even if organic carbon is not limiting, inputs of labile organic carbon should increase remineralization kinetics (Berner, 1980; Arndt et al., 2013), leading to more remineralization in saline portions of the STE. Because organic carbon remineralization is a component of many other biogeochemical reactions including nutrient and greenhouse gas production, the shift in organic carbon quality with salinity may impact fluxes of these solutes from SGD.

Distribution of Residuals and Implications for Controls of Biogeochemical Reactions

Despite differences in flow regime between Yucatan and Indian River Lagoon sites, reactions within STEs impact CDOM similarly and lead to its production within the freshwater-saltwater mixing zone, while DOC is consumed at the Yucatan site as well as at EGN (Fig. 2-3a and c). Production of CDOM may result from in situ degradation of particulate organic matter or microbial activity (Blough and Del Vecchio, 2002). DOC may also be produced by similar mechanisms, although its consumption at Yucatan and EGN sites may reflect preferential remineralization of non-chromophoric DOC. The mechanism for different signs of DOC and CDOM residuals at the Yucatan and EGN

sites are unknown but could relate to differences in the reactivity of CDOM versus non-chromophoric DOC: CDOM may contain relatively more recalcitrant biomolecules than bulk DOC and is therefore may be less readily degraded than non-chromophoric portions (Blough and Del Vecchio, 2002).

Given the consistent non-conservative behavior of CDOM between sites, I use distribution of the non-conservative CDOM as an indicator for enhanced biogeochemical activity to compare the magnitude and locations of reactions between STE sites. In all cases, the non-conservative CDOM displays systematic variations with salinity that reflect the zones of enhanced biogeochemical activity. Enhanced biogeochemical activity suggests that a limiting reactant has been delivered to the zone and increases the intensity of reactions involving organic carbon. Therefore, the discussion below examines the distribution of CDOM residuals along salinity gradients at STE sites to evaluate controls of enhanced biogeochemical reactions. In this framework, the source of limiting reactants determines the location of organic carbon processing within the salinity gradient, while the mixing rate relative to reaction rate determines the deviation from conservative mixing lines as a measure of the magnitude of the reactions (Fig. 2-5).

Three of the four STE sites (Yucatan, BRL, and RWP) contain greater CDOM concentrations in freshwater compared to saltwater, and freshwater redox potential is low (Fig. 2-2). Low ORP and high CDOM concentrations indicate that organic carbon remineralization is limited by the availability of terminal electron acceptors. Thus, enhanced remineralization following freshwater-saltwater mixing may occur through the delivery of electron acceptors in the seawater, such as sulfate, to the freshwater-

saltwater mixing zone (Fig. 1-5). Water containing organic carbon but lacking sulfate may be sufficiently reducing to support methanogenesis (Weston et al., 2011) but methanogenesis is inhibited by sulfate concentrations > 1 mM (Whiticar and Schoell, 1986). Once sulfate mixes with reducing and low-sulfate freshwater, methanogenesis should cease and sulfate reduction begin because of the greater energy yield of sulfate reduction relative to methanogenesis (Table 1-1).

This shift in redox pathway appears to have occurred at RWP and BRL, where maximum CDOM residuals are located at the fresher portion of the salinity gradient and where delivery of sulfate would have the greatest impact on organic carbon remineralization (Fig. 2-5c). However, at the Yucatan STE, the freshest sample measured has a salinity of 10, which if simply diluted by sulfate-free freshwater should have over 8 mM of SO_4^{2-} and should inhibit methanogenesis. Moreover, sulfate concentrations at this salinity are far greater than organic carbon concentrations (up to 3 mg/L or 0.25 mM), and sulfate should therefore not limit remineralization. Alternatively, the turbulent flow dynamics in karst conduits may allow for surface water to deliver oxygen up to several 10s of meters into conduits (Parra et al., 2015). In this case, rapid depletion of oxygen could enhance biogeochemical activity to a greater extent than sulfate reduction because of the greater energy yield (Table 1-1). Reduction of dissolved oxygen by organic carbon remineralization has been found at the Yucatan site previously (Young et al., 2017), and likely results at least in part to the enhanced remineralization observed at intermediate salinities here (Fig. 2-5b)

EGN is distinct from other sites because freshwater has positive ORP values and contains lower organic carbon concentrations than saltwater. The low total CDOM and

DOC concentrations correspond with elevated ORP values, which indicate that TEA availability is high (Fig. 2-2c). This correspondence suggests that biogeochemical reactions at this site are carbon-limited, rather than TEA limited, which allows aerobic conditions to be maintained in the fresh portion of the STE. Non-conservative behavior of CDOM at EGN results from biogeochemical reactions in the more saline portion of the STE where relatively labile marine organic carbon is delivered to the STE. Because of its relatively higher content of protein-like organic matter, as represented by PARAFAC component C5, the inputs of marine organic matter in saline portions of the STE may serve to further increase organic carbon remineralization in carbon-limited STEs. Increased remineralization would result from both an increase in the quantity and the relative reactivity of organic carbon available to drive reactions (Fig. 2-5a).

Conclusions

This study reveals hydrogeological controls on the distribution of organic carbon and the extent of its processing in subterranean estuaries. Organic carbon distribution in the Yucatan STE, characterized by conduit-dominated flow, appears to be mostly controlled by end-member mixing, though salinity-based conservative mixing models reveal some in situ production of CDOM coinciding with DOC consumption. This observation suggests that biogeochemical processing of carbon is sufficiently rapid to alter its concentrations with salinity, despite short timescales of mixing. In Indian River Lagoon STEs, which are characterized by widely distributed seepage through siliciclastic sediments, organic carbon quantities are controlled by mixing as well as reactions. These reactions can enhance DOC and CDOM concentrations several times greater than conservative mixing concentrations. Despite these differences, all four sampled STEs exhibit similar variations in organic carbon quality across salinity

gradients, where the relative abundances of terrestrial humic-like compounds (%C2) decreases and protein-like compounds (%C5) increases with salinity. Because proteins tend to be more reactive than humic acids, these findings may illustrate a change in the overall reactivity of organic carbon within STEs, in which reactivity increases with increasing contributions of marine organic matter. This trend occurs regardless of the organic carbon concentrations in fresh vs. marine end members or the differences in hydrology inherent in karst carbonate versus siliciclastic systems. This finding highlights the importance of organic carbon reactivity, which depends on its origins, to biogeochemical reactions in STEs. Because organic carbon remineralization drives many reactions that alter the concentration and speciation of solutes such as nutrients (Slomp and Van Cappellen, 2004; Gonnera and Charette, 2014), metals (Roy, et al., 2010; Johannesson et al., 2011), and carbon, the intensity and distribution of reactions with salinity may exert an important control on solute fluxes via SGD.

Table 2-1. PARAFAC component matches as identified via OpenFluor.

Component	Component Description
C1	Terrestrial humic-like, suggested as photo-refractory (C2; Yamashita et al., 2010)
C2	Terrestrial humic-like, high molecular weight (C1; Kothawala et al., 2012)
C3	Microbial humic-like fluorescence (C2; Murphy et al., 2011)
C4	Terrestrial humic (C3, Walker et al., 2009)
C5	Protein-like (C4; Cawley et al., 2012)

Table 2-2. R² and p-value for correlations between PARAFAC components in PARAFAC model, n=322. All components are positively correlated. *p<0.0001

	C1	C2	C3	C4
C1	--	0.46*	0.88*	0.36*
C2	0.46*	--	0.74*	0.95*
C3	0.88*	0.74*	--	0.62*
C4	0.36*	0.95*	0.62*	--
C5	0.84*	0.19*	0.66*	0.13*

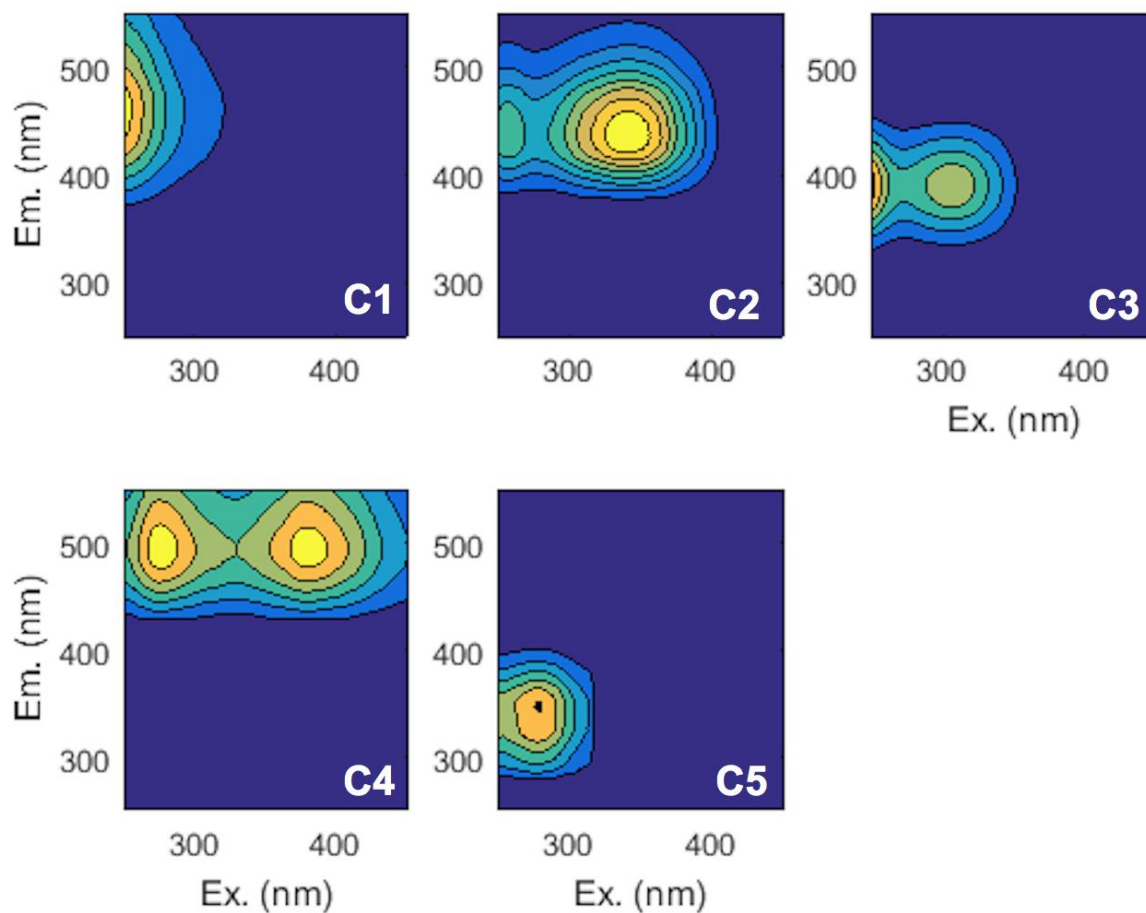


Figure 2-1. Five-component PARAFAC model for subterranean estuary samples. Components C1, C2 and C4 are characterized as terrestrial humic-like, C3 is microbial humic-like, and C5 is protein-like (Table 2-1).

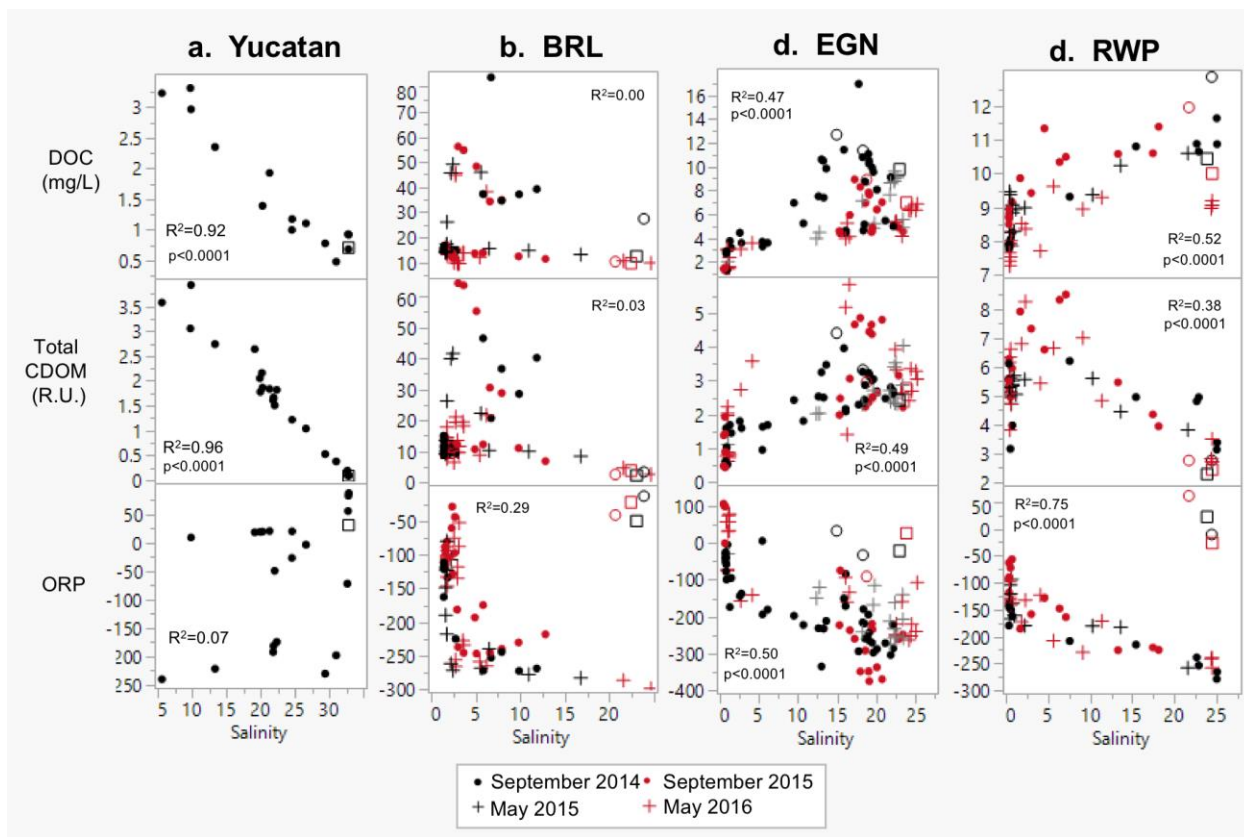


Figure 2-2. Cross plots of salinity versus DOC, total CDOM, and ORP for (a) Yucatan, (b) BRL, (d) EGN, and (d) RWP sites. Closed data points represent groundwater samples and open data points represent surface water for the Yucatan samples, and for samples collected in Indian River Lagoon in September 2014 (black circle), May 2015 (black square), September 2015 (red circle) and May 2016 (red square)

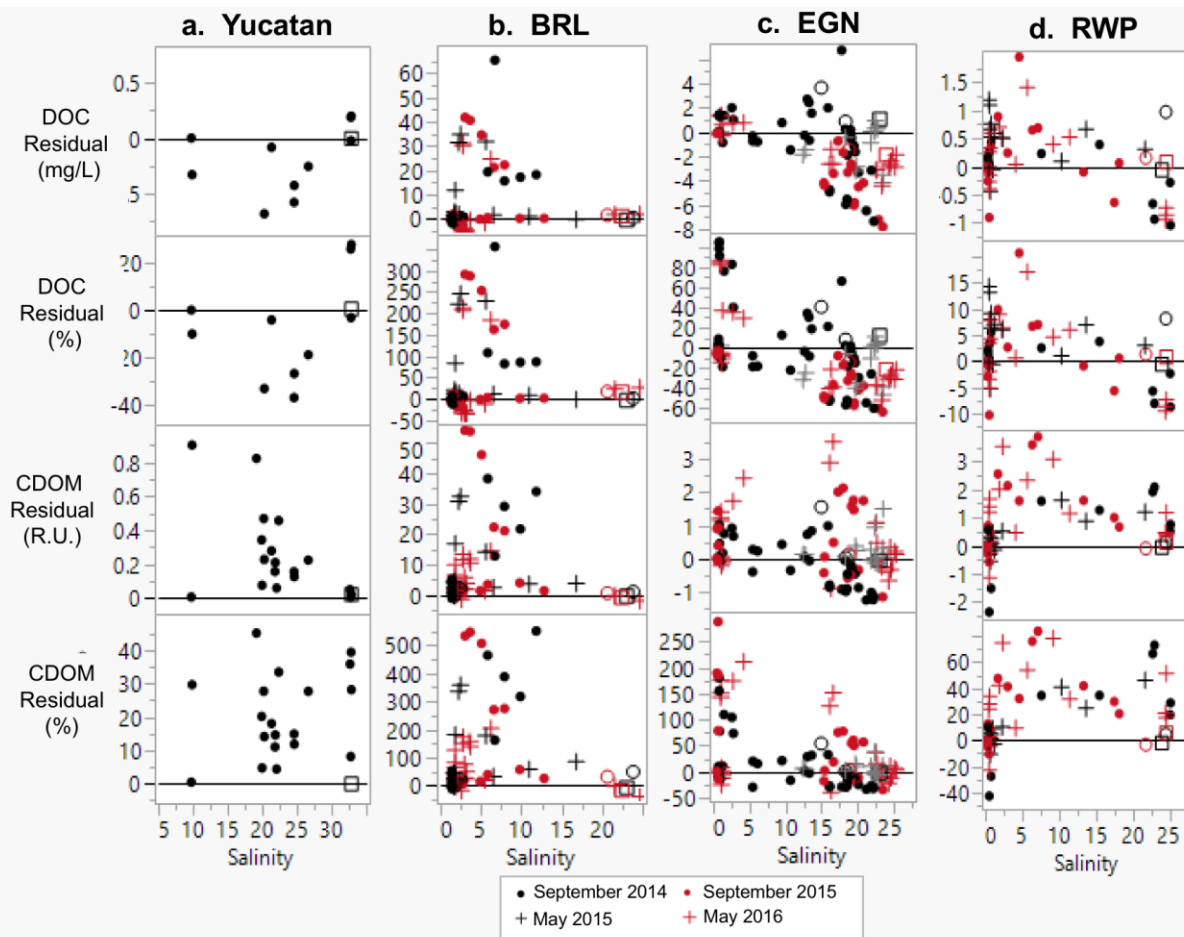


Figure 2-3. Residuals of salinity-based conservative mixing models for DOC and total CDOM for (a) Yucatan, (b) BRL, (c) EGN, and (d) RWP sites. Deviations from residuals are reported in concentrations as well as percent deviation from the conservative mixing line. Closed data points represent groundwater samples and open data points represent surface water for the Yucatan samples, and for samples collected in Indian River Lagoon in September 2014 (black circle), May 2015 (black square), September 2015 (red circle) and May 2016 (red square).

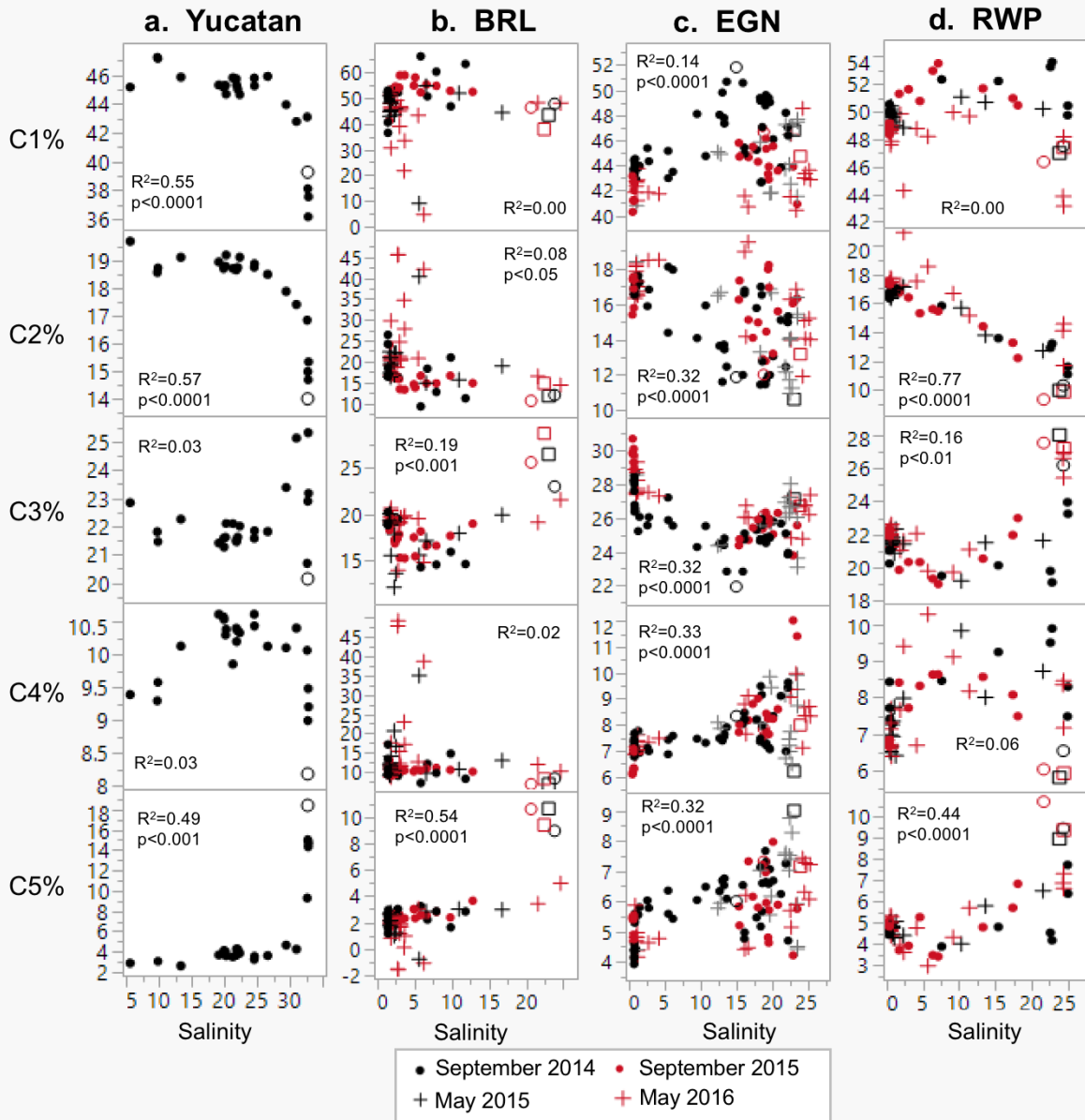


Figure 2-4. Relative PARAFAC component abundance versus salinity for (a) Yucatan, (b) BRL, (c) EGN, and (d) RWP sites. Closed data points represent groundwater samples and open data points represent surface water for the Yucatan samples, and for samples collected in Indian River Lagoon in September 2014 (black circle), May 2015 (black square), September 2015 (red circle) and May 2016 (red square).

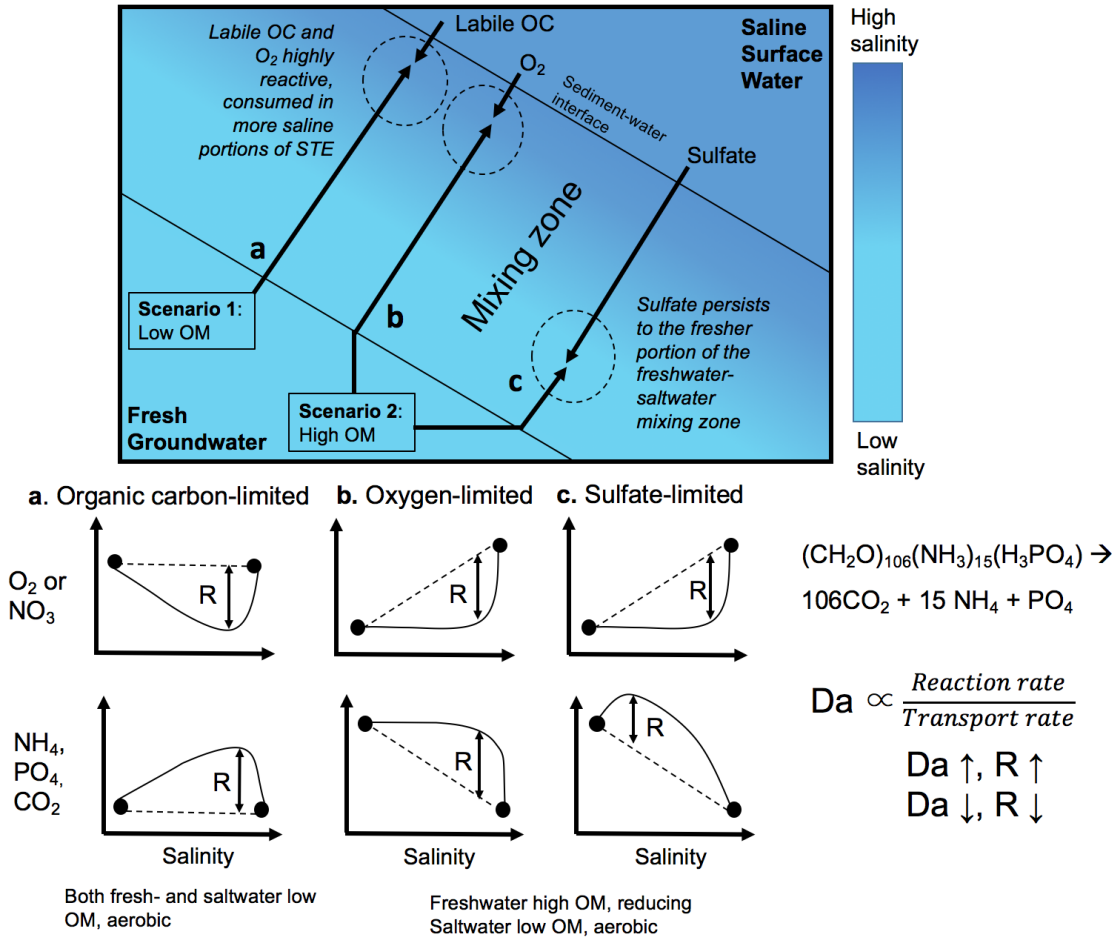


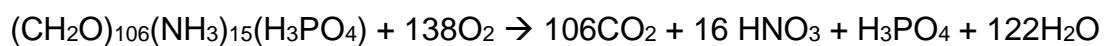
Figure 2-5. Conceptual model of CDOM concentrations versus salinity for (a) Carbon-limited STEs (representative of EGN) (b) Oxygen-limited STEs (representative of Yucatan) and (c) Sulfate-limited STEs (representative of BRL and RWP). Graphs present hypothetical concentrations (solid black lines) compared to conservative mixing lines (dashed black lines) of solutes due to remineralization of a generic organic molecule, $(\text{CH}_2\text{O})_{106}(\text{NH}_3)_{15}(\text{H}_3\text{PO}_4)$. Black dots represent concentrations in freshwater and saltwater end members. The change in concentrations due to reactions are represented by R. The location of production on the salinity gradient is a function of the limiting reactant, while the absolute deviation from the conservative mixing line is determined by reaction rate relative to mixing. Expected changes in solute concentrations are indicated in panels for (a) organic-carbon limited STEs, where both fresh and saltwater end members contain equivalent concentrations of O₂/NO₃ but low concentrations of nutrients. Remineralization in the saline portion due to labile organic carbon delivery increases NH₄/PO₄/CO₂ concentrations. (b) oxygen-limited STEs, where freshwater is reducing (low O₂/NO₃) and contains products of remineralization (NH₄, PO₄, CO₂). Delivery of O₂ by saltwater depletes O₂ and generates NH₄, PO₄ and CO₂, and (c) sulfate-limited STEs, which is similar to (b) but processing occurs near the freshwater portion of the STE where sulfate concentrations begin to increase.

CHAPTER 3
ORGANIC-INORGANIC CARBON FEEDBACKS IN A CARBONATE KARST AQUIFER
AND IMPLICATIONS FOR NUTRIENT AVAILABILITY

Introduction

Carbonate aquifers are characterized by high permeability due to secondary porosity that results from the dissolution of calcium carbonate minerals, leading to the formation of karst features that allow rapid water infiltration to the groundwater table (Fleury et al., 2007). Consequently, freshwater is predominantly stored as groundwater and surface runoff may be scarce or negligible. For coastal karst aquifers, these characteristics make submarine groundwater discharge (SGD) the predominant or sole source of terrestrial fresh water and solutes to the coastal zone (Fleury et al. 2007) and thus a critical component of coastal biogeochemical budgets. The terrestrial water is unlikely to discharge from subterranean estuaries (STE) without chemical modification along the flow paths. These modifications are likely to have important impacts to budgets of biogeochemically important solutes in coastal zones (Moore, 1999; Slomp and Van Cappellen, 2004).

Biogeochemical reactions in STEs are largely driven by organic carbon remineralization (Ch. 2). This reaction leads to the production of carbonic acid via hydration of the produced CO₂ (Froelich et al., 1979). I depict aerobic remineralization as a generic remineralization pathway below. Aerobic respiration is the most energetically favorable reaction and therefore proceeds when oxygen is available in sufficient concentrations:

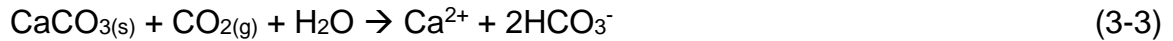


(3-1)

CO₂ generated by remineralization induces further feedbacks as it hydrates to carbonic acid that dissociates to decrease the pH of the water according to:



The decreased pH leads to undersaturation with respect to carbonate minerals which dissolve according to:



While organic carbon remineralization and associated CaCO₃ dissolution are known to occur in carbonate aquifers (Gulley et al., 2011; Brown et al., 2014; Gulley et al., 2015), the relative magnitude of these processes are unknown in STEs where mixing of terrestrial and marine organic carbon enhances biogeochemical reactions (Ch. 2). Because reactions within STEs modify the composition of SGD, the relative magnitudes of CO₂ sources (remineralization, Eq. 3-1) and sinks (CaCO₃ dissolution, Eq. 3-3) may regulate surface water CO₂ fluxes to the atmosphere.

Apart from producing CO₂, organic carbon remineralization also leads to the generation of nutrients (Eq. 3-1), producing CO₂ and inorganic nitrogen (N) and phosphorus (P) at a ratio of 106:16:1, otherwise known as the Redfield Ratio (Redfield, 1934). This ratio aligns with the typical nutrient requirements of photosynthetic algae in the ocean, and processes that alter the ratios of dissolved nutrients drive ecosystems toward nutrient limitation (Redfield, 1934). P is commonly limiting in carbonate settings due to a high affinity for sorption of PO₄³⁻ to carbonate mineral surfaces, which reduces dissolved P concentrations (DeJonge and Villerius, 1989). Conversely, carbonate dissolution driven by elevated CO₂ concentrations may increase P availability in coastal zones (Price and Herman, 1991; Price et al., 2010). Therefore, both carbonate

dissolution and precipitation could alter fluxes of P from sediment to surface water (Short et al. 1990).

If P is a limiting nutrient, as is commonly the case in carbonate systems, liberation of P from organic carbon remineralization coupled with carbonate mineral dissolution may drive a negative feedback loop for surface water CO₂ concentrations: excess P delivered by SGD can drive primary productivity, which sequesters CO₂ as organic matter. While links between organic carbon remineralization, carbonate mineral saturation, and P availability are known to exist, the magnitude of these feedbacks within STEs and their impact on fluxes from SGD are unknown.

Here, I assess the relationships between the organic carbon processing and feedbacks with CO₂ and P concentrations in a carbonate karst aquifer in Quintana Roo, Mexico, where groundwater discharges to coastal lagoons through submarine springs. Previous work at this location indicates that both organic matter reactivity and terminal electron acceptor availability change along salinity gradients: the proportion of protein-like organic carbon increases with salinity (Ch. 2) as well as oxygen concentrations derived from surface water, which is rapidly consumed in spring vents during period of saltwater intrusion (Young et al., 2017). Constraining coupled nutrient and carbon transformations prior to discharge to the coastal ocean could improve understanding of carbon cycling and biogeochemical processes in carbonate karst STEs.

Study Location

The field site is located in a coastal lagoon offshore of Puerto Morelos approximately 40 km south of Cancun in the state of Quintana Roo, Mexico, on the Yucatan Peninsula (Fig. 1-4a). The Yucatan Peninsula is a karstic carbonate platform of Triassic to Holocene age, and is characterized by dissolutional secondary porosity. This

secondary porosity generates high aquifer permeability and hydraulic conductivity, which limits surface water and causes groundwater to discharge at the coast as SGD from submarine springs, while surface runoff is negligible (González-Herrera et al., 2002; Beddows et al., 2007). Groundwater is recharged as rainwater infiltrates thin soil layers overlying the carbonate matrix, and most recharge occurs during the rainy season from June to October. Recharged water carries elevated P_{CO_2} (the partial pressure of dissolved CO_2) from soil OC remineralization that aids dissolution (Gulley et al., 2016). Although surface water is scarce, the region is dotted with dissolution features known as cenotes which expose the water table and may extend to saltwater below the freshwater lens (Schmitter-Soto et al., 2002). Mangrove wetlands, which fix large amounts of carbon, occupy ~2 km wide benches between Marine Isotope Stage (MIS) 5e high stand deposits (Fig. 1-4b and 1-4c; Blanchon et al. 2009) and coastal dunes. Secondary porosity form long water-filled cave systems that connect inland cenotes to offshore springs.

Spring discharge to the coastal fringing reef lagoon is controlled in part by lagoon hydrodynamics. Some of the submarine springs reverse flow with elevated lagoon level at high tide and during wave and wind set-up events (Parra et al., 2014; Parra et al., 2015). Saline and freshwater components of SGD have been separated using multiple methods including isotopic tracers (^{222}Ra), salinity, and silica mixing models (Hanshaw and Back 1980; Hernández-Terrones et al. 2010; Null et al. 2014). Discharge varies seasonally due to increased recharge in the rainy season, but peak discharge lags peak precipitation by several months (Perry et al. 2003; Null et al. 2014). Null et al. (2014) estimated fresh SGD at Puerto Morelos at $29.3 \text{ m}^3 \text{ day}^{-1}$ per meter of shoreline, 78.5%

of which was derived from spring discharge, with the remainder derived from diffuse seepage from the beach face. Beach face discharge originates from an unconfined surficial aquifer while spring discharge originates from a deep confined aquifer (Null et al., 2014). The lagoon is microtidal but tidal flushing regulates lagoon residence time, which averages 3 hours but can be as low as 0.35 hours following lagoon level setup following storm swells (Coronado et al., 2007).

Nutrient concentrations can be elevated in Yucatan groundwater from wastewater contamination (Metcalf et al., 2011). Contamination can occur through diffuse run-off as well as through point-sources such as widely distributed individual septic tanks and disposal wells that inject untreated wastewater into the saline groundwater below the freshwater lens. Injected wastewater pollutants migrate upward into the freshwater lens, elevating the concentrations of contaminants, nutrients, and pathogens (Metcalf et al., 2011). Domestic wastewater contamination also leads to heterogeneous nutrient concentrations in coastal freshwater wells (Hernandez-Terrones et al., 2011). Wastewater contamination of springs is reflected in elevated *E. coli* concentrations of spring discharge, suggesting some OC and nutrients in the STE may have an anthropogenic source. Nutrient concentrations in spring discharge are high compared to average lagoon water concentrations (Null et al., 2014). N:P ratios are greater than the Redfield ratio of 16 though P loads are several times higher than those from similar SGD systems such as Florida Bay (Hernández-Terrones et al., 2011; Null et al., 2014). Because P is a limiting nutrient, its delivery from SGD increases primary productivity around submarine springs, and groundwater P inputs are critical for ecosystem dynamics (Carruthers et al. 2005).

Methods

Field Methods

Water was sampled over a two-week period in September 2014 along a transect from cenotes ~21 km inland to the lagoon. Although these samples are not along a known flow line, each represents characteristics of water along a flow path from the recharge to discharge areas (conceptual model given in Fig. 3-1). Most samples were collected offshore including four submarine springs (Hol Kokol, Gorgos, Laja, and Pargos) that are distributed along ~5 km of shoreline in Puerto Morelos (Fig. 1-4c). During the sampling periods, tides, wave setup, and storms elevated sea level and caused surface lagoon water to backflow into springs. This backflow caused variable salinity of vent discharge that serves as a conservative tracer to assess mixing, from which biogeochemical processing in the STE may be evaluated. All spring samples were collected as the springs discharged. A lagoon surface water end member was collected in the lagoon outside the direct influence of discharging vents (approx. 1 km from shore; Fig. 1-4c).

Inland water was collected from three cenotes (Cenote Siete Bocas, Cenote Zapote, and Cenote Kin-Ha) approximately 21 km from the shoreline (Fig. 1-4b). These samples represent the primary recharge area of the Yucatan aquifer. Surface water was collected from a mangrove wetland that parallels the coastline along a 2-km wide bench between MIS stage 5e highstand deposits. This water represents a potential freshwater source and was sampled in April 2014 prior to the main sampling trip in September. Finally, a near-shore well (UNAM), located approximately 100 m inland, was sampled to represent groundwater from the dune field that parallels the coast. Although these sites are unlikely to represent a single continuous flow path, we use these samples to estimate

potential sources and transformation of solutes that flow to the STE sampled in the offshore wells (Fig. 3-1).

Sampling was accomplished by pumping water to the surface through a 0.5 cm diameter flexible PVC tube from spring openings, cenotes and the well. A YSI Pro-Plus sensor was installed in an overflow cup in-line with the tubing to measure salinity, temperature, pH, dissolved oxygen, and oxidation-reduction potential (ORP). Once these parameters were stable, samples were collected after being filtered through 0.45 μm trace-metal grade Geotech medium capacity disposable canister filters and preserved in the field. Samples for cations and anions were collected in HDPE bottles; cation samples were preserved with trace metal grade nitric acid ($\text{pH}<2$) while no preservative was added to anion samples. Samples for dissolved organic carbon (DOC) and fluorescent DOC analysis were collected in amber borosilicate vials that were combusted at 550°C prior to use. DOC samples were acidified with hydrochloric acid to $\text{pH}<2$. Fluorescent DOC samples were not acidified and were frozen until analysis within one month of collection. Nutrient samples were filtered directly into polypropylene vials with no preservative and frozen until analysis. DIC samples were filtered at $0.2 \mu\text{m}$ directly into glass vials and sealed tightly with no headspace. All other samples were kept chilled in the field (ice) and refrigerated in the laboratory until analysis.

Laboratory Methods

Anion and cation concentrations were measured on an automated Dionex ICS-2100 and ICS-1600 Ion Chromatograph, respectively. Error on replicates was less than 5%. Nutrient concentrations were analyzed on a Seal AA3 AutoAnalyzer. Error on replicates was less than 10%. DOC concentrations were analyzed on a Shimadzu TOC-VCSN total organic carbon analyzer, and the coefficient of variance was less than 2%.

DIC concentrations were measured on a UIC (Coulometrics) 5011 CO₂ coulometer coupled with an AutoMate Preparation Device. Samples were acidified and the evolved CO₂ was carried through a silver nitrate scrubber to the coulometer where total C was measured. Accuracy was calculated to be ± 0.1 mg/L. We depicted organic carbon character through the generation of excitation emission matrices (EEMs) via fluorescence spectroscopy, and modeled the results with PARAFAC analysis according to methods outlines in Chapter 2. Note that the relationship between concentration and fluorescence intensity is unknown but likely to be variable between components, therefore the proportion of fluorescence is not analogous to the relative concentration of components, but only reflects relative changes in component abundance compared to the total amount of fluorescent matter.

Modeling

STE conservative mixing models

Carbon chemistry is depicted through geochemically modeled parameters P_{CO_2} (partial pressure of dissolved CO₂) and SI_{cal} (calcite saturation index). SI_{cal} is calculated to determine whether a system is at equilibrium with respect to calcite (CaCO₃), and is defined as the log of the ratio of the ion activity product (IAP) to the solubility product (K_{sp}) with respect to calcite. At equilibrium, the IAP should be equal to K_{sp} , and thus the saturation index should be 0. Under-saturated systems will have negative SI_{cal} values, and super-saturated systems will have positive SI values. SI_{cal} values indicate whether mineral dissolution is expected to occur. SI_{cal} and P_{CO_2} were calculated with geochemical modeling software PHREEQc (USGS) with the PHREEQc.dat database (Parkhurst, 1995). Input parameters included major cation and anion concentrations, pH, temperature, and DIC concentrations of water samples (Appendix B).

To depict changes in STE chemistry due to reactions versus mixing, I constructed conservative mixing models between a saltwater end member (represented by surface lagoon water), and a freshwater end member, which I define as the freshest SGD sample measured (Hol Kokol; Table 3-1). The mixing models were applied to reaction products including DIC, P_{CO_2} , SI_{cal} , Ca^{2+} , NH_4^+ , and PO_4^{3-} . Mixing was assumed to be linear except for P_{CO_2} and SI_{cal} , which are non-linear (Langmuir, 1997). For these parameters, conservative mixing models were constructed by using salinity to calculate the fraction of fresh and saltwater end members in each sample (Eq. 3-4 and 3-5), where f designates the proportional contribution of end members and S designates salinity. I modeled mixtures corresponding to each sample salinity in PHREEQC to determine the expected value to mixing.

$$f_{freshSGD} + f_{seawater} = 1 \quad (3-4)$$

$$S_{Sample} = f_{freshSGD} * S_{freshSGD} + f_{lagoon} S_{lagoon} \quad (3-5)$$

For all conservative mixing models, the residual between measured data and the conservative mixing value is considered to represent changes in chemistry due to reactions within the STE. Residual concentrations, indicating changes due to reactions, are indicated by Δ symbols, which equals measured value minus the value expected solely from mixing (Eq. 3-6); positive values represent a gain and negative values represent a loss of the solute.

$$\Delta Solute = [Solute_{measured}] - [Solute_{mixingmodel}] \quad (3-6)$$

Surface water organic carbon mass balance

To evaluate the fate of terrestrially derived OC in surface lagoon water, I constructed a mass balance for the surface lagoon water composition based on its

measured salinity, assuming it was a mixture of average seawater and freshest SGD (Table 3-1). Seawater outside the lagoon was not sampled in this study, so average seawater was assumed to have a salinity of 35.

$$\text{Salinity}_{\text{lagoon}} = f_{\text{freshSGD}} * \text{Salinity}_{\text{freshSGD}} + f_{\text{seawater}} \text{Salinity}_{\text{seawater}} \quad (3-7)$$

Total fresh SGD was split into SGD from submarine springs versus beach face SGD based on the results of Null et al. (2014), where spring SGD was 78.5% of total fresh SGD and both SGD types were assumed to have the same salinity:

$$f_{\text{springSGD}} = 0.785 * f_{\text{freshSGD}} \quad (3-8)$$

Estimating the fraction of spring water is needed because it is assumed to be the only source of CDOM, because seawater organic carbon concentrations are typically low and beach face concentrations are likely to be insignificant compared to springs (Chapelle et al. 2016). Solving for f_{freshSGD} in Eq. 3-7 and inserting into Eq. 3-8 yields an expression estimating the proportion of lagoon surface water derived from spring SGD. Values of salinity and fluorescent OC content of lagoon water and fresh SGD end members were identical to those used in mixing models (Table 3-1).

Results

Salinity and Biogeochemical Parameters

Terrestrial water increases in salinity with proximity to shore: cenotes have the lowest average salinity (0.72) followed by mangroves (1.60) and UNAM well (5.63) (Table 3-2). Fresh groundwater (cenotes and UNAM well) have low dissolved oxygen concentrations and negative ORP values although the UNAM well is more reducing than cenotes. Mangrove surface water has a positive ORP value and higher pH than the cenotes and UNAM well samples. SGD samples span a salinity range from 9.77 to 26.6

and all are reducing. Lagoon surface water has the highest salinity sampled (32.7), which on average is 90% saturated with DO and has a positive ORP (Table 3-2).

Within the STE, both measured and conservative mixing concentrations for DIC, P_{CO_2} , and NH_4 concentrations are inversely correlated with salinity, while measured and conservative mixing for SI_{cal} and Ca concentration are positively correlated (Fig. 3-2a-e). Although the conservative mixing model shows an inverse relationship between salinity and PO_4 concentrations, the measured PO_4 concentrations are not significantly related to salinity. For STE samples, positive values of ΔDIC , ΔP_{CO_2} , ΔCa , ΔNH_4 and ΔPO_4 indicate they are enriched and reflect production within the STE, while SI_{cal} values are more undersaturated than would be expected based on simple mixing between the saline and fresh end members (Fig. 3-2c).

Freshwater end members (UNAM well, cenotes, and mangroves) are distinct from STE samples in the concentrations of solutes in Fig. 3-2. Cenotes have higher DIC concentrations, lower P_{CO_2} values, and higher SI_{cal} values than other freshwater end members, while they contain lower concentrations of NH_4 and PO_4 relative to STE samples. Similarly, mangrove samples are depleted in all solute concentrations relative to conservative mixing relationships, except for DIC, SI_{cal} or P_{CO_2} for which no data are available for the mangrove site. In contrast, the UNAM well falls close to a projection of the mixing line of STE samples for all solutes, though NH_4 concentrations are slightly elevated and PO_4 concentrations are slightly lower than the lower salinity extension of the conservative mixing line (Fig. 3-2).

Organic Carbon Character and Distribution

Total CDOM abundance in spring vent samples shows a strong negative correlation with salinity (Fig.3-3a). The CDOM is broken into various components by PARAFAC modelling, that is described in Chapter 2 and includes 322 samples from subterranean estuaries in the Yucatan as well as Indian River Lagoon, Florida. The five different PARAFAC component abundances vary with salinity in STE samples as well as compared to freshwater sources (mangrove surface water, cenotes, and inland wells) (Fig. 3-3b-f). PARAFAC components are collinear for Yucatan samples, with R^2 values near 1 for all comparisons (Table 3-3). Terrestrial freshwater end members have variable component abundances: the UNAM well falls close to an extension of the salinity-abundance observed in STE samples similar to the solute concentrations, while the mangrove surface water sample has much higher and cenote freshwater samples have much lower abundances (Fig. 3-3a).

Changes in organic matter composition are depicted by variation in the proportion of fluorescence attributable to each PARAFAC component. For STE samples, most component abundances remain constant across the salinity gradient but considerable composition changes occur in the most saline samples (Fig.3-4b-f). Except for component C5, the mangrove surface water and cenote differ from STE and UNAM well samples, where mangroves have relatively greater C1 and lower C2, C3 and C4 abundances, while cenotes have relatively higher C3 but lower C1 and C4 abundances.

Utilizing the mass balance relationships outlined in Eq. 3-7 and 3-8 and based on the salinity of lagoon surface water (32.7 compared to the salinity of standard seawater (35) and fresh SGD (9.77; Table 3-1), I estimate that SGD comprises 9% of surface lagoon water. If 78.5% of fresh SGD is derived from submarine springs with the

remainder from diffuse seepage at the beach face (Null et al., 2014), 6.5% of surface lagoon water is derived from submarine spring discharge. I assume that this spring discharge contributes all CDOM to surface water, and that surface water CDOM content is regulated by simple dilution of organic-carbon rich SGD (Table 3-4). This assumption allows me to evaluate potential changes in CDOM from reactions in the lagoon through comparisons of the measured PARAFAC component in surface lagoon water to that predicted by dilution of CDOM-rich spring discharge. Based on this analysis, modeled concentrations are approximately two times greater than measured concentrations (indicating net consumption in surface water) for components C1-C4, but about one third the measured abundance of C5 (indicating net production in surface water; Table 3-4).

Discussion

The following discussion addresses the magnitudes of feedbacks between organic carbon remineralization, carbonate mineral dissolution, and phosphorus concentrations in carbonate karst STEs. I assess organic matter quality at two different locations: within the inland aquifer, and at discharge sites of the hydrologic system (Fig. 3-1). These discussions center on PARAFAC signatures and biogeochemical solute concentrations of end members. I first discuss the sources and transformations of organic matter in the inland aquifer system by comparing the quantity and quality of organic carbon from terrestrial freshwater sources in a system wide flow model (e.g., Baker et al. 2003; Baker and Spencer 2004; Lapworth et al. 2008), along with indicators of biogeochemical reactions (P_{CO_2} , SI_{cal} , Ca, NH_4 , and PO_4). I then evaluate biogeochemical reactions within the freshwater-saltwater mixing zone of the STE. Based on the ratios of solutes produced compared to the stoichiometries of reactions, I

describe a conceptual model of OC-driven biogeochemical reactions within the STE. Finally, I discuss implications for organic carbon fluxes to the lagoon and CO₂ fluxes to the atmosphere.

Terrestrial Sources and Processing of Organic Carbon

Organic carbon in the STE is largely derived from terrestrial freshwater sources, as indicated by the strong negative correlations between salinity and CDOM abundance (Fig. 3-3a) and with DOC (Chapter 2, Fig. 2-2). While components are collinear (Table 3-3), the relative proportion of PARAFAC components varies with salinity in terrestrial freshwater end members (cenotes, mangrove surface water, and UNAM well), as well as offshore in STE samples and surface lagoon water (Fig. 3-3). These variations suggest changes in organic carbon quality that may impact the distribution and magnitudes of biogeochemical reactions during transport from terrestrial freshwater sources offshore and discharge as SGD.

Possible sources of terrestrial OC in the STE could include water recharged directly through soils, infiltration from mangrove forests, and anthropogenic wastewater. Although freshwater sampling points do not represent points along a specific flow paths in the conceptual model presented in Fig. 3-1, they should represent characteristics of coast-parallel environments. Specifically, cenotes represent inland areas where precipitation recharges groundwater (Fig. 3-1a), mangroves represent the strip between the 5e highstand reef deposits and coastal dunes (Fig. 3-1b), and the UNAM well represents the coastal dunes (Fig. 3-1d). Inland groundwater recharge areas (characterized by cenotes), appear to contribute little OC and contains less organic matter than the well, mangroves, or water in the STE (Fig. 3-3a). The mangrove wetlands have higher CDOM concentrations and relative C1 component abundances,

corresponding with lower relative abundances of C2, C3 and C4 than other freshwater sources (Fig. 3-3a-e). Mangrove organic carbon may be a source to the STE, because intertidal mangrove forests transpire sufficient water to create pore water brines that can alter SGD dynamics (McGowan and Martin, 2007) and similar salt concentration may set up density instability in the freshwater wetlands and cause downward infiltration into the groundwater flow path in our field area (Fig. 3-1b). While no wastewater was sampled, disposal is unregulated in the region and known to contaminate freshwater sources (Hernández-Terrones et al. 2011; Metcalfe et al. 2011). The injection of wastewater below the halocline and its subsequent upward mixing (Metcalfe et al., 2011) indicates this source could also contribute to organic matter in the STE.

While mangrove wetlands may contribute to terrestrial OC at the STE, the PARAFAC signature of mangrove wetlands is distinct from both the UNAM well and the STE by being dominated by C1 with lower abundances of C2-C5 (Fig. 3-1b). These distinctions suggest it is altered along the flow paths to the coast (Fig. 3-1c). Alteration is not simply caused by dilution with low OC groundwater, a process that would retain the relative abundance of PARAFAC components. Alteration of organic carbon composition through remineralization could modify both the quantity and quality of organic carbon and change PARAFAC component composition along freshwater flow paths. Remineralization is evidenced by elevated P_{CO_2} and nutrient concentrations, and lower SI_{cal} values in the UNAM well and STE samples compared to cenotes (Fig. 3-2b-f). The salinity and nutrient concentrations, and P_{CO_2} , and SI_{cal} values of the UNAM well fall close to the expected conservative mixing (Fig. 3-2), which suggests most alteration

occurs inland of location of the UNAM well (e.g. Fig. 3-1c) and little additional alteration occurs as water flows from the dunes to the springs (e.g., between d and e on Fig. 3-1).

Biogeochemical processing in the STE

Organic carbon remineralization between inland freshwater end members (cenotes, mangroves) and the STE is shown by increasing P_{CO_2} and nutrient (NH_4 and PO_4) concentrations (Fig. 3-2). However, further remineralization within the freshwater-saltwater mixing zone occurs within the STE, as indicated by positive values of ΔP_{CO_2} , ΔNH_4 and ΔPO_4 (Fig. 3-2). Additionally, carbonate mineral saturation indices within STE samples are lower than the conservative mixing line while ΔCa values are positive, suggesting that $CaCO_3$ dissolution also occurs (Fig. 3-2c and d). Remineralization may result from intrusion of oxygen-containing surface lagoon water to the STE (Chapter 2; Young et al., 2017), which may enhance remineralization rates because oxygen produces the most energy of redox reactions (Chapter 2; Table 1-2). Alternatively, labile organic carbon, such as that depicted by the C5 component in PARAFAC modeling, is present in relatively high concentrations in lagoon water and could enhance remineralization reactions in the mixing zone (Chapter 2).

Given the evidence from conservative mixing models that both organic carbon remineralization and $CaCO_3$ dissolution occur within the STE, the following discussion focuses on the magnitude of carbon feedbacks as well as impact on P concentrations by comparing the change in solute concentration to that predicted by reaction stoichiometry (Eq. 3-1 and 3-3). I assume that inorganic C and P distributions are predominantly controlled by organic carbon remineralization, which I assume generates C:N:P at the Redfield Ratio of 106:16:1 (Eq. 3-1), $CaCO_3$ dissolution, which produces

Ca and DIC at a molar ratio of one (Eq. 3-3), and sorption interactions between P and CaCO_3 minerals, which has no fixed stoichiometry.

Remineralization reactions in the STE generate CO_2 , which decreases SI_{cal} to values lower than those expected from conservative mixing (Fig. 3-2c). Enrichment of Ca (ΔCa) by up to 1.3 mM above conservative mixing reflects carbonate dissolution within the mixing zone (Fig. 3-2d). Dissolution of CaCO_3 minerals may occur due to fresh and saltwater end member mixing alone because of the cubic rather than linear dependence of SI_{cal} on Ca concentrations (Plummer 1975; Smart et al. 1988; Sanford and Konikow 1989). However, in this case, mixing alone is unlikely to cause dissolution because mixing only generates positive SI_{cal} values (Fig. 3-2c). OC remineralization, CO_2 production, and hydration to carbonic acid (Eq. 3-1 and 3-2) may reduce SI_{cal} to negative values and drive dissolution (e.g., Gulley et al. 2014; Gulley et al. 2015). This mechanism is more likely here, resulting from enhanced OC remineralization (Gulley et al., 2016) from the introduction of terminal electron acceptors or labile organic carbon with seawater.

The net impact of coupled organic carbon remineralization (Eq. 3-1) and CaCO_3 dissolution (Eq. 3-3) on CO_2 concentrations depends on the relative magnitudes of these two processes. This may be assessed by comparing the proportions of DIC and Ca production (ΔDIC and ΔCa) within the STE, which are taken as the residual of salinity-based conservative mixing models (Fig. 3-2a and 3-2c). OC remineralization produces CO_2 (Eq. 3-1) while carbonic acid-driven carbonate mineral dissolution is a CO_2 sink as it converts CO_2 to bicarbonate (Eq. 3-3). Consequently, positive DIC residuals (Fig. 3-2a) result from both OC remineralization and carbonate mineral

dissolution. However, positive P_{CO_2} residuals (Fig. 3-2b) indicate that increases in DIC largely reflect OC remineralization rather than carbonate mineral dissolution. If only OC remineralization and carbonate mineral dissolution impact ΔDIC and ΔCa concentrations, all residuals should plot within the shaded field in Fig. 3-4 bounded by the expected changes of molar $\Delta DIC:\Delta Ca$ ratios due to these two reactions. However, nearly half the STE samples plot outside this field, indicating that additional reactions contribute Ca or consume DIC.

Many additional reactions could contribute Ca or consume DIC including ion exchange processes, precipitation of carbonate minerals, outgassing of CO_2 and/or primary productivity. Although Ca concentrations in groundwater may increase due to ion exchange processes following saltwater intrusion (Sayles and Mangelsdorf, 1977), this process should be minor in carbonate aquifers, which have little cation exchange capacity. In addition, the Yucatan aquifer exhibits conservative mixing of Na^+ , indicating little exchange occurs (Price and Herman 1991). Calcite precipitation reduces Ca and DIC concentrations at a molar ratio of 1 and thus could not fractionate DIC/Ca residual ratios. Only precipitation of other metal carbonates (magnesite, siderite, dolomite etc.) would fractionate the Ca/DIC ratio. Precipitation of these metals seems unlikely as little Fe is present in the systems and magnesite is close to saturation (Whelan et al. 2011).

The Ca/DIC disequilibrium in Fig. 3-4 more likely results from DIC lost from the system. Such a loss could be due to outgassing of CO_2 as observed in other coastal carbonate aquifer systems (Price and Herman, 1991) or from primary productivity. Because the freshest spring water has P_{CO_2} values around 1.5 orders of magnitude higher than the atmospheric P_{CO_2} of $10^{-3.4}$ atm, and all STE samples have P_{CO_2} values

higher than atmospheric CO₂ (Fig. 3-2b), outgassing is a plausible mechanism to reduce dissolved DIC concentrations but water would have to come into contact with surface water in order to be able to exchange with the atmosphere (Fig. 3-6). Alternatively, primary productivity would also reduce the DIC concentration without affecting the Ca concentration. The lack of light in the STE requires DIC fixation by chemolithoautotrophic bacteria, a process which has not been well studied in STE systems. However, chemolithoautotrophic bacteria fix large amounts of carbon in anoxic, sulfidic cave systems, such as in the Yucatan offshore springs, as well as deep sea vents and could contribute to loss of DIC (Jannash, 1995; McCollum and Shock, 1997; Engel et al., 2004; Arndt et al., 2013).

Implications for STE Nutrient Sources and Sinks

Though organic carbon remineralization in STEs generates inorganic N and P (Eq. 3-1) and CaCO₃ dissolution may lead to liberation of sorbed P, the impact of these reactions on P delivery from SGD depends on their relative magnitudes compared to P sorption to CaCO₃ minerals. The extent of additional P sinks within the STE can be assessed by comparing $\Delta\text{NH}_4:\Delta\text{PO}_4$ ratios to the Redfield Ratio, assuming all NH₄ and PO₄ are derived from organic carbon remineralization at the Redfield Ratio of 16:1. Production of nutrients from remineralization of organic carbon with an N:P ratio of 16 should produce $\Delta\text{NH}_4:\Delta\text{PO}_4$ ratios of 16 if no additional sources or sinks of N or P alter ratios. Ratios that are higher than 16:1 indicate an additional N source or P sink. Since N lacks a mineral source in carbonate aquifers and is largely derived from remineralization of organic N to NH₄, P sorption is a more likely candidate to explain high ratios (Santoro, 2010). Alternatively, if P is derived from CaCO₃ dissolution, ratios

should reflect that of carbonate rocks. The concentration of P contained in the Yucatan carbonate rocks is unknown, but Ca:P ratios in the Floridan carbonate karst aquifer range from 360-5700 (Price et al., 2008). This comparison may not be perfect because a source of P exists in the Floridan aquifer from the P-rich siliciclastic Hawthorn Group rocks (Scott, 1988), which is missing from the Yucatan aquifer (Back and Hanshaw, 1970). With this caveat in mind, I assess sources and sinks of N and P through comparisons of measured N:P ratios, and residual $\Delta N:\Delta P$ and $\Delta Ca:\Delta P$ ratios to ratios typical of organic matter and carbonate minerals (Fig. 3-5).

Bulk N:P ($NH_4:PO_4$) ratios suggest that nutrients contained in fresh and saltwater end members are derived predominantly from organic carbon remineralization, because the N:P ratios of the freshwater end member is slightly elevated above the Redfield ratio, while that of the saltwater end member is approximately 16:1 (Fig. 3-5a). However, N:P ratios at intermediate salinities reach values of 400. This indicates that, while both nutrients are produced within the STE (Fig. 3-2e and f), the concentrations of P relative to N are considerably reduced, likely due to sorption of P to $CaCO_3$ minerals.

Similar to bulk N:P ratios, $\Delta N:\Delta P$ molar ratios are near Redfield ratios (16:1) in the freshwater end member and lagoon surface water, suggesting remineralization of marine organic matter as a likely source of excess N and P (Fig. 3-5b). However, $\Delta N:\Delta P$ ratios reach values of nearly 800 at intermediate salinity, suggesting a loss of P from the system because of the lack of mineral N to cause the excess. High $\Delta N:\Delta P$ values compared to the Redfield Ratio suggest that the P concentrations are reduced in the discharging fresh water. Losses could occur through sorption to carbonate mineral surfaces (Price and Herman 1991; Price et al. 2010; Leader et al. 2007). Decreasing

N:P and $\Delta\text{N}:\Delta\text{P}$ ratios with salinity may reflect a reduction in the magnitude of the CaCO_3 sorption sink because desorption of P from carbonate mineral surfaces typically occurs at salinities above 90% of seawater values (Price et al. 2008). The salinity dependence of N:P and $\Delta\text{N}:\Delta\text{P}$ ratios is consistent with this mechanism, where ion exchange at high salinity would lead to desorption of P associated with carbonate minerals, thus decreasing both the N:P and Ca:P ratios in the STE. The desorption of P with increasing salinity does not liberate all sorbed P, however, because the N:P and $\Delta\text{N}:\Delta\text{P}$ ratio remains above the Redfield ratio for most samples. The retention of P within the carbonate aquifer lowers P delivery via SGD, and may impact surface water carbon cycling if P is a limiting nutrient (Fig. 3-6).

Most $\Delta\text{Ca}:\Delta\text{P}$ residuals are within the range of Floridan carbonate rock values, except for the freshest water sample, which has a Ca:P ratio of over 15000 at a salinity of 10 (Fig. 3-5c). While CaCO_3 dissolution may be a source of P, it appears to be relatively minor here. For instance, since other evidence of organic carbon remineralization exists (e.g. elevated P_{CO_2} and ΔNH_4 concentrations), remineralization should produce P at an N:P ratio of approximately 16:1. Because N:P ratios are much higher than this value in many STE samples, considerable P sorption to CaCO_3 minerals must occur. Therefore, even though CaCO_3 dissolution may contribute excess P, CaCO_3 appears to be a net sink of P in this setting due to sorption interactions.

Impact on Surface Water Carbon Cycling

The conceptual model of STE biogeochemical processing (Fig. 3-6) reflects chemical modifications of the discharging water, which should impact coastal biogeochemical budgets by providing a source of carbon and nutrients (Slomp and Van

Cappellen 2004; Kim and Swarzenski 2010; Roy et al. 2013). Using a mass balance approach for lagoon water salinity (Eq. 3-7 and 3-8), I assess the fate of SGD-derived organic carbon (CDOM) in surface lagoon water utilizing the measured versus modeled (mass balance) abundances of PARAFAC components in lagoon water, and discuss implications for lagoon surface water P_{CO_2} values and fluxes to the atmosphere.

For organic carbon, I estimate production or degradation of PARAFAC components in the lagoon and compare it with the measured abundances in lagoon water to assess its fate after being discharged from the STE. The salinity mass balance indicates lagoon water contains approximately 7% fresh SGD from springs and thus C1-C5 in lagoon surface water should be 7% of the fresh SGD concentration, assuming negligible contributions from seawater. However, modeled C1 to C4 abundances using this mass balance are more than 200% greater than measured abundances, indicating that significant loss of CDOM occurs following discharge (Table 3-4). In contrast, C5 is three times more abundant in lagoon surface water than predicted from the mass balance, suggesting an additional source in surface lagoon water, such as through production via photosynthesis. The relative depletion of C5 in SGD may also reflect preferential remineralization if it is more labile, or the lack of a source in the subterranean environment because it is isolated from sunlight and photosynthesis may not occur. Multiple mechanisms could reduce the C1-C4 abundances in surface seawater, including remineralization, coagulation/flocculation, or photo-oxidation. Photo-oxidation causes losses ranging from 50% in laboratory studies to 70% in natural systems, similar to our estimates, but is a relatively slow process that operates on long timescales (100's-1000's of hours) compared to the average residence time of the

Puerto Morelos lagoon (~3 hours; Vodacek et al., 1997; Blough and Del Vecchio, 2002; Coronado et al., 2007). Therefore, rapid reactions such as microbial remineralization or coagulation/flocculation are likely more important removal mechanisms than photo-oxidation. This mass balance suggests that the majority of terrestrial organic carbon discharged via SGD is remineralized in surface water within the lagoon residence time of three hours (Coronado et al., 2007). This rate of remineralization may be reflected in the P_{CO_2} of lagoon surface (589 ppm, or $\log P_{\text{CO}_2} = -3.23$), which elevated above atmospheric values (400 ppm).

The supersaturated P_{CO_2} of the lagoon water suggests that SGD may impact atmospheric CO_2 fluxes either by CO_2 supersaturation of SGD itself or remineralization of terrestrial carbon delivered by SGD. However, nutrients delivered by SGD could induce a negative feedback for atmospheric CO_2 fluxes if increased availability of limiting nutrients (N or P) increases primary productivity and fixes dissolved CO_2 . The P_{CO_2} of lagoon water is likely to vary over time, at diel and longer frequencies, depending on productivity, and thus to evaluate the total CO_2 flux would require longer term measurements than available from this study. Nonetheless, elevated P_{CO_2} in the STE from biogeochemical processing indicates SGD could be an important source of CO_2 to the lagoon and atmosphere as suggested for STEs elsewhere (Dorsett et al. 2011; Szymczycha et al. 2013). At the time of our sampling, primary productivity did not fix all additional CO_2 delivered by SGD because lagoon surface water remains supersaturated with respect to the atmosphere. Because P appears to be a limiting nutrient in this setting (e.g., Carruthers et al. 2005), the preferential retention of P within the STE may limit surface water primary productivity, and therefore limit the C fixation

rate and drive surface lagoon water to be a source of CO₂ to the atmosphere during this sampling period.

Conclusions

Organic carbon in carbonate karst STEs drives biogeochemical reactions that generate nutrients and dissolved CO₂ and leads to carbonate mineral dissolution. Organic carbon is processed in the STE prior to discharge and leads to increased nutrient concentrations as well as carbonate mineral dissolution. Remineralization in the STE may be enhanced due to the introduction of oxygen contained in surface lagoon water or the contribution of relatively labile organic carbon, here represented by PARAFAC component C5. Although P may be derived from both OC remineralization and carbonate mineral dissolution, elevated $\Delta N:\Delta P$ and $\Delta Ca:\Delta P$ ratios indicate that P sinks in the STE, such as sorption to the carbonate matrix, may reduce P fluxes in SGD. Because $\Delta N:\Delta P$ ratios are greater than the Redfield ratio, the sinks may cause P-limitation in this type of carbonate coastal setting. OC remineralization in the STE also increases CO₂ concentrations of water that is discharged to the lagoon, and may contribute to supersaturation of lagoon water with respect to atmospheric CO₂ concentrations. Nutrient delivery by SGD could offset this CO₂ source by increasing C fixation via primary productivity, although P retention in the STE may limit the amount of primary productivity that may occur in surface waters.

Table 3-1. Chemical characterization of end members for conservative mixing models.

	Fresh SGD (Hol Kokol)	Lagoon surface water
Salinity	9.77	32.74
pH	7.21	8.08
ORP	-205.2	83.4
D.O. (%)	6.2	89.3
DOC (μM)	344	59
C1 (R.U.)	1.44	0.04
C2 (R.U.)	0.57	0.01
C3 (R.U.)	0.67	0.02
C4 (R.U.)	0.28	0.01
C5 (R.U.)	0.09	0.02
DIC (mM)	4.34	2.15
Log P_{CO_2}	-1.81	-2.95
Si_{cal}	0.02	0.68
Ca^{2+} (mM)	5.11	11.63
NH_4^+ (μM)	46.96	2.08
PO_4^{3-} (μM)	0.54	0.04

Table 3-2. Water chemistry parameters of terrestrial water, near-shore springs, and seawater.

	n	Type	Collection depth (m)	Salinity	Temp (°C)	DO (%)**	pH	ORP (mV)
Cenotes	3	GW	2, 20, 20	0.72± 0.04	25.33± 0.87	21.6± 9.0	7.12± 0.08	-84.27 ± 12.98
Mangrove	1	SW	0.9	1.60	25.8	49.8	7.41	109.2
Well	1	GW	18	5.63	32	4.4	7.13	-239.7
Hol Kokol	2	SGD	--	9.82± 0.07	28.75± 0.07	6.9± 1.0	7.25± 0.06	-196.40 ± 12.45
Gorgos	5	SGD	--	19.91± 0.44	29.16± 0.35	15.2± 3.5	7.17± 0.13	-191.86 ± 44.94
Laja	1	SGD	--	21.33	28.70	8.0	7.14	-207.60
Pargos	7	SGD	--	23.43± 1.87	29.64± 0.44	15.1± 7.0	7.28± 0.11	-86.27 ± 92.41
Lagoon water	3	SW	2	32.74	30.1	89.3	8.08	83.4

Range shown is ± 1 standard deviation.

* GW = groundwater, SW = surface water, SGD = submarine groundwater discharge.

** Percent saturation

Table 3-3. R² between PARAFAC components in Yucatan samples.

	C1	C2	C3	C4
C2	0.99			
C3	0.99	0.99		
C4	0.99	0.99	0.98	
C5	0.94	0.94	0.93	0.96

Table 3-4. Mass balance of terrestrial PARAFAC components based on salinity.

Component	Abundance in Fresh SGD (R.U.)	Modeled Abundance in Surface Lagoon (R.U.)	Measured Abundance in Surface Lagoon (R.U.)	Modeled/measured (%)
C1	1.444	0.093	0.004	234%
C2	0.567	0.036	0.014	258%
C3	0.666	0.043	0.021	211%
C4	0.284	0.018	0.008	221%
C5	0.094	0.006	0.018	33%

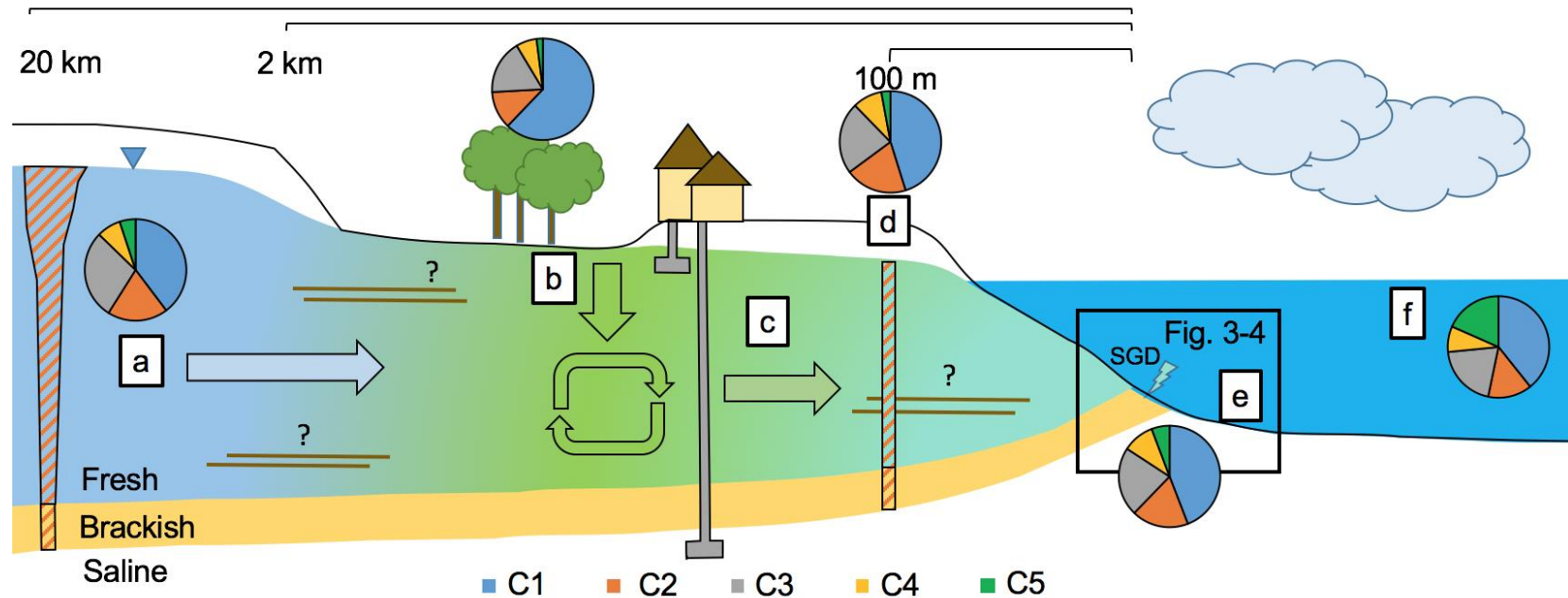


Figure 3-1. Conceptual model of a hypothetical flow line to the near-shore springs delineating potential sources and sites of transformation of organic matter broken into five fluorescent components shown in the pie diagrams. Confining units, depicted as horizontal brown lines with question marks, may restrict water exchange and separate the aquifer into upper unconfined and lower confined portions, particularly near the shore (e.g., Null et al., 2014). (a) Inland cenotes intersect the freshwater lens. Aquifer recharge drives flow of groundwater toward coast. (b) Surficial water at mangroves contains high concentrations of CDOM, possibly also including anthropogenic organic carbon in wastewater infiltrates the aquifer, increasing groundwater CDOM concentrations between cenotes and the shoreline. Mangrove PARAFAC signature is dominated by C1 over other terrestrial components. Injected wastewater may also contribute to groundwater chemistry. (c) Organic matter is remineralized and increases P_{CO_2} and inorganic nutrient content of groundwater. (d) Water in the UNAM well is composed of groundwater mixed with surface organic source. (e) Groundwater flows offshore to be discharged in springs as SGD. PARAFAC signature of spring discharge is similar to UNAM well water. Freshwater mixes with saltwater prior to discharge in STE underlying freshwater lens, shaded in yellow. (f) Lagoon surface water contains relatively more protein-like C5 than all terrestrial groundwater sources or spring discharge. Note compression in the horizontal scale.

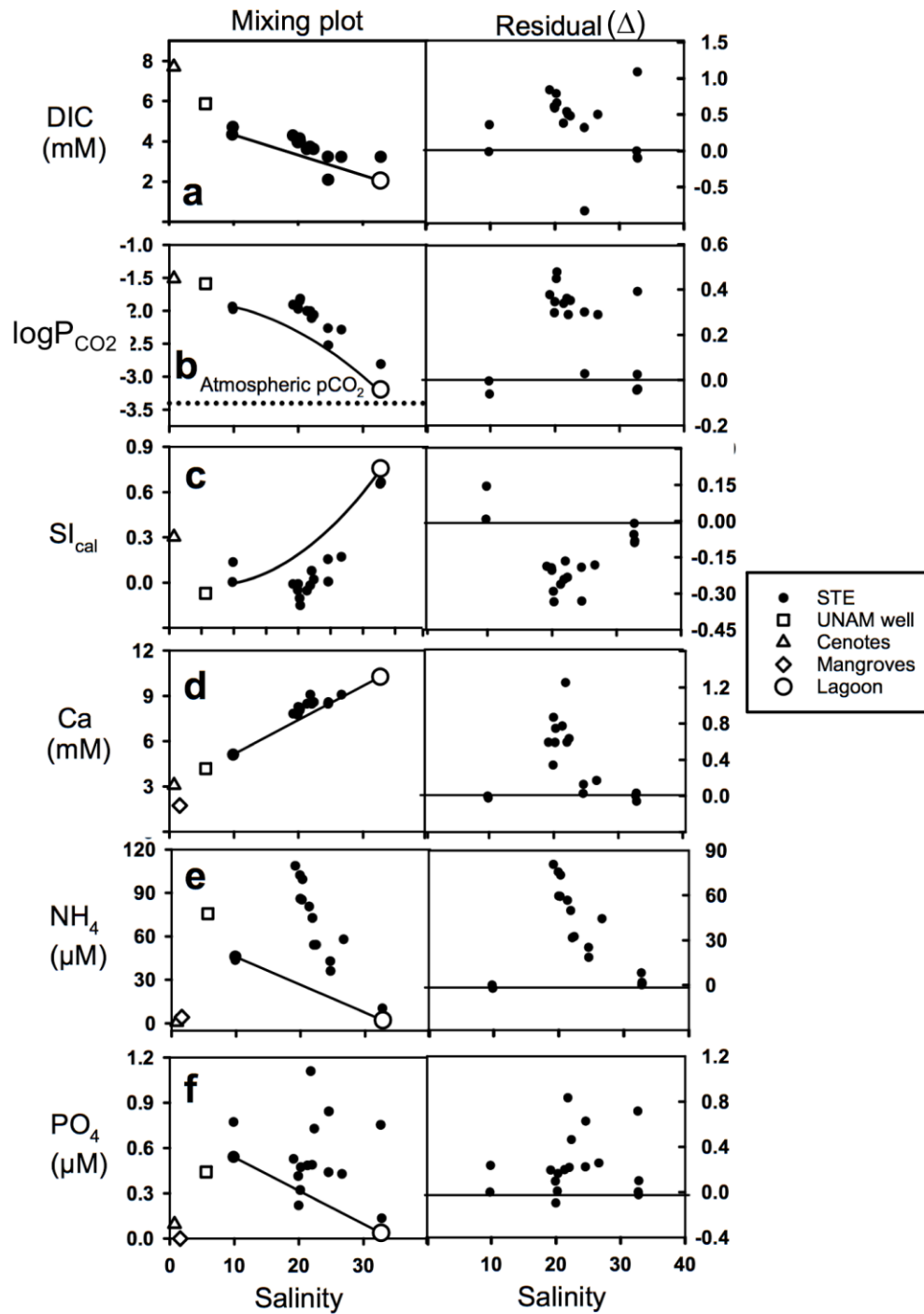


Figure 3-2. Salinity versus (a) DIC, (b) $\log P_{CO_2}$ ($p < 0.001$), (c) SI_{cal} , (d) Ca^{2+} , (e) NH_4^+ , and (f) PO_4^{3-} (Left panels) and residuals from the mixing models (right panels). Filled circles represent SGD samples and lagoon surface water. Black lines represent conservative mixing between freshest SGD sample and surface lagoon water. Residuals are reported in same units as data. DIC data was not available for mangroves so no data for DIC, P_{CO_2} , and SI_{cal} are reported.

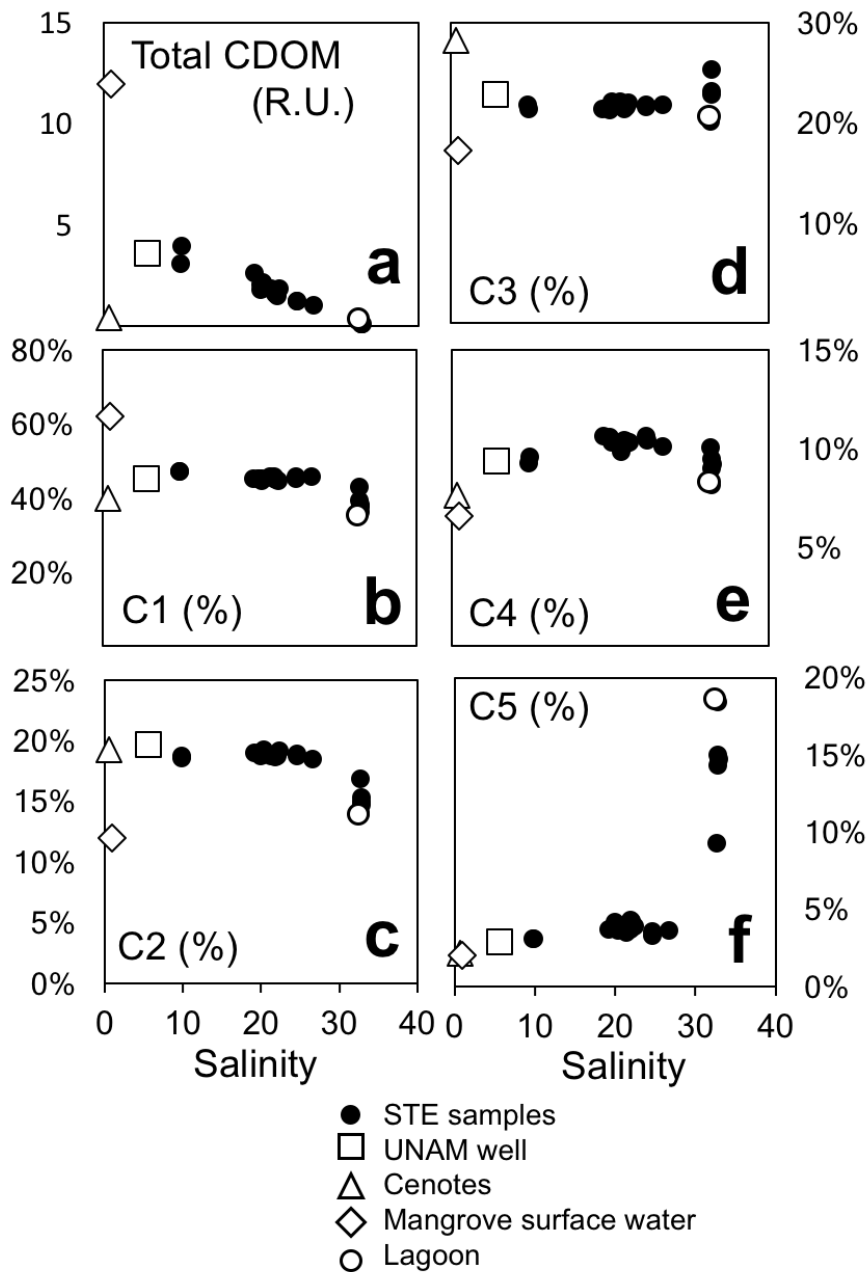


Figure 3-3. Salinity versus (a) total CDOM and various PARAFAC components including (b) C1), (c) C2, (d) C3, (e) C4, and (f) C5. The total CDOM is the sum of the various components. The black dots represent the values for samples collected from the STEs and the open squares represent water from the cenotes, open diamonds water from the mangrove forest, and open triangles water from the well. These data represent the quantity (a) and quality (b-f) of chromophoric organic carbon.

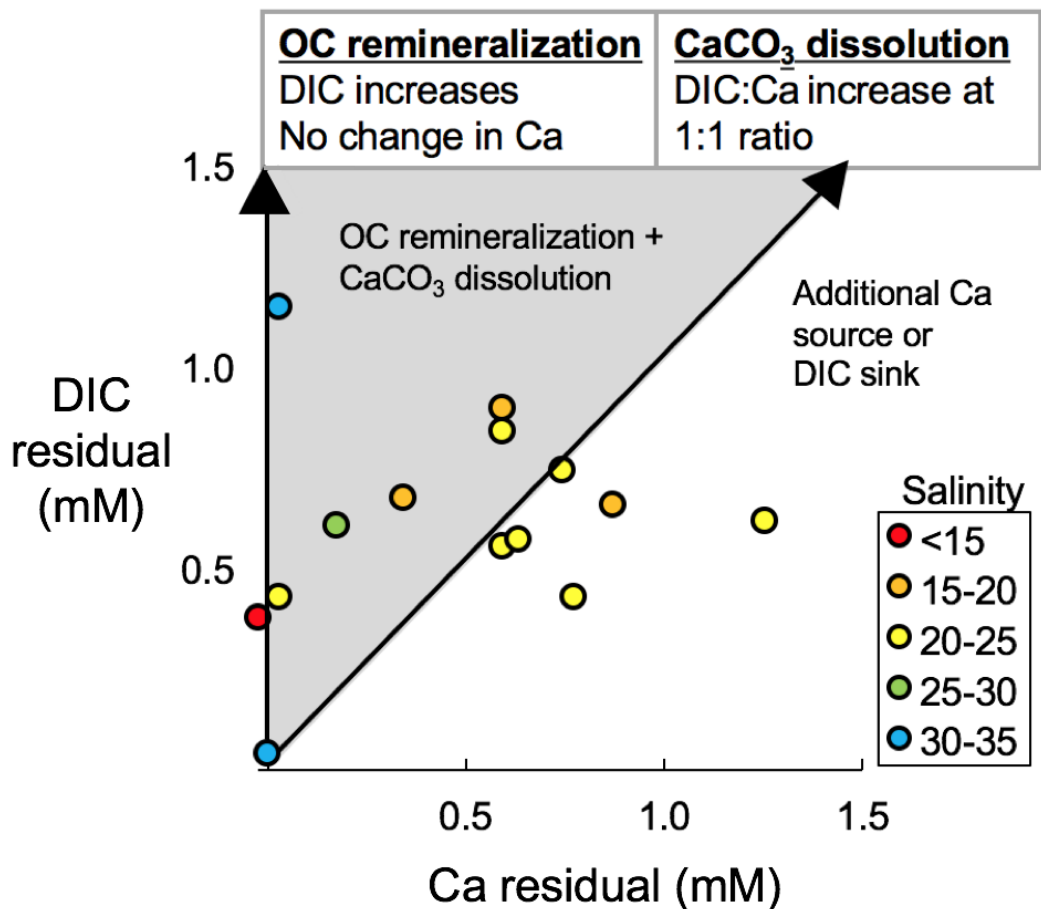


Figure 3-4. Cross plot of Ca versus DIC residuals in STE water samples. Arrows and fields represent DIC and Ca residuals if the main sources are organic carbon (OC) remineralization and CaCO₃ dissolution. Salinity ranges of data points are color coded from low salinity (red) to high salinity (blue).

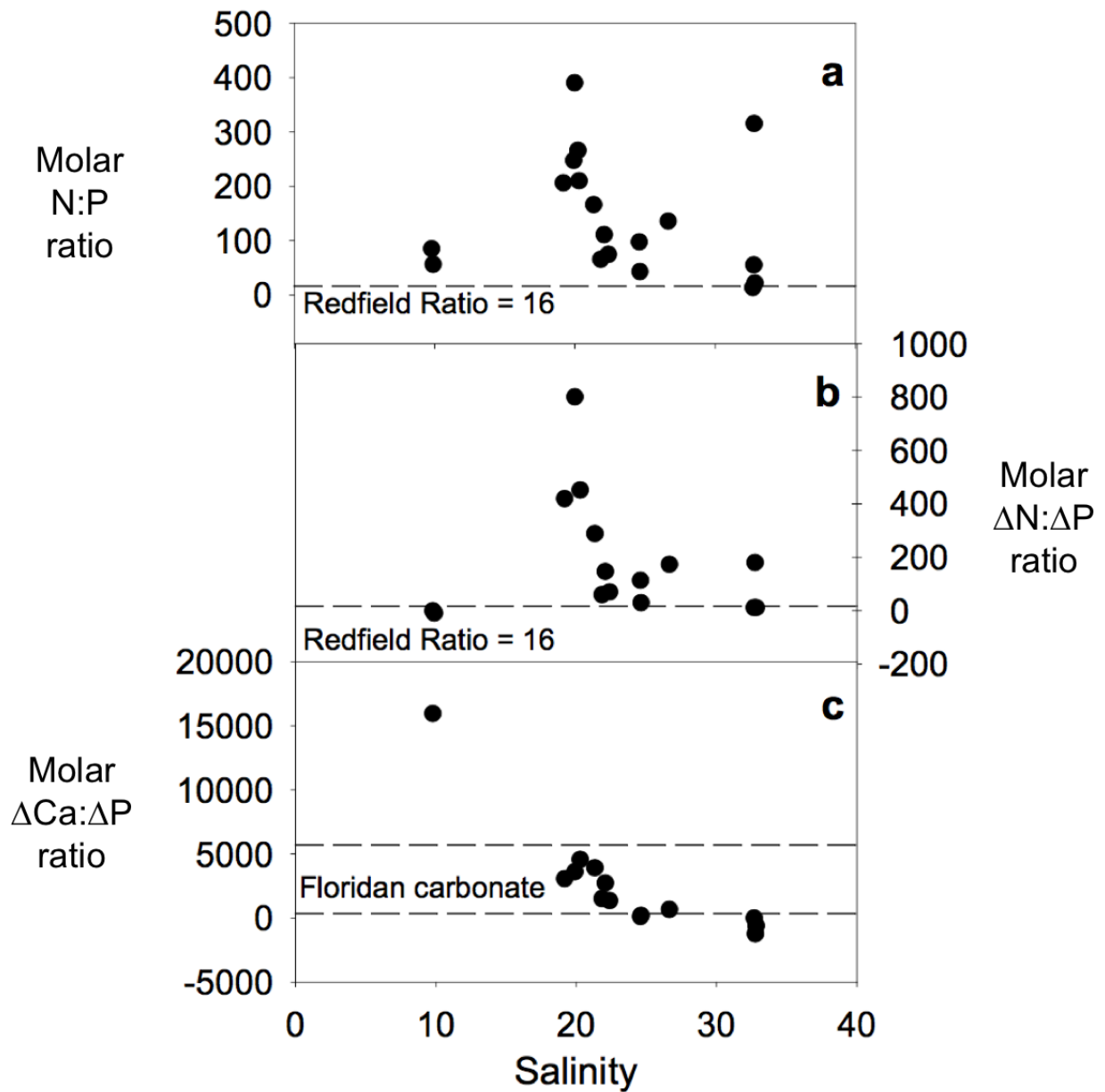


Figure 3-5. Cross plots of salinity versus (a) molar N:P ratios (b) $\Delta N:\Delta P$ ratios and (c) $\Delta Ca:\Delta P$ ratios.

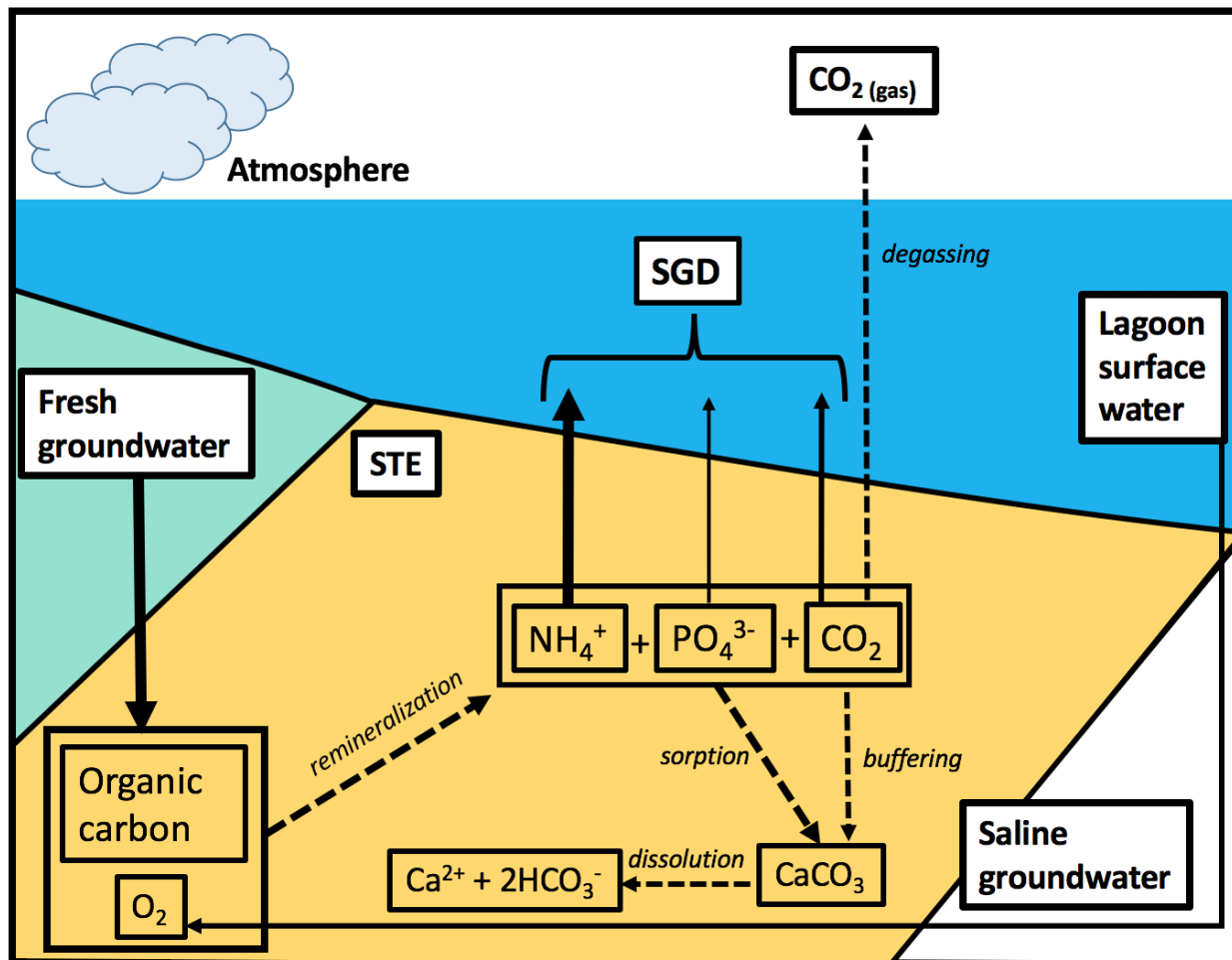


Figure 3-6. Conceptual model of STE biogeochemistry within STE. Black boxes represent solute reservoirs, solid arrows represent fluxes between reservoirs, dashed arrows represent transformations due to reactions. Arrow thickness indicates the magnitude of fluxes and transformations. Fresh groundwater delivers organic carbon to the STE. Surface seawater delivers oxygen. Organic carbon from fresh groundwater is remineralized with oxygen from surface saltwater to produce NH_4 , PO_4 , and CO_2 . NH_4 is discharged in high concentrations in SGD due to lack of sink in the STE, while some P is retained due to Ca-P sorption interactions, reducing SGD concentrations. CO_2 is consumed in CaCO_3 dissolution and outgassing, reducing SGD concentrations.

CHAPTER 4 BIOGEOCHEMICAL CONTROLS OF GREENHOUSE GAS PRODUCTION AND SEQUESTRATION IN SILICICLASTIC SUBTERRANEAN ESTUARIES

Introduction

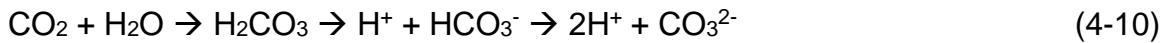
Gradients of organic carbon quantity, quality, and terminal electron acceptor concentrations regulate the distribution of redox reactions in subterranean estuaries (STEs) and generate solutes that may be transported to surface waters via submarine groundwater discharge (SGD). A consequence of organic carbon remineralization reactions is the production of greenhouse gases including carbon dioxide (CO₂) and methane (CH₄), which may be transported to surface waters and evade to the atmosphere. CO₂ and CH₄ are produced alongside well-studied reactions that alter nutrient and metal concentrations. However, carbon fluxes from SGD have received relatively little attention compared to nutrients (Slomp and Van Cappellen, 2004; Kroeger and Charette, 2008; Spiteri et al., 2008a) and metals (Roy, M. et al., 2010; Whelan et al., 2011; Johannesson et al., 2011). Several studies have found SGD to be a significant source of carbon to surface waters (Cai et al., 2003; Liu et al., 2012; Liu et al., 2017), though little consensus exists as to whether STEs are sources or sinks of CO₂ because interactions between remineralization reactions and sediment mineralogy may alter CO₂ concentrations and pore water buffering capacity (Cai et al., 2003; Liu et al., 2017). CH₄ fluxes from STEs have received relatively more attention than CO₂ because CH₄ is used as a quasi-conservative tracer of SGD due to its typically high concentrations in groundwater compared to surface water (Cable et al., 1996; Corbett et al., 2000; Dulaiova et al., 2010).

Both CO₂ and CH₄ are generated during redox reactions (Table 4-1), and their concentrations in STEs should therefore in part be controlled by redox gradients that

depend on changes in terminal electron acceptor and organic carbon availability and reactivity (Chapter 2). In the case of CH₄, production occurs during organic carbon remineralization when other terminal electron acceptors have been depleted (Meynert et al., 2005). Because seawater contains high concentrations of sulfate, methanogenesis does not occur in marine settings unless supplies of organic carbon are sufficiently high to deplete sulfate. Methanogenesis is therefore a relatively more important process in freshwater settings where sulfate availability is low (Meynert et al., 2005). Because sulfate reduction is energetically favorable compared to methanogenesis (Table 1-2), and because sulfate concentrations are highly correlated with salinity, variations in STE sulfate concentrations should regulate zones of methanogenesis. While CH₄ is known to be delivered in large quantities to surface water via SGD (e.g. Bugna et al., 1996; Borges et al., 2016), fewer studies have assessed the impact of methanogenesis on carbonate chemistry, though both methanogenesis and methane oxidation produce CO₂ (Table 4-1, Eq. 4-5 and 4-9). Studies using CH₄ as a tracer typically assume that it is quasi-conservative (Bugna et al., 1996; Dulaiova et al., 2010; Lecher et al., 2015), but more recent assessments of CH₄ oxidation in coastal aquifers have observed that methanotrophy can consume a large proportion of CH₄ and strongly reduce fluxes to surface water (Schutte et al., 2016).

Carbon Dioxide and Carbonate Equilibria

Carbon dioxide is produced during all organic carbon remineralization reactions, including methanogenesis, but may be sequestered as HCO₃⁻ or CO₃²⁻ depending on the carbonate chemistry of pore waters (Eq. 4-10) (Froelich et al., 1979; Stumm and Morgan, 1996).



The degree of sequestration depends on buffering capacity, which is a function of total dissolved inorganic carbon (DIC) concentrations:

$$\text{DIC} = [\text{H}_2\text{CO}_3^*] + [\text{HCO}_3^-] + [\text{CO}_3^{2-}] \quad (4-11)$$

and

$$[\text{H}_2\text{CO}_3^*_{(\text{aq})}] = [\text{CO}_{2(\text{aq})}] + [\text{H}_2\text{CO}_{3(\text{aq})}] \quad (4-12)$$

as well as pore water pH, and alkalinity (Alk) (Egleston et al., 2010). DIC is defined as the sum of dissolved CO_2 , including its hydrated form (H_2CO_3) and dissociation products, bicarbonate (HCO_3^-) and carbonate (CO_3^{2-}) ions (Eq. 4-11). Note that hydration of dissolved CO_2 ($\text{CO}_{2(\text{aq})}$) to H_2CO_3 occurs more rapidly than dissolution of CO_2 in water, therefore the sum of dissolved CO_2 plus H_2CO_3 is referred to as H_2CO_3^* (Eq. 4-12), because the distribution between dissolved CO_2 and H_2CO_3 does not impact the speciation of DIC (Eq. 4-11). The speciation of DIC in Eq. 4-11 is predominantly a function of pH, where progressively higher pH (lower concentrations of H^+ ions) causes deprotonation of H_2CO_3 and causes more DIC to be speciated as HCO_3^- and CO_3^{2-} .

Alkalinity is a critical parameter in carbonate chemistry because it determines the acid-neutralizing capacity of water, for example as carbonic acid concentrations increase following organic carbon remineralization. Increased alkalinity reduces the magnitude of decreases in pH as weak acid is added to water, and represents the excess of base (proton acceptors) over acids (proton donors). Proton acceptors form complexes with H^+ ions, which reduces concentration of free H^+ . Alkalinity (Alk) may operationally be expressed as the sum of the most common bases (Eq. 4-13) or by the

charge balance of all strong acids and bases that are unaffected by acid additions (Eq. 4-14; Sarmiento and Gruber, 2006).

$$\text{Alk} = [\text{HCO}_3^-] + 2[\text{CO}_3^{2-}] + [\text{OH}^-] - [\text{H}^+] - [\text{B}(\text{OH})_4^-] + \text{minor bases} \quad (4-13)$$

$$\begin{aligned} \text{Alk} = & [\text{Na}^+] + [\text{K}^+] + 2[\text{Mg}^{2+}] + 2[\text{Ca}^{2+}] + \text{minor cations} \quad (4-14) \\ & - [\text{Cl}^-] - 2[\text{SO}_4^{2-}] - [\text{Br}^-] - [\text{NO}_3^-] - \text{minor anions} \end{aligned}$$

For the carbonic acid system, the buffering capacity of water changes based on changes in the ratio of alkalinity to DIC (Sabine et al., 2004), where a greater Alk:DIC ratio increases the buffering capacity of water, which allows more CO₂ to be dissolved and sequestered as HCO₃⁻ and CO₃²⁻. Both DIC and alkalinity are altered by many diagenetic reactions, which in turn alter buffering capacity. However, these reactions differ between carbonate or siliciclastic systems. In carbonate systems and in the open ocean, DIC and alkalinity are predominantly controlled by carbonate mineral (CaCO₃) dissolution and precipitation and atmospheric CO₂ concentrations (Sarmiento and Gruber, 2006). However, in siliciclastic settings where CaCO₃ minerals are less abundant, redox reactions, including organic carbon remineralization by different electron acceptors (Table 1-2), may play a larger role in regulating Alk:DIC ratios than CaCO₃ mineral dissolution or precipitation.

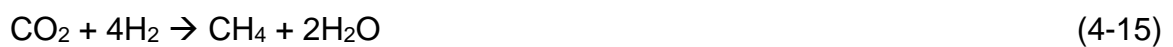
DIC is produced from organic carbon remineralization because it produces dissolved CO₂ that become speciated as DIC (Eq. 4-11) according to pore water chemistry, but also produces or consumes alkalinity depending on the remineralization pathway (Table 4-1). For instance, aerobic remineralization and methanogenesis produce DIC but no alkalinity, while denitrification, iron reduction, and sulfate reduction produce alkalinity and DIC at molar ratios of ~ 0.8, 8, and 1, respectively (Table 4-1;

Kuivila and Murray, 1984). The impact of redox pathway on Alk:DIC ratios is well known, and reaction stoichiometries are frequently used to determine the relative importance of the suite of diagenetic reactions changes in alkalinity and DIC, expressed as $\Delta\text{Alk}:\Delta\text{DIC}$ (Berner et al., 1970; Davison and Woof, 1990; Chen and Wang, 1999; Cai et al., 2003; Thomas et al., 2009; Liu et al., 2017). In general, the main sources of alkalinity in anaerobic marine sediments include denitrification, iron reduction, and sulfate reduction (Berner et al., 1970; Thomas et al., 2009; Liu et al., 2017). The impact of these reactions on carbonate equilibria in STEs should thus alter SGD CO_2 fluxes to surface waters in different amounts, which may in turn alter fluxes of CO_2 from surface water to the atmosphere, depending on processing in the water column, and makes redox reactions a critical parameter in CO_2 fluxes in siliciclastic systems compared to carbonate systems.

Methanogenesis and Carbonate Equilibria

Methanogenesis is typically a minor redox pathway in marine sediments due to inhibition by sulfate, and is generally restricted to freshwater systems or organic-rich marine sediments where sulfate may be entirely depleted (Whiticar and Schoell, 1986; Mitterer, 2010). Freshwater entering STEs should allow methanogenesis to occur, making methanogenesis in STEs more common than in saline marine sediments. However, its impact on carbonate chemistry across salinity gradients in STE sediments is not well known, though isolated studies suggest it could contribute significant DIC (Cai et al., 2003).

Methane may be produced via two pathways, CO_2 reduction:



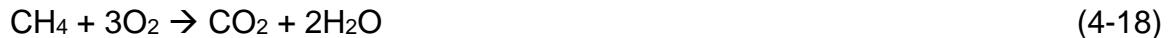


and acetate fermentation:



CO_2 reduction (Eq. 4-15) is coupled with fermentation (Eq. 4-16) because H_2 is required in CO_2 reduction and is often the limiting reactant. Because of this coupling, the net impact of both pathways is to produce CO_2 and CH_4 at a molar ratio of 1. Methanogenesis has no impact on alkalinity, however, and results in a $\Delta\text{Alk}:\Delta\text{DIC}$ ratio of 0 (Table 4-1, Eq. 4-5), and therefore should decrease the CO_2 buffering capacity of the pore waters since $\text{Alk}:\text{DIC}$ ratios are proportional to buffering capacity (Sabine et al., 2004) .

Additionally, methane produced by either CO_2 reduction or acetate fermentation may subsequently be oxidized through aerobic



or anaerobic pathways



Because anaerobic oxidation of methane (AOM) produces HCO_3^- and reduces SO_4^{2-} to sulfide, it results in a $\Delta\text{Alk}:\Delta\text{DIC}$ value of 3 because every mole of sulfate reduced increases alkalinity by 2 moles (Eq. 4-14), and HCO_3^- is included in both DIC and alkalinity (Eq. 4-11 and 4-13). In contrast, aerobic oxidation results in a $\Delta\text{Alk}:\Delta\text{DIC}$ ratio of 0 because no alkalinity is produced (Eq. 4-18).

To assess the controls of carbonate chemistry in siliciclastic STEs where alkalinity is likely to be determined by the distribution of redox reactions rather than CaCO_3 saturation, I report dissolved gas concentrations and redox-sensitive solutes

(NO₃, Fe(II), and HS⁻) at three siliciclastic STEs bordering Indian River Lagoon, Florida (EGN, BRL, and RWP; Fig. 1-3). I isolate the impacts of reactions from those due to mixing by the use of salinity-based conservative mixing models, and consider that changes in CO₂ concentrations reflect production from organic carbon remineralization, but may also reflect changes in DIC speciation from alteration of pore water buffering capacity. If changes in buffering capacity results in changes in CO₂ concentrations, CO₂ concentrations should be altered as well the proportion of DIC as CO₂ and Alk:DIC ratios. Because reactions have disparate impacts on Alk:DIC ratios (Table 4-1), I assess which reactions control gas distributions by comparing compare zones of changes in DIC and alkalinity to zones delineated by reactions outlines in Table 4-1. I also compare the ratios of changes in DIC and alkalinity ($\Delta\text{Alk}:\Delta\text{DIC}$) in STE samples to those of reaction stoichiometry. These results are used to evaluate controls of CO₂ concentrations in siliciclastic STEs, which is critical for determining the role of SGD on coastal carbon cycles.

Methods

I collected samples from multi-level piezometers that had previously been installed at EGN, RWP and BRL sites (Fig. 1-3; see Chapter 1 for thorough site description). Briefly, piezometers were installed in 2004 at EGN and during May 2014-September 2015 at RWP and BRL. At EGN, sampled piezometers were installed at 0, 10, and 20 m offshore (EGN-0, EGN-10, EGN-20), at RWP were 10, 20, and 35 m offshore (RWP-10, RWP-20, RWP-35) and at BRL were 1, 11, 21, and 45 m offshore (BRL-1, BRL-11, BRL-21, BRL-45; piezometer schematic illustrated in Fig. 1-2). Samples described in this study were collected in May, 2016.

Sample Collection

Sampling was accomplished by pumping pore water to the surface through a 0.5 cm diameter flexible PVC tube attached to the multisampler ports. A YSI Pro-Plus sensor was installed in an overflow cup in-line with the tubing to measure salinity, temperature, pH, dissolved oxygen (DO), and oxidation-reduction potential (ORP). Although instrumented with a DO sonde, hydrogen sulfide interfered with DO measurements, and thus I lack reliable DO concentration measurements. Once all of these parameters were stable, samples were filtered through 0.45 μm trace-metal grade Geotech medium capacity disposable canister filters into sample vials. Samples for cations and anions were collected in HDPE bottles; cation samples were preserved with trace metal grade nitric acid ($\text{pH} < 2$) while no preservative was added to anion samples. DIC samples were filtered at 0.2 μm directly into glass vials and sealed tightly with no headspace.

Redox-sensitive solutes, Fe(II) and hydrogen sulfide, were measured on 0.45- μm filtered water in the field immediately after pumping from the multisampler tubing using colorimetric methods. Fe(II) was measured using the ferrozine method (Stookey, 1970). Samples were measured in triplicate. Water was sampled from the flowing pore water stream and 1 mL of ferrozine was immediately added to 10 mL of sample and agitated to mix. The absorbance of developed color was measured after 5 minutes of reaction with a Hach DR 890 portable colorimeter at 560 nm. Blanks were prepared with ferrozine and distilled water and measured before each triplicate pore water sample. Measured absorbance values were converted to concentrations with laboratory calibrations prepared with Fe(II) standards, utilizing an aliquot of the prepared ferrozine that was used in the field. Sampling for hydrogen sulfide occurred simultaneously with

the Fe sampling and H₂S was measured immediately in triplicate using the methylene blue method according to US EPA methods outlined in Hach (2015). Precision is reported at 0.1 mg/L.

Gas samples were collected via headspace extractions. Unfiltered water was pumped into the bottom of 500 mL bottles until they overflowed and immediately capped with rubber stoppers fitted with two 3-way inlet valves. 60 mL of water was extracted from one inlet and replaced with 60 mL of CO₂-free N₂ gas. Bottles were shaken for 2 minutes to equilibrate headspace gas with water, and headspace gas was extracted and immediately injected into pre-evacuated 60 ml glass serum bottles. Samples were stored at room temperature until analysis within one week of collection. Method check standards were collected by injecting gases of known concentrations of CO₂ and CH₄ into evacuated vials and treated identically to samples.

Laboratory Methods

Gas samples were analyzed for CO₂ and CH₄ concentrations, and $\delta^{13}\text{C-CO}_2$ and $\delta^{13}\text{C-CH}_4$ on a Picarro cavity ring-down spectrometer. Carbon isotopic compositions are reported in reference to Vienna Pee Dee Belemnite (VPDB). Because hydrogen sulfide interferes with CO₂ concentrations and $\delta^{13}\text{C-CO}_2$ measurements, sample gas was passed through an in-line elemental copper scrubber before analysis (Malowany et al., 2015). The error on check standards was less than 10%.

Anion and cation concentrations were measured on an automated Dionex ICS-2100 and ICS-1600 Ion Chromatograph, respectively. Error on replicate analyses was less than 5%. DIC concentrations were measured on a UIC (Coulometrics) 5011 CO₂ coulometer coupled with an AutoMate Preparation Device. Samples were acidified and

the evolved CO₂ was carried through a silver nitrate scrubber to the coulometer where total C was measured. Accuracy was calculated to be ±0.1 mg/L.

Data Processing

Dissolved gas concentrations

Headspace dissolved gas concentrations are reported in dissolved raw ppm values to facilitate comparison with atmospheric gas concentrations as well as molar concentrations to allow for stoichiometric modeling. Conversion to molar units followed the methods outlined in Bastviken et al., (2004). To solve for the moles of gas originally dissolved in solution, I first converted measured gas concentration (ppm) in headspace to moles:

$$n_g = \frac{P_x * V_g}{R * T} \quad (4-20)$$

Where n_g equals the moles (n) of gas in the gaseous phase, P_x is the measured partial pressure of CH₄ or CO₂ (atm), V_g is the volume of headspace gas (L), R is the common gas constant (0.0821 L atm K⁻¹ mol⁻¹) and T is the temperature (K), here taken as 298.15 K (25°C). The number of moles of gas dissolved in the aqueous phase (n_{aq}) is calculated by:

$$n_{aq} = C_{aq} * V_{aq} = P_x * K_H * V_{aq} \quad (4-21)$$

where C_{aq} is aqueous concentration and V_{aq} is aqueous volume (500 mL minus 60 mL replaced by headspace gas to give a total volume of 440 mL), and K_H is Henry's Law constant (M atm⁻¹). The value of K_H was taken at 25°C as 1.4×10^{-3} for CH₄, and as 3.5×10^{-2} for CO₂ (Lide and Frederikse, 1995). The final concentration of dissolved gas in water samples (C_{aq}) was then calculated as the sum of the number of moles of gas in aqueous and gaseous phases divided by the aqueous volume:

$$C_{\text{aq}} = \frac{n_{\text{g}} + n_{\text{aq}}}{V_{\text{aq}}} \quad (4-22)$$

CH₄ oxidation was calculated using the isotopic method outlined in Mahieu et al. (2008) and Preuss et al. (2013). The fraction of oxidized methane (f_{ox}) in an open system is given by:

$$f_{\text{ox}} = \frac{\delta_{\text{E}} - \delta_{\text{P}}}{1000 \cdot (\alpha_{\text{ox}} - \alpha_{\text{trans}})} \quad (4-23)$$

where δ_{E} is the measured $\delta^{13}\text{C-CH}_4$ value for each pore water sample, δ_{P} is $\delta^{13}\text{C-CH}_4$ of produced methane, α_{ox} is the oxidation fractionation factor, and α_{trans} is a fractionation factor resulting from transportation of CH₄. While the exact value of δ_{P} is unknown, diagenetic alteration of $\delta^{13}\text{C-CH}_4$ values through oxidation or transport only enrich $\delta^{13}\text{C-CH}_4$ signatures, therefore the value of δ_{P} is take as the most depleted $\delta^{13}\text{C-CH}_4$ signature per STE site, because it is likely the least impacted by diagenetic alteration. Literature-reported values for α_{ox} range between 1.003 and 1.049. I calculate the fraction of oxidized methane with the largest fraction factor ($\alpha_{\text{ox}} = 1.049$), (Mahieu et al., 2008), which will give the minimum amount of CH₄ oxidation required to explain the observed variations in $\delta^{13}\text{CH}_4$, and thus is a conservative estimate for CH₄ oxidation. Literature-reported values for α_{trans} vary from 1 for advection-dominated systems to 1.0178 for diffusion-dominated porous media (Visscher et al., 2004; Mahieu et al., 2008; Preuss et al., 2013). Based on Roy et al., (2011), I assume that transport is advection dominated and thus assume $\alpha_{\text{trans}} = 1$.

The concentration of oxidized methane (CH_{4-ox}) is derived by solving the set of equations:

$$\text{CH}_{4\text{-produced}} = \text{CH}_{4\text{-measured}} + \text{CH}_{4\text{-ox}} \quad (4-24)$$

$$\text{CH}_{4\text{-ox}} = f_{\text{ox}} * \text{CH}_{4\text{-produced}} \quad (4-25)$$

where the measured concentration of methane ($\text{CH}_{4\text{-measured}}$) is considered to represent the original concentration of produced methane ($\text{CH}_{4\text{-produced}}$) minus the oxidized portion $\text{CH}_{4\text{-ox}}$.

Modeling

I used concentrations of major cations and anions, pH, temperature, and DIC concentrations to model the alkalinity and speciation of carbonate ions in PHREEQc using the PHREEQc database (Parkhurst, 1995). Alkalinity was estimated from the charge balance of the model input (Parkhurst, 1997).

To assess the impacts due to mixing versus reactions in the STE, I constructed salinity-based conservative mixing models between the freshest STE sample at each site and surface saltwater. Mixing models assume that the freshest groundwater sample is representative of groundwater with the least impact from diagenetic reactions due to freshwater-saltwater mixing in the STE. The models use lagoon water compositions as the saltwater end member.

Results

Dissolved Gas Concentrations and Carbonate Chemistry

Dissolved CO_2 and CH_4 concentrations in STE pore water samples are elevated above surface water concentrations at all STE sites, and gas concentrations are higher in fresh portions of STEs (Fig. 4-1). CO_2 concentrations reach highest concentrations in freshest sampled of BRL (up to 120,000 ppm) and EGN (up to 46,000 ppm; Fig. 4-1a). The maximum CO_2 concentration at RWP (22,000 ppm) occurs in a sample with salinity of approximately 10. Surface water CO_2 concentrations are elevated above atmospheric CO_2 concentrations (currently around 400 ppm) at all sites and measure 1030 ppm at

BRL, 2130 ppm at EGN, and 1850 ppm at RWP (Fig. 4-1b). CH₄ concentrations are highest in freshwater portions of STEs at BRL and RWP, but in brackish portions of EGN (Fig. 4-1c). At BRL, CH₄ reaches concentrations of 29,000 ppm at BRL-1, while concentrations reach 58,960 ppm at RWP-20. At EGN, maximum CH₄ occurs at EGN-20 and reaches 390 ppm. Salinity at this pore water interval is 16.5. All STE samples and surface water samples have CH₄ concentrations higher than atmospheric concentrations of approximately 2 ppm (Fig. 4-1d).

Conservative mixing models between freshest pore water and surface saltwater indicate that DIC, alkalinity, and Ca are predominantly produced at all three STE sites (Fig. 4-2a, b, and c). A high degree of variability of CO₂ concentrations with salinity occur at BRL-1 and EGN-0, which are indicated separately from other samples due to their distinct chemistries. At BRL-1, which is located at the mangrove-colonized shoreline, CO₂ concentrations are greater than expected from conservative mixing, and the proportion of DIC as CO₂ increases while Alk:DIC ratios decrease relative to salinity. At EGN-0, CO₂ concentrations are lower than conservative mixing, while the proportion of DIC as CO₂ decreases with salinity, and Alk:DIC ratios increase (Fig. 4-2d, g, and h). Apart from these changes in chemistry at EGN-0 and BRL-1, CO₂ concentrations generally decrease with salinity at all seepage faces, as well as the proportion of DIC as CO₂, while Alk:DIC ratios increase (Fig. 4-2d, g, and h).

Distribution of Redox Reactions

Salinity, ORP, and the distributions of redox-sensitive species are displayed in Fig. 4-3. ORP values are all negative except for the shoreline piezometer of EGN. This site also contains up to 200 μM nitrate, while maximum NO₃ concentrations are only 25 μM at BRL and 2.5 μM at RWP. Fe(II) is present at highest concentrations near EGN-

20(40 μM) and BRL-11 (35 μM). Hydrogen sulfide (HS^-) exhibits concentrations up to 60 μM at EGN, directly overlying the zone of $\text{Fe}(\text{II})$ production. BRL contains up to 120 μM HS^- at the shoreline piezometer, which is colonized by mangroves, as well as shallow sediments of the piezometer 45 m offshore. At RWP, HS^- is produced in shallow sediments in piezometers 10 and 35 m offshore, as well as in deep sediments 35 m offshore. CH_4 concentrations at EGN reach maximum concentrations of 3 μM at EGN-22.5 in brackish pore waters (salinity=22.4), but reach 200 μM in freshwaters at BRL-1, and 400 μM at RWP-20. CO_2 concentrations are highest at the nearshore piezometer for all seepage faces, and concentrations decrease in magnitude from 6500 μM at BRL, 1600 μM at EGN, and 800 μM RWP.

The difference between measured DIC, alkalinity and Ca concentrations and the salinity-based conservative mixing lines depicted in Fig. 4-2a, b and c are expressed as ΔDIC , ΔAlk , and ΔCa (Fig. 4-4). Values of ΔAlk compared to ΔCa , and NO_3^- , $\text{Fe}(\text{II})$ and HS^- concentrations indicate similarities in zones of alkalinity production and ΔCa values at EGN, while zones correspond more closely to HS^- concentrations at BRL and RWP (Fig. 4-3).

CH_4 Concentrations and Oxidation

At all seepage faces, $\delta^{13}\text{C}-\text{CH}_4$ signatures are lowest where CH_4 concentrations are highest (Fig. 4-5a). The lowest $\delta^{13}\text{C}-\text{CH}_4$ signatures at each seepage face are measured at -56.97‰ at BRL, -57.70‰ at EGN and -78.89‰ at RWP. I assume this low value represents the $\delta^{13}\text{C}-\text{CH}_4$ value of methane production prior to fractionation by oxidation because oxidation and transport of CH_4 by diffusion or advection enriches the residual CH_4 pool and leads to isotopically heavier values (Whiticar, 1999). The quantity

of CH₄ oxidized is highest at low-salinity samples, reaching maximum concentrations of 45 μM at RWP, 30 μM at BRL, and 8 μM at EGN (Fig. 4-5b).

ΔAlk:ΔDIC Ratios Compared to Reaction Stoichiometries

Plots of ΔAlk and ΔDIC calculated from conservative mixing models compared to the ratios of ΔAlk to ΔDIC from biogeochemical reactions (Table 4-1) reflect which reaction may dominate the changes in pore water concentrations. Most saline pore water samples from all sites plot slightly under the 1:1 line corresponding to values expected from sulfate reduction and denitrification (Fig. 4-6). Ratios of freshwater samples from EGN-0 and BRL-1 plot farther from the 1:1 line. ΔAlk:ΔDIC ratios are closer to the value expected from CaCO₃ dissolution at EGN-0 and ΔAlk:ΔDIC ratios are close to those expected from methanogenesis at BRL.

Most pore water Alk:DIC ratios are low compared to surface water values (Fig. 4-7). Comparison of observed Alk:DIC ratios to ratios predicted by conservative mixing between fresh and saltwater end members indicates that pore waters at EGN-0 and EGN-10 have relatively higher Alk:DIC ratios than expected from conservative mixing, while pore waters at BRL-1 have relatively lower Alk:DIC ratios than those predicted by conservative mixing (Fig. 4-7).

Discussion

CO₂ and CH₄ concentrations elevated above surface water and atmospheric concentrations (Fig. 4-1) suggest that SGD is a source of both CO₂ and CH₄ to surface waters and the atmosphere. While freshwater appears to be one source of CO₂ and CH₄ for STEs due to negative relationships with salinity (Fig. 4-1) deviations from conservative mixing models indicate that concentrations are modified by reactions. The

relative magnitudes of these reactions should control changes in CO₂ concentrations and DIC speciation. Because of differences in chemical reactions in fresh compared to marine portions of the STE, I first discuss controls of changes in CO₂ speciation in samples with salinity <15, particularly at BRL and EGN where sharp chemical gradients with salinity lead to large changes in CO₂ concentrations. I subsequently discuss processes in portions of STEs where salinity >15. Because the overall impact of reactions on CO₂ fluxes from SGD depends on net changes in alkalinity and DIC that result from a range of biogeochemical reactions, I compare the residuals of conservative mixing models of alkalinity and DIC (ΔAlk and ΔDIC), to ratios expected based on each reaction stoichiometry shown in Table 4-1. These results elucidate the biogeochemical controls of CO₂ concentrations and DIC speciation in siliciclastic STEs, and may be used to predict potential impacts of SGD from siliciclastic STEs on surface water carbon budgets.

Impacts on CO₂ Concentrations and DIC speciation

Lower salinity portions of STEs (salinity < 15)

Conservative mixing models indicate that reactions consume CO₂ at EGN-0, but produce CO₂ at BRL-1 and mid-salinity samples at RWP (Fig. 4-2d). The largest differences in chemical composition from conservative mixing values occur at the EGN and BRL shoreline piezometers (EGN-0 and BRL-1). Along with changes in CO₂ concentrations, the proportion of DIC as CO₂ decreases at EGN and increases at BRL and RWP, and the Alk:DIC ratios increase at EGN-0 and decrease at BRL-1 and RWP. These changes suggest that deviation of CO₂ concentrations from the conservative mixing line is in part determined by changes in the buffering capacity of pore water, but

buffering capacity increases at EGN, thus sequestering CO₂ as HCO₃⁻ or CO₃²⁻, and decreases at BRL and RWP, causing increases in CO₂ concentrations.

EGN-0 is distinct from other locations because it has positive ORP values and high concentrations of NO₃⁻ (Fig. 4-3), which may drive denitrification. Further offshore from EGN-0, NO₃ concentrations decrease along with ORP values suggest that NO₃ may be consumed by denitrification, but a more detailed assessment of N transformation is required to confirm the role of denitrification. Denitrification would produce alkalinity and DIC ($\Delta\text{Alk}:\Delta\text{DIC}$) at a ratio of approximately 0.8 (Table 4-1; Eq. 4-1b). Because the Alk:DIC ratio in the freshwater end member of EGN is around 0.5 (Fig. 4-2h), denitrification could increase alkalinity relative to DIC and thus the pore water buffering capacity and promote sequestration of CO₂ as DIC. This could account for the increase in Alk:DIC ratios from the freshwater end member at EGN and contribute to the increase in Alk:DIC observed at EGN-0 (ranging from 0.5-0.9; Fig 4-2h). Additional reactions may contribute, however, including CaCO₃ dissolution. ΔCa concentrations at EGN-0 are between 1-2 mM (Fig. 4-4). The distribution of ΔCa in the seepage face closely aligns with ΔAlk (Fig. 4-4) and suggests that CaCO₃ dissolution is a source of alkalinity. Because CaCO₃ dissolution results in a $\Delta\text{Alk}:\Delta\text{DIC}$ ratio of 2, well above the Alk:DIC ratio of the EGN freshwater end member, it could result in the increasing Alk:DIC ratios observed at EGN-0 and promote CO₂ sequestration.

Reactions at the BRL shoreline piezometer (BRL-1) result in CO₂ concentrations (Fig. 4-2d) and proportion of DIC as CO₂ (Fig. 4-2g) elevated above values expected from conservative mixing. These reactions also result in Alk:DIC ratios lower than expected from conservative mixing (Fig. 4-2h). Alk:DIC ratios at BRL-1 are low (0.4-0.6)

compared to the freshwater end member (0.85; Fig. 4-2h), which could reflect alteration by diagenetic reactions that produce a $\Delta\text{Alk}:\Delta\text{DIC}$ ratio at 0.4 or lower. Elevated HS^- and CH_4 concentrations at BRL-1 suggest that sulfate reduction and methanogenesis occur, and are likely fueled by high organic carbon concentrations (Fig. 4-3). Sulfate reduction has a $\Delta\text{Alk}:\Delta\text{DIC}$ ratio of approximately 1 (Table 4-1, Eq. 4-4), and therefore would not contribute to the decrease in Alk:DIC ratios from the freshwater end member value of 0.85. Methanogenesis produces DIC but not alkalinity, and could lower Alk:DIC ratios (Table 4-1, Eq. 4-5). However, the magnitude of CH_4 production at BRL-1 (100-200 μM ; Fig. 4-2e) is small compared to the CO_2 produced (2000-4000 μM ; Fig. 4-2d) and methanogenesis would therefore not provide all additional CO_2 , and would only contribute to the reduction. Other reactions could include sulfide or iron oxidation, which may be catalyzed by mangrove roots (Lee, 1999). These reactions consume alkalinity but do not impact DIC (Table 4-1, Eq. 4-7 and 4-8), and thus could also lower Alk:DIC ratios at BRL-1.

Similar to BRL, methanogenesis or sulfate reduction coupled with sulfide oxidation could lead to the elevated CO_2 concentrations at mid-salinities of RWP. Samples that plot above the conservative mixing line have salinities of approximately 10, and are also the shallowest samples at RWP-10 and RWP-20, which are located at depths of 60 cm and 20 cm below the sediment water interface, respectively. The high CH_4 concentrations at RWP (Fig. 4-3) suggest that methanogenesis contributes to the increase in Alk:DIC ratio and elevated CO_2 concentrations. Alternatively, since these samples are relatively shallow, iron and/or sulfide oxidation may also play a role. For instance, bioirrigation is known to mix surface water to depths of at least 25-35 cm at

Indian River Lagoon (Martin et al., 2006). However, low Fe(II) concentrations relative to sulfide concentrations suggest that sulfide oxidation may contribute more than Fe oxidation. Decreases in Alk:DIC ratios from CH₄ oxidation is less likely to play a role because it contributes an Alk:DIC ratio of 3:1 (Table 4-1, Eq. 4-9).

Higher salinity portions of STEs (salinity > 15)

Saline portions of STEs (salinity >15) have more homogeneous distributions of CO₂, DIC, and alkalinity than fresher portions, which are reflected in $\Delta\text{Alk}:\Delta\text{DIC}$ ratios that cluster around the 1:1 line (Fig. 4-4). In general, Alk:DIC ratios increase from ratios found in the freshwater to values around or slightly greater than 1 in the most saline STE samples and in surface water. These increases in Alk:DIC ratios may be due to sulfate reduction, because the distribution of ΔDIC and ΔAlk in the saline portions of BRL and RWP (Fig. 4-4) correspond to zones delineated by elevated sulfide concentrations (Fig. 4-3). Sulfate reduction has a $\Delta\text{Alk}:\Delta\text{DIC}$ ratio of approximately 1, which is close to the Alk:DIC ratios observed in surface waters and in the most saline samples of STEs. Sulfate reduction is likely the dominant redox reaction in saline portions of STEs because of low potential for aerobic respiration (evidenced by negative ORP values), low potential for denitrification due to low NO₃ concentrations, low Fe(II) concentrations compared to HS⁻ concentrations, and low CH₄ concentrations due to the inhibition of methanogenesis by sulfate (Fig. 4-2h).

$\Delta\text{Alk}:\Delta\text{DIC}$ ratios

The likely controls of carbonate chemistry as delineated by the above discussion for EGN-0 (predominantly controlled by denitrification and CaCO₃ dissolution), and BRL-1 (predominantly controlled by methanogenesis, sulfate reduction and sulfide

oxidation) are supported by comparison of $\Delta\text{Alk}:\Delta\text{DIC}$ ratios to those predicted by reactions in Table 4-1 (Fig. 4-6). Samples from EGN-0 have $\Delta\text{Alk}:\Delta\text{DIC}$ ratios greater than 1 (Fig. 4-6a), and plot between the $\Delta\text{Alk}:\Delta\text{DIC}$ expected from denitrification and CaCO_3 dissolution. This high $\Delta\text{Alk}:\Delta\text{DIC}$ ratio should promote the sequestration of CO_2 as HCO_3^- or CO_3^{2-} . A reduction of pore water buffering capacity at BRL-1 is shown by $\Delta\text{Alk}:\Delta\text{DIC}$ ratios near zero, which would be expected from methanogenesis but could alternatively result from a combination of processes including sulfate reduction, methanogenesis, and iron/sulfide oxidation (Fig 4-6a). All of these processes are plausible at BRL-1 considering elevated concentrations of CH_4 and HS^- (Fig. 4-3). At this site with lower buffering capacity would result in elevated CO_2 concentrations and possibly fluxes of CO_2 .

In contrast with freshwater samples of BRL and EGN, most saline samples plot near or slightly lower than the 1:1 line, or between the ratios expected from sulfate reduction and denitrification (Fig. 4-6b). Because low or non-detectable NO_3^- concentrations occur in all but EGN-0 samples, denitrification is unlikely to impart its ratio on saline samples. Moreover, up to 1.5 mM of DIC production and 2 mM of alkalinity production is observed for saline samples of BRL and EGN. This production of DIC via denitrification would require 1.2 mM of NO_3^- , assuming the stoichiometry of denitrification in Table 4-1, which is six times higher than the highest NO_3^- concentrations measured at EGN-0. Therefore, saline $\Delta\text{Alk}:\Delta\text{DIC}$ ratios are more likely controlled by sulfate reduction, although other processes, such as methanogenesis or sulfide oxidation, could also contribute.

Redox and Mineralogical Controls of Dissolved Gas Concentrations

As discussed above, the distribution of redox reactions controls carbonate chemistry because of variations in the production of DIC relative to alkalinity. Although biogeochemical processes in freshwater portions of STEs alter carbonate chemistry, particularly at BRL-1 and EGN-0, they have contrasting impacts on CO₂ concentrations. I hypothesize that these differences result from variability in the distribution of CaCO₃ in sediment, as well as differences in redox potential between EGN and BRL freshwater. Specifically, EGN-0 appears to have CaCO₃ mineral phases to dissolve and buffer CO₂ production, while the CaCO₃ content of sediment may be lower at RWP and BRL. Additionally, freshwater at EGN has positive ORP values and contains NO₃, contrasting with BRL and RWP, where freshwater is reducing and supports methanogenesis.

Redox potential may determine the impact of reactions on carbonate chemistry because denitrification has a $\Delta\text{Alk}:\Delta\text{DIC}$ ratio of 0.8, greater than most freshwater samples, and would increase the buffering capacity of pore waters. The relatively high redox potential at EGN-0 appears to be related to the concentration of organic carbon in freshwater, which is low at EGN compared to other sites (Fig. 4-3). Low organic carbon concentrations allow the persistence of terminal electron acceptors such as oxygen and nitrate due to lower organic carbon remineralization rates, and would allow for denitrification to be a dominant redox pathway. Relatively low redox potentials at BRL-1 may result in low $\Delta\text{Alk}:\Delta\text{DIC}$ ratios due to the contributions of methanogenesis, which has a $\Delta\text{Alk}:\Delta\text{DIC}$ ratio of 0, though sulfate reduction coupled with sulfide oxidation would result in low $\Delta\text{Alk}:\Delta\text{DIC}$. This coupling is plausible where CO₂ production occurs at BRL in mangrove-dominated shorelines and at RWP surficial sediments. At these locations,

sulfate reduction is evident due to elevated sulfide concentrations (Fig. 4-3), but are also sites of plausible sulfide oxidation which may be catalyzed by mangrove roots (Lee, 1999) or oxidation of sulfide via the introduction of oxygen to sediments through bioturbation (Martin et al., 2006).

I quantify the changes in DIC and alkalinity due to the combination of reactions (denitrification, iron reduction, sulfate reduction, methanogenesis, methane oxidation, and CaCO_3 dissolution) using reaction stoichiometry (Table 4-1) in order to determine if the sum of these reactions yields a $\Delta\text{Alk}:\Delta\text{DIC}$ ratio that corresponds to $\Delta\text{Alk}:\Delta\text{DIC}$ ratios determined via conservative mixing models (Fig. 4-2a and b). For many samples, this stoichiometric analysis does not yield results similar to the magnitude or sign of ΔDIC and ΔAlk based on conservative mixing models in Fig. 4-2 (Tables 4-2 and 4-3, Fig. 4-8). These differences may be due to the lack of inclusion of iron and sulfide oxidation in the stoichiometric model, which are known to occur at EGN sediments and likely occur at BRL and RWP, but require further geochemical modeling to estimate their relative importance. Additionally, uncertainty is introduced due to the use of salinity-based conservative mixing models because of the considerable variability observed in composition of freshwater entering the STE, particularly at EGN and BRL. The selection of the freshest STE sample at each site as the freshwater end member allows an assessment of the impact of reactions using salinity as a tracer. However, variability in freshwater chemistry may result in mixing models that over- or under-predict the impacts of reactions. While quantitative assessments of the role of redox reactions in carbonate chemistry may not be ideal for this study setting due to the sensitivity of end member selection, the qualitative assessments based on $\Delta\text{Alk}:\Delta\text{DIC}$ ratios suggest that

specific reactions control carbonate chemistry. Moreover, the roles of these reactions (e.g. denitrification and CaCO_3 at EGN-0, and combined sulfate reduction, sulfide oxidation, and methanogenesis at BRL-1) are corroborated by the distribution of solutes in Fig. 4-3.

Implications for CO_2 and CH_4 Fluxes

Concentrations of CO_2 and CH_4 in all three STEs are orders of magnitude higher than surface water concentrations, and surface water concentrations are elevated above atmospheric concentrations (Fig. 4-1). Despite the apparent increased buffering capacity of pore water with increasing salinity, the STE is still a source of CO_2 as well as CH_4 to surface waters and likely to the atmosphere.

The impact of SGD on surface water chemistry depends on the difference between SGD Alk:DIC ratios and surface water Alk:DIC ratios. For instance, if STE samples have Alk:DIC ratios lower than surface water ratios, SGD should decrease the CO_2 buffering capacity of surface water. This decrease will limit uptake of anthropogenic atmospheric CO_2 (Egleston et al., 2010) or CO_2 from other sources such as organic matter remineralization (Liu et al., 2017). Most pore water in the Indian River Lagoon STEs have Alk:DIC ratios lower than surface waters (Fig. 4-7) because of low Alk:DIC ratios in the freshwater (Fig. 4-2h) compared to surface saltwater. Despite multiple diagenetic pathways (sulfate reduction, Fe reduction, denitrification) that produce Alk:DIC ratios at or above molar ratios of 1, the combined impact of reactions is insufficient to produce Alk:DIC ratios in pore waters that are greater than surface water values (Fig. 4-6). Higher DIC exports relative to alkalinity have been noted in aerobic siliciclastic STEs (Liu et al., 2017), and researchers concluded that SGD reduces the buffering capacity of surface water. In aerobic settings, this result is not surprising

because aerobic respiration requires coupling with CaCO_3 dissolution to generate alkalinity and increase buffering capacity (Kuivila and Murray, 1984). The results suggest that SGD from siliciclastic STEs should decrease CO_2 buffering capacity of surface water unless sufficient CaCO_3 is available to buffer pore waters from increased H_2CO_3 concentrations (Kuivila and Murray, 1984). This effect has been noted in other groundwater systems and CO_2 fluxes from carbonate aquifers may be several times lower than siliciclastic due to increased buffering capacity following CaCO_3 dissolution (Khadka et al., 2014).

Conclusions

The results of this study suggest that the distribution of redox reactions with salinity gradients in STEs is critical for CO_2 and CH_4 concentrations. Reactions in freshwater portions of STEs both increase and decrease the sequestration of CO_2 , depending on the redox status of pore waters. $\Delta\text{DIC}:\Delta\text{Alk}$ ratios compared to reaction stoichiometries reveals that most brackish to saline pore waters are impacted by sulfate reduction with potential contributions of methanogenesis or sulfide oxidation, leading to $\Delta\text{Alk}:\Delta\text{DIC}$ ratios slightly less than 1. Fresh pore waters exhibit a larger deviation from the 1:1 ratio, and reactions both increase and decrease the Alk:DIC ratios of STE pore waters. These results suggest that, despite the production of alkalinity through multiple anaerobic pathways, SGD from STEs lacking CaCO_3 minerals are likely to decrease the CO_2 buffering capacity of surface water, which could lead to greater CO_2 fluxes from surface waters to the atmosphere. Given the importance of estuaries and the coastal ocean in the global carbon cycle, carbon fluxes from SGD may represent an understudied but important net source or net sink of CO_2 . Whether SGD serves as a

net source or sink of CO_2 may be ultimately determined by the abundance of CaCO_3 minerals available to buffer pore waters against CO_2 generated by organic carbon remineralization.

Table 4-1. Impact of redox pathways and biogeochemical reactions on alkalinity and DIC.

Equation	Reaction	$\Delta\text{Alkalinity}:\Delta\text{DIC}$
4-1	Aerobic respiration $(\text{CH}_2\text{O})_{106}(\text{NH}_3)_{16}\text{H}_3\text{PO}_4 + 138\text{O}_2 \rightarrow$ $106\text{CO}_2 + 122\text{H}_2\text{O} + 16\text{HNO}_3 + \text{H}_3\text{PO}_4$	$-(16)(\text{NO}_3)/((106)(\text{CO}_2)) = -0.15$ ¹
4-2	Denitrification $(\text{CH}_2\text{O})_{106}(\text{NH}_3)_{16}\text{H}_3\text{PO}_4 + 84.8\text{HNO}_3 \rightarrow$ $106\text{CO}_2 + 42.4\text{N}_2 + 148.4\text{H}_2\text{O} + 16\text{NH}_3 +$ H_3PO_4	$+(84.8)(\text{NO}_3)/((106)(\text{CO}_2)) = 0.8$ ¹
4-3	Iron reduction $(\text{CH}_2\text{O})_{106}(\text{NH}_3)_{16}\text{H}_3\text{PO}_4 + 424\text{FeOOH} +$ $848\text{H}^+ \rightarrow 106\text{CO}_2 + 742\text{H}_2\text{O} + 424\text{Fe}^{+2} +$ $16\text{NH}_3 + \text{H}_3\text{PO}_4$	$+(848)(\text{H}^+)/((106)(\text{CO}_2)) = 8$ ¹
4-4	Sulfate reduction $(\text{CH}_2\text{O})_{106}(\text{NH}_3)_{16}\text{H}_3\text{PO}_4 + 53\text{SO}_4^{2-} + 106\text{H}^+$ \rightarrow $106\text{CO}_2 + 106\text{H}_2\text{O} + 53\text{H}_2\text{S} + 16\text{NH}_3 + \text{H}_3\text{PO}_4$	$+(53*2)(\text{SO}_4)/((106)(\text{CO}_2)) = 1$ ¹
4-5	Methanogenesis $(\text{CH}_2\text{O})_{106}(\text{NH}_3)_{16}\text{H}_3\text{PO}_4 \rightarrow$ $53\text{CO}_2 + 53\text{CH}_4 + 16\text{NH}_3 + \text{H}_3\text{PO}_4$	$0/53(\text{CO}_2) = 0$
4-6	CaCO ₃ dissolution $\text{CaCO}_3 \rightarrow \text{CO}_3^{2-} + \text{Ca}^{2+}$	$(2*1)\text{Ca}^{2+}/1(\text{CO}_3^{2-}) = 2$
4-7	Sulfide oxidation ² $\text{H}_2\text{S} + 2\text{O}_2 \rightarrow \text{SO}_4^{2-} + 2\text{H}^+$	$-(2*1)(\text{SO}_4^{2-})/0 = \infty$
4-8	Fe oxidation ² $4\text{Fe}^{2+} + \text{O}_2 + 6\text{H}_2\text{O} \rightarrow 4\text{FeOOH} + 8\text{H}^+$	$-(8)(\text{H}^+)/0 = \infty$
4-9	AOM $\text{CH}_4 + \text{SO}_4^{2-} \rightarrow \text{HCO}_3^- + \text{HS}^- + \text{H}_2\text{O}$	$(2*1)(\text{SO}_4^{2-}) + 1(\text{HCO}_3^-) / 1(\text{HCO}_3^-) = 3$

¹ Chen and Wang, 1999

² Anderson and Schiff, 1987

Table 4-2. Δ DIC concentrations compared to concentrations produced from denitrification (DN-DIC; Eq. 4-2), iron reduction (FeR-DIC; Eq. 4-3), sulfate reduction (SR-DIC; Eq. 4-4), methanogenesis (Methane-DIC; Eq. 4-5), methane oxidation (Meth_{ox}-DIC; Eq. 4-9) and CaCO₃ dissolution (CaCO₃-DIC; Eq. 4-6). All data are reported in μ M. Sample depths are cm below the sediment-water interface.

Piezometer	Depth (cm)	SAL (PSU)	Δ DIC	DN-DIC	FeR-DIC	SR-DIC	Methane-DIC	Meth _{ox} -DIC	CaCO ₃ -DIC
BRL-1	20	6.13	3900	0	0	26	103	7	2300
BRL-1	30	2.68	4600	0	0	27	171	3	1300
BRL-1	60	2.65	5700	0	0	37	206	3	-900
BRL-1	100	2.19	4300	0	0	68	109	9	800
BRL-11	20	1.7	-500	2	9	0	4	3	2300
BRL-11	60	1.69	0	0	9	0	2	6	0
BRL-11	100	1.71	100	32	9	0	2	30	0
BRL-11	150	1.69	0	2	9	1	0	0	0
BRL-11	180	1.69	-100	0	8	0	1	1	100
BRL-11	210	1.76	100	0	8	1	5	2	100
BRL-11	210	1.81	0	34	8	0	2	3	200
BRL-21	20	5.38	-600	0	6	30	16	1	4100
BRL-21	60	3.57	-200	10	8	20	31	1	5000
BRL-21	91	3.48	0	1	6	16	28	0	1800
BRL-21	150	1.73	200	0	5	1	0	0	300
BRL-21	200	1.72	100	0	6	1	5	1	0
BRL-21	250	1.72	-100	0	7	1	3	1	-100
BRL-45	20	24.56	1900	0	0	46	16	0	600
BRL-45	60	21.48	1700	0	0	45	20	1	1200
BRL-45	120	2.87	-800	0	0	21	2	0	-1500
BRL-45	50	2.49	-700	0	0	1	1	0	-1800
BRL-45	180	2.89	-600	0	0	1	1	0	-1100
BRL-45	210	3.07	-500	0	0	0	1	0	-1000
BRL-45	210	3.02	-500	4	0	1	1	0	800
BRL-45	0	22.33	0	0		0	0	0	0
EGN-0	15	0.76	0	218	0	0	0	0	0
EGN-0	25	0.97	-2400	250	0	0	0	0	0

Table 4-2. Continued

Piezometer	Depth (cm)	SAL (PSU)	Δ DIC	DN-DIC	FeR-DIC	SR-DIC	Methane- DIC	Meth _{ox} - DIC	CaCO ₃ - DIC
EGN-0	95	1.14	1900	206	0	0	0	0	1800
EGN-0	115	1.09	2000	211	0	0	0	0	1800
EGN-10	15	16.2	600	0	1	4	0	0	1600
EGN-10	25	4.07	1000	0	2	2	0	0	1000
EGN-10	75	2.59	1300	0	3	0	0	0	2000
EGN-10	95	0.9	1200	0	0	0	0	0	1200
EGN-10	115	0.9	1200	0	3	0	0	0	1600
EGN-10	115	0.9	1200	0	3	0	0	0	1600
EGN-10	0	23.8	0	0	0	0	0	0	1600
EGN-20	7	25.17	0	0	0	2	0	0	0
EGN-20	15	24.47	200	0	0	14	0	0	0
EGN-20	25	24.35	700	0	1	22	0	0	200
EGN-20	55	22.39	1300	0	10	18	2	0	300
EGN-20	95	16.49	1800	0	9	4	3	0	400
EGN-20	115	16.01	1800	0	1	0	1	0	400
EGN-22.5	36	24.13	700	0	0	35	0	0	800
EGN-22.5	36	25.03	700	0	0	31	0	0	400
EGN-22.5	106	23.23	1600	0	10	1	3	0	200
EGN-22.5	156	22.52	1800	0	6	5	3	8	1000
RWP-10	60	9.05	1800	0	0	19	124	3	500
RWP-10	100	0.45	300	0	0	5	226	2	100
RWP-10	150	0.4	400	0	0	6	283	0	-400
RWP-10	200	0.36	400	0	0	2	0	6	-300
RWP-20	20	11.29	2200	4	1	11	51	6	100
RWP-20	60	0.5	400	0	0	3	312	7	2400
RWP-20	100	0.4	300	0	0	2	411	9	400
RWP-20	200	4	1100	0	0	3	288	5	100
RWP-20	250	0.36	400	0	0	4	261	0	100
RWP-35	10	24.36	5200	0	0	4	0	0	-700
RWP-35	20	24.36	5200	0	0	37	1	0	0

Table 4-2. Continued

Piezometer	Depth (cm)	SAL (PSU)	Δ DIC	DN-DIC	FeR-DIC	SR-DIC	Methane- DIC	Meth _{ox} - DIC	CaCO ₃ - DIC
RWP-35	30	24.26	5200	0	0	30	1	1	200
RWP-35	100	2.23	700	0	0	16	0	25	100
RWP-35	150	1.77	600	0	4	3	216	32	-400
RWP-35	200	5.56	1200	0	0	9	114	43	-400
RWP-35	200	5.53	300	0	0	28	89	0	1300
RWP-35	0	24.37	0	0	0	12	0	0	1000

Table 4-3. Δ Alk concentrations compared to concentrations produced from denitrification (DN-Alk; Eq. 4-2), iron reduction (FeR-Alk; Eq. 4-3), sulfate reduction (SR-Alk; Eq. 4-4), methanogenesis (Methane-Alk; Eq. 4-5), methane oxidation (Meth_{ox}-Alk; Eq. 4-9) and CaCO₃ dissolution (CaCO₃-Alk; Eq. 4-6). All data are in μ eq/L. Sample depths are cm below the sediment-water interface.

Piezometer	Depth (cm)	SAL (PSU)	Δ Alk	DN-Alk	FeR-Alk	SR-Alk	Methane-Alk	Meth _{ox} -Alk	CaCO ₃ -Alk
BRL-1	0.2	6.13	0	0	0	26	103	21	4500
BRL-1	0.3	2.68	300	0	1	27	171	8	2600
BRL-1	0.6	2.65	900	0	1	36	206	8	-1700
BRL-1	1.0	2.19	800	0	1	67	109	27	1600
BRL-11	0.2	1.7	-300	2	36	0	4	8	4500
BRL-11	0.6	1.69	100	0	35	0	2	17	0
BRL-11	1.0	1.71	0	26	36	0	2	90	0
BRL-11	1.5	1.69	0	2	35	1	0	0	0
BRL-11	1.8	1.69	0	0	34	0	1	4	100
BRL-11	2.1	1.76	100	0	32	0	5	7	300
BRL-11	2.1	1.81	200	27	33	0	2	9	300
BRL-21	0.2	5.38	-500	0	22	30	16	3	8200
BRL-21	0.6	3.57	-100	8	34	20	31	2	10000
BRL-21	0.9	3.48	-100	1	22	15	28	0	3600
BRL-21	1.5	1.73	200	0	18	1	0	0	700
BRL-21	2.0	1.72	100	0	24	1	5	4	0
BRL-21	2.5	1.72	100	0	28	1	3	3	-300
BRL-45	0.2	24.56	1400	0	0	45	16	0	1200
BRL-45	0.6	21.48	1200	0	0	45	20	2	2400
BRL-45	1.2	2.87	-400	0	0	20	2	1	-3000
BRL-45	0.5	2.49	-300	0	0	1	1	1	-3600
BRL-45	1.8	2.89	-300	0	0	1	1	1	-2200
BRL-45	2.1	3.07	-100	0	0	0	1	1	-1800
BRL-45	0.0	22.33	0	0	0	0	0	0	0
EGN-0	0.2	0.76	0	175	0	0	0	0	0
EGN-0	0.3	0.97	-1000	194	0	0	0	1	0
EGN-0	0.8	1.11	2700	169	0	0	0	0	2000

Table 4-3. Continued

Piezometer	Depth (cm)	SAL (PSU)	Δ Alk	DN-Alk	FeR-Alk	SR-Alk	Methane-Alk	Methox-Alk	CaCO ₃ -Alk
EGN-0	1.0	1.14	2900	165	0	0	0	0	3600
EGN-0	1.2	1.09	2800	169	0	0	0	1	3500
EGN-10	0.2	16.2	800	0	4	4	0	0	3200
EGN-10	0.3	4.07	2100	0	7	2	0	0	1900
EGN-10	0.8	2.59	2400	0	14	0	0	0	4200
EGN-10	1.0	0.9	2400	0	1	0	0	0	2500
EGN-10	1.2	0.9	2500	0	12	0	0	0	3100
EGN-10	1.2	0.9	2400	0	13	0	0	0	3200
EGN-10	0.0	23.8	0	0	0	0	0	0	3200
EGN-20	0.1	25.17	0	0	0	2	0	0	0
EGN-20	0.2	24.47	100	0	0	14	0	0	-100
EGN-20	0.3	24.35	700	0	5	22	0	0	400
EGN-20	0.6	22.39	1200	0	40	18	2	1	500
EGN-20	1.0	16.49	1700	0	37	4	3	1	700
EGN-20	1.2	16.01	1700	0	3	0	1	0	700
EGN-22.5	0.4	24.13	500	0	1	35	0	0	1600
EGN-22.5	0.4	25.03	600	0	0	31	0	1	900
EGN-22.5	1.1	23.23	1300	0	38	1	3	0	400
EGN-22.5	1.6	22.52	1800	0	22	5	3	25	2000
RWP-10	0.6	9.05							
RWP-10	1.0	0.45							
RWP-10	1.5	0.4							
RWP-10	2.0	0.36							
RWP-20	0.2	11.29	-400	3	6	11	51	17	100
RWP-20	0.6	0.5	0	0	0	3	312	20	4800
RWP-20	1.0	0.4	-200	0	0	2	411	28	800
RWP-20	2.0	4	-200	0	0	3	288	16	200
RWP-20	2.5	0.36	600	0	0	4	261	0	200
RWP-35	0.1	24.36	0	0	0	4	0	1	-1400
RWP-35	0.2	24.36	500	0	0	36	1	1	0

Table 4-3. Continued

Piezometer	Depth (cm)	SAL (PSU)	Δ Alk	DN-Alk	FeR-Alk	SR-Alk	Methane- Alk	Methox- Alk	CaCO ₃ - Alk
RWP-35	0.3	24.26	500	0	0	30	1	3	400
RWP-35	0.6	20	400	0	0	27	4	0	200
RWP-35	1.0	2.23	900	0	0	16	0	74	200
RWP-35	1.5	1.77	300	0	15	3	216	95	-800
RWP-35	2.0	5.56	400	0	1	9	114	130	-800
RWP-35	2.0	5.53	700	0	0	28	89	0	2600
RWP-35	0.0	24.37	800	0	0	12	0	0	2000

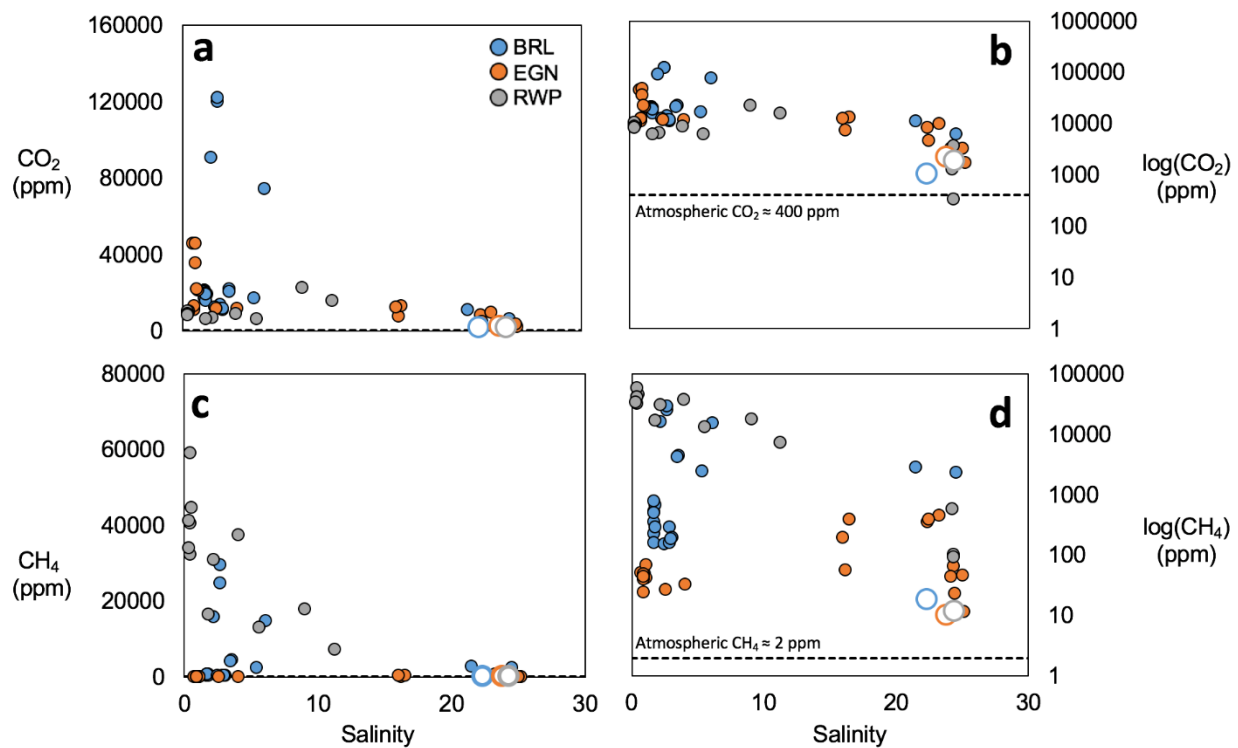


Figure 4-1. Relationship between dissolved gas concentrations and salinity at each STE site. Panels a) and b) present CO₂ concentrations, and panels c) and d) present CH₄ concentrations. To facilitate comparison of low-concentration samples, panels b) and d) present log concentrations. Open symbols represent surface water concentrations.

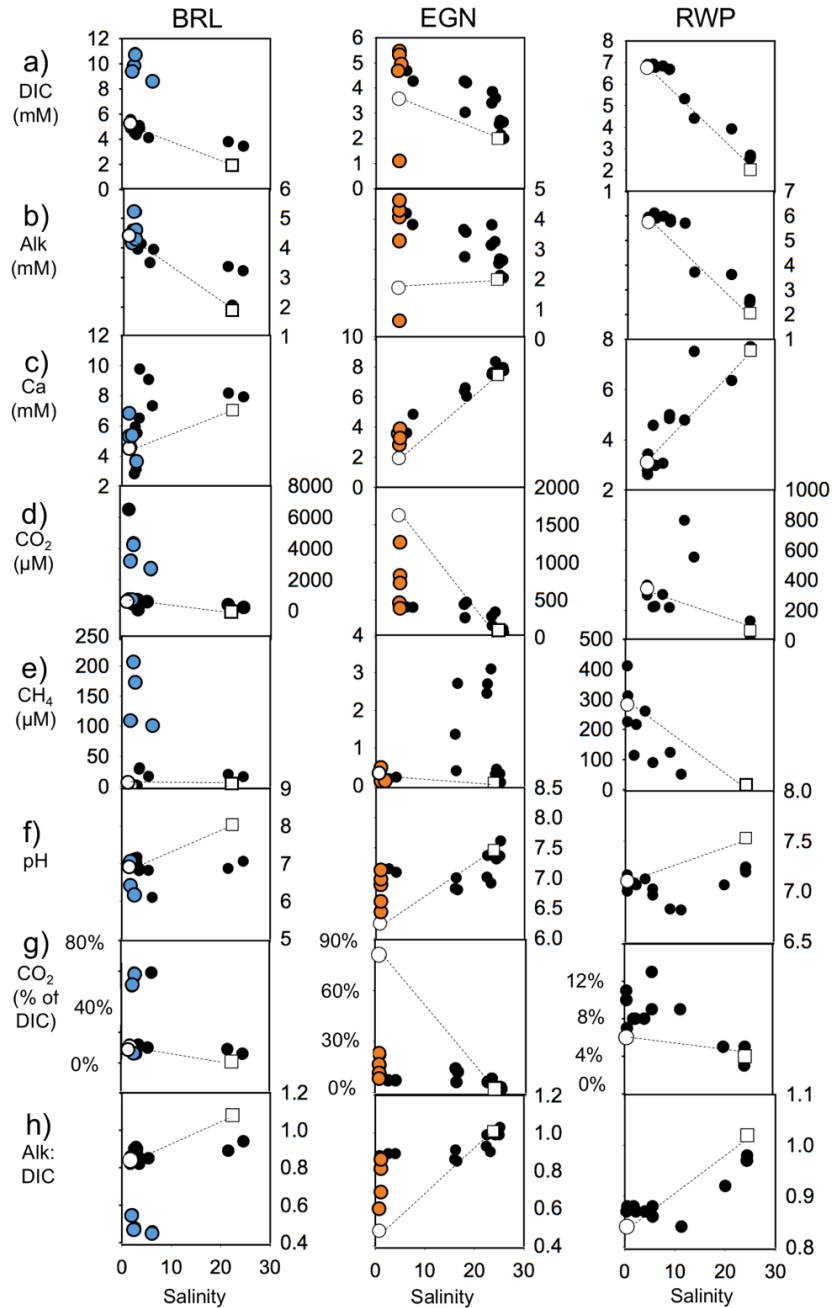


Figure 4-2. Concentrations of solutes with salinity between Indian River Lagoon seepage faces, including (a) DIC, b) alkalinity, c) Ca, d) CO₂, e) CH₄, f) pH, g) proportion of DIC as CO₂, and h) Alk:DIC ratios. Dotted lines represent conservative mixing between the freshest STE sample (indicated with white circle) and surface seawater (indicated with white square) at each seepage face, and are only shown when a mixing model was constructed. Fresh and saltwater end members are indicated for CO₂, CH₄ and pH although no mixing model was constructed for these parameters. Due to their distinct chemistries, samples from BRL-1 and EGN-0 are indicated in blue and orange, respectively.

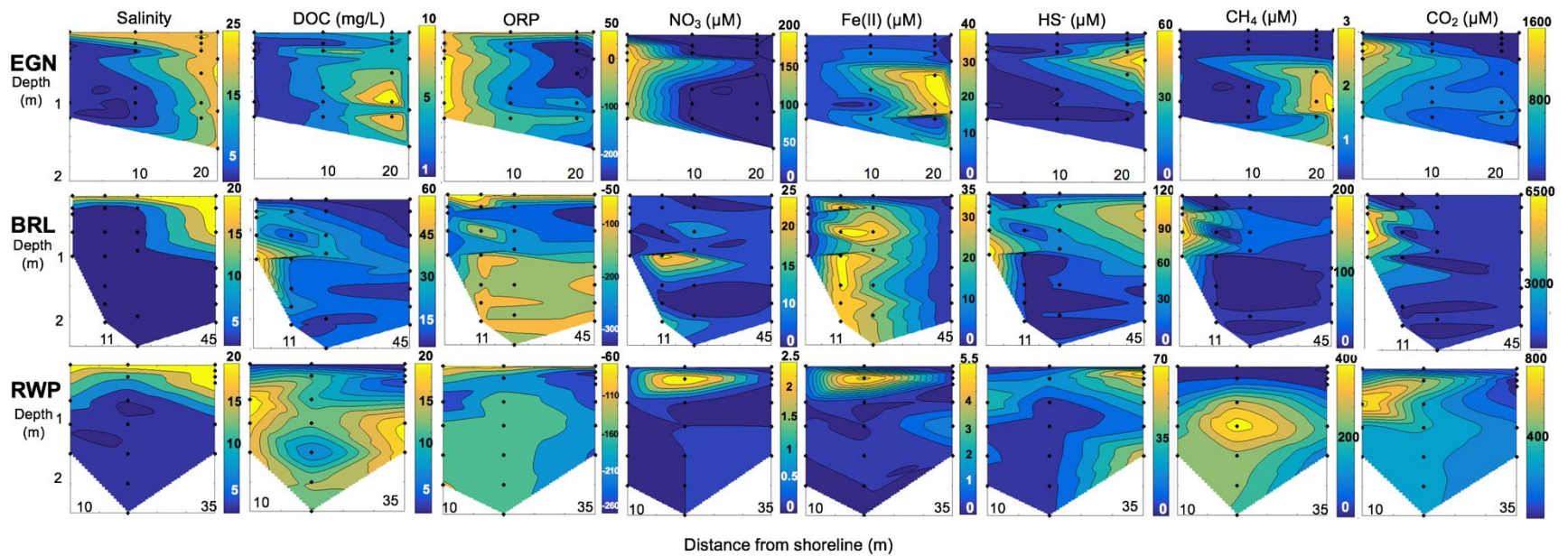


Figure 4-3. Distribution of salinity, DOC, redox species, and dissolved gases between Indian River Lagoon seepage faces. Note that the vertical and horizontal scales of each STE site are different.

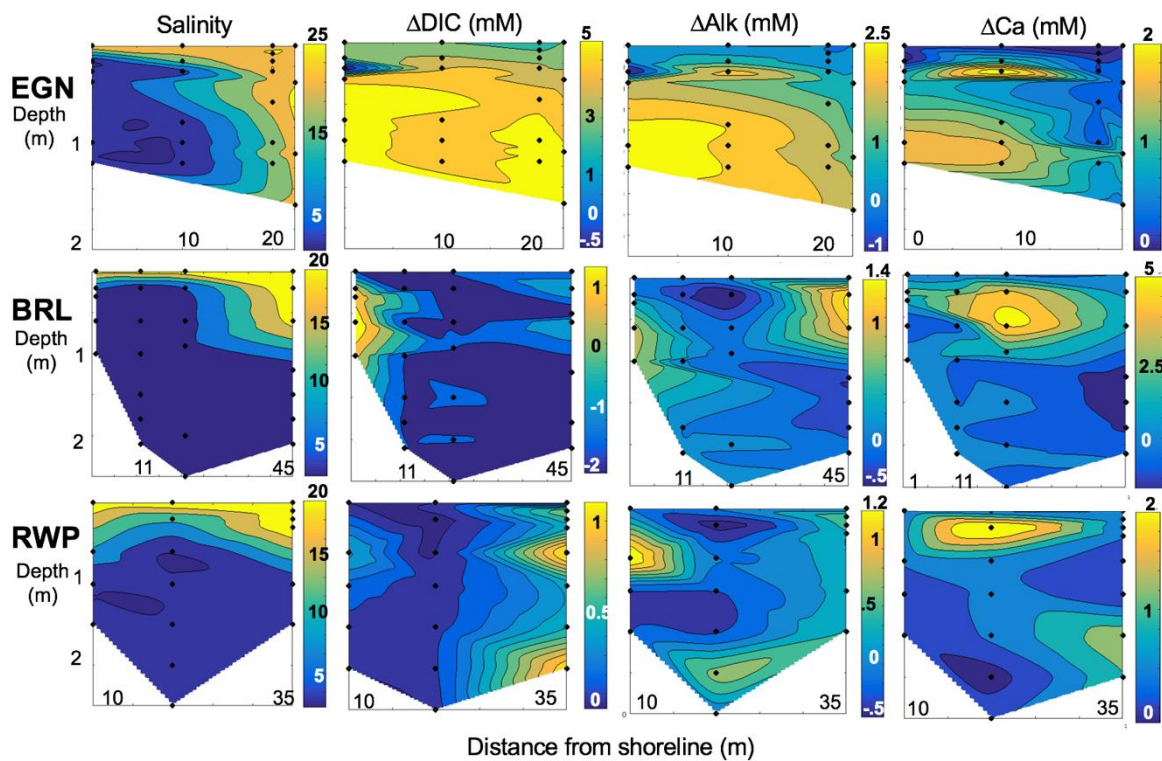


Figure 4-4. Distribution of salinity Δ DIC, Δ Alk, and Δ Ca between Indian River Lagoon seepage faces. Note that the vertical and horizontal scales of each STE site are different.

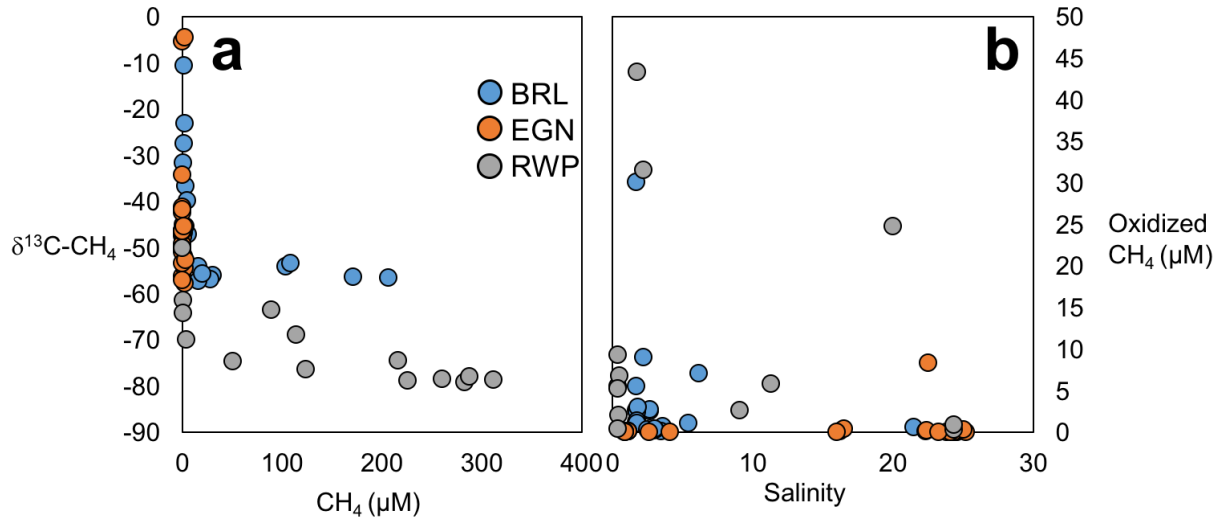


Figure 4-5. CH₄ concentrations and isotopic compositions at Indian River Lagoon sites. (a) CH₄ concentrations and δ¹³C-CH₄ signatures and (b) the quantity of CH₄ oxidized versus salinity.

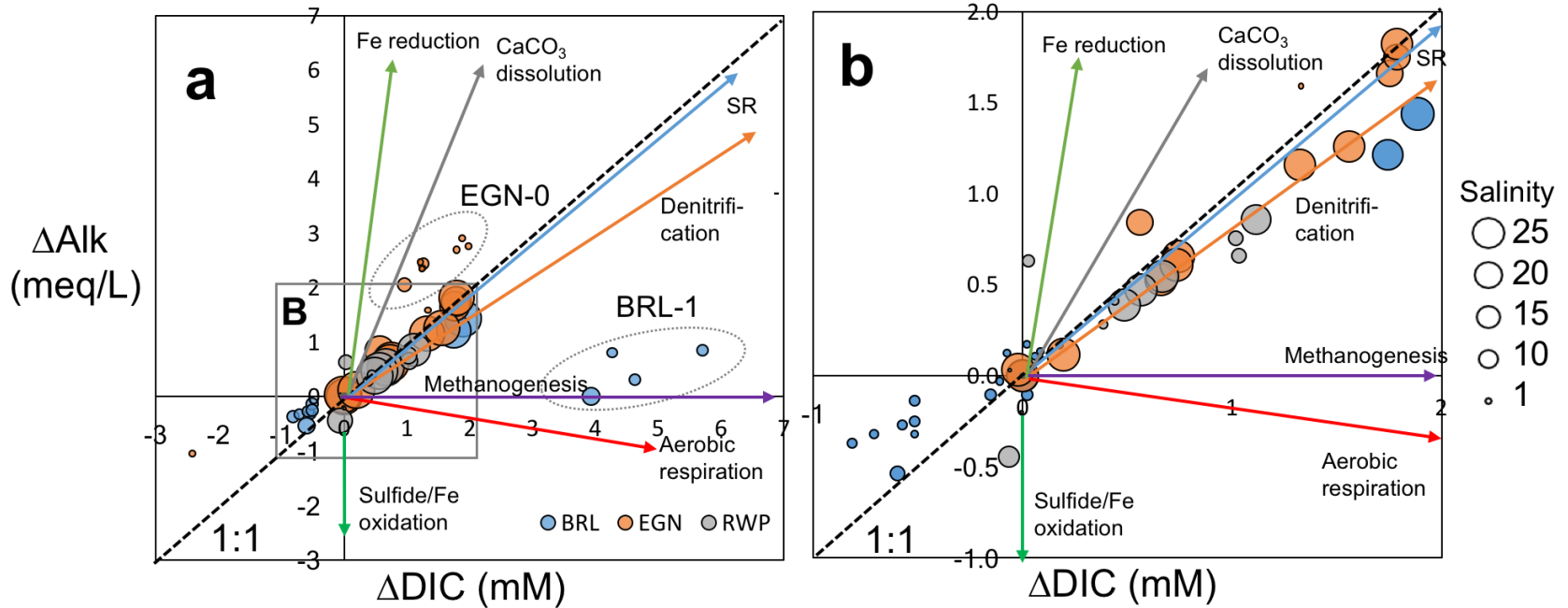


Figure 4-6. ΔAlk and ΔDIC compared to $\Delta\text{Alk}:\Delta\text{DIC}$ ratios produced by reactions. The diagonal dotted black line represents a 1:1 line, while vectors represent ratios of $\Delta\text{Alk}:\Delta\text{DIC}$ produced by reactions (SR= sulfate reduction). Panel (a) presents the full range of data, while (b) is scaled to depict the cluster of data points with salinity > 15. The size of data points corresponds to salinity. Modified from Liu et al. (2017).

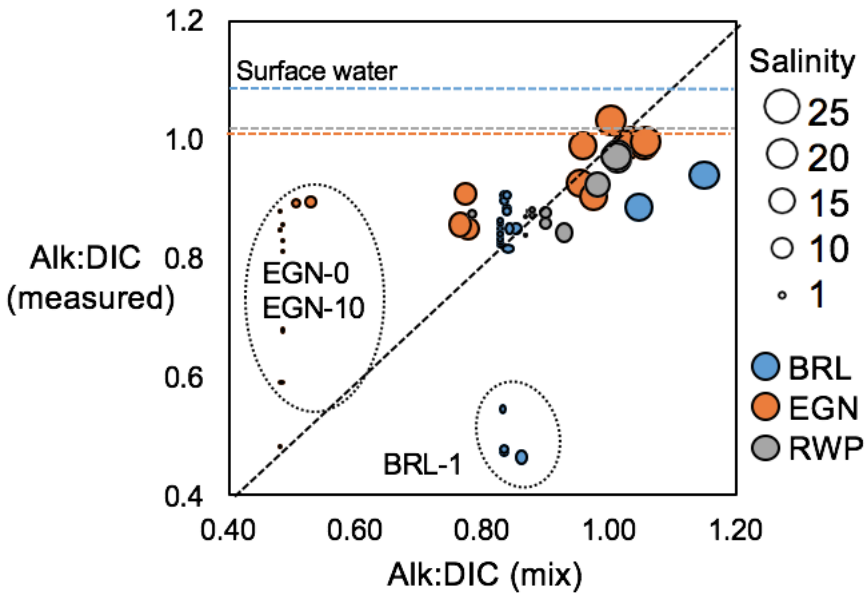


Figure 4-7. Alk:DIC ratios modeled by conservative mixing model (Alk:DIC (mix)) compared to Alk:DIC (measured). The size of data points represents sample salinity. Color coded dotted lines represent the surface water measured Alk:DIC ratio at each seepage face. Samples from EGN-0 and EGN-10, as well as BRL-1 are indicated due to their distinct chemistries from other STE samples.

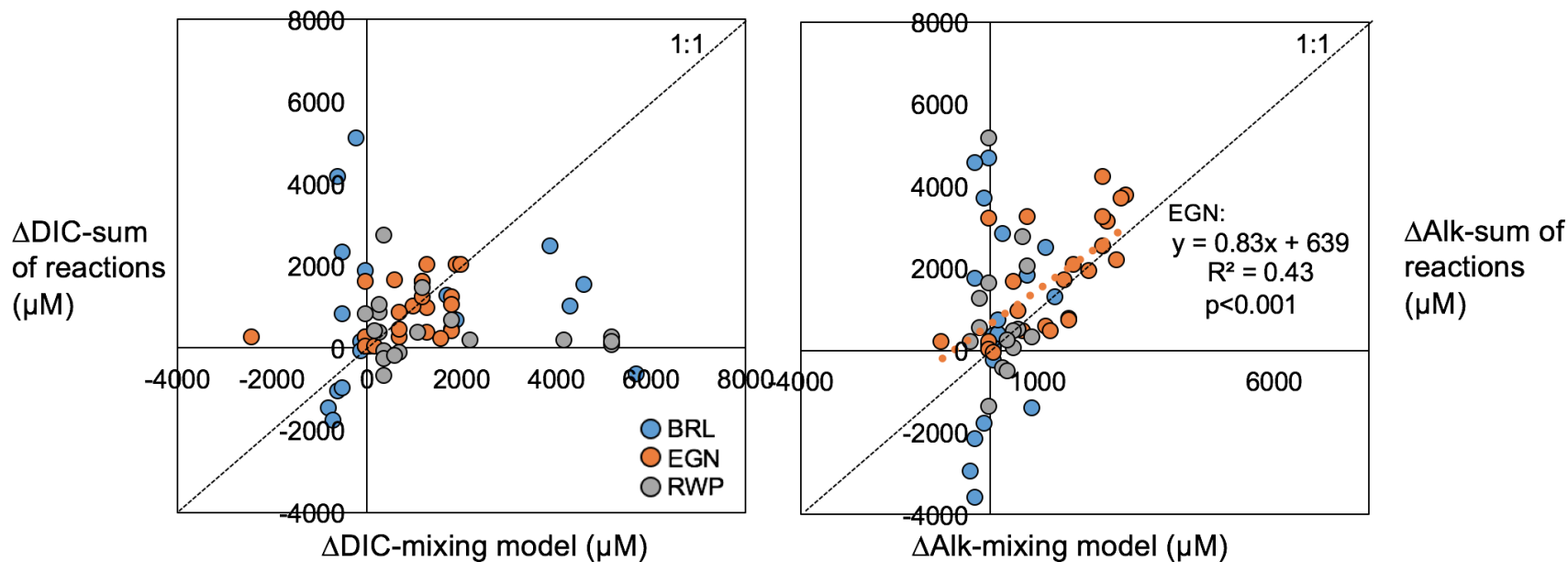


Figure 4-8. Relationships between Δ DIC and Δ Alk estimated via salinity-based conservative mixing models (deviations from conservative mixing lines indicated in Fig. 4-2a and b) compared to that calculated from the net impact of reactions. Reactions included in this calculation include denitrification, iron reduction, sulfate reduction, methanogenesis, methane oxidation, and CaCO_3 dissolution (data presented in Tables 4-2 and 4-3). The only significant relationship is between Δ Alk estimates at EGN.

CHAPTER 5 SUMMARY AND CONCLUDING REMARKS

Biogeochemical processing in subterranean estuaries modifies the composition of submarine groundwater discharge, which is an important source of freshwater and terrestrial solutes to coastal zones. Comparison between carbon processing in siliciclastic STEs of Indian River Lagoon, FL and a karst carbonate STE in Quintana Roo, Mexico, demonstrates that the impacts of reactions on carbon transformations, and likely on carbon fluxes, vary due to aquifer hydrogeology. These differences may be classified into differences due to flow, which alters residence time within the freshwater-saltwater mixing zone, and differences due to interactions with aquifer solid material. These variations may lead to considerable yet systematic variability in the composition of SGD derived from siliciclastic compared to carbonate karst aquifers.

Impacts Due to Flow

Carbonate karst STEs have high groundwater transport rate and low groundwater residence time in the freshwater-saltwater mixing zone compared to widely distributed siliciclastic systems. Lower residence time in carbonate karst STEs leads to relatively less organic carbon processing compared to siliciclastic STEs (Chapter 2). The magnitudes of differences are considerable: compared to concentrations predicted by conservative mixing, STE processing increased CDOM by 40% in the Yucatan, while this increase was up to 600% at Indian River Lagoon. This finding suggests that fluxes of organic carbon per unit volume of SGD should be considerably higher from siliciclastic STEs with a lower water:rock ratio and greater potential to interact with sedimentary organic carbon pools, depending on the absolute volumes of discharge water, which will control solute loading. This finding also implies that fluxes of by-

products of remineralization, which include remineralized nutrients, metals, and greenhouse gases, should be greater per unit volume in siliciclastic systems compared to karst carbonate systems.

The impact of STE hydrogeology on SGD fluxes depends on the concentrations of solutes in SGD as well as total SGD volume from the two end member systems. Many studies quantifying SGD fluxes have focused on the fresh component of SGD because it represents a source of “new” solutes to the system, contrasting with solutes regenerated from marine sediments (Knee and Paytan, 2011). These techniques often multiply estimates of total fresh SGD, quantified via seepage meters, chemical tracers, water balance approaches, piezometers, or numerical methods (Burnett et al., 2006) by the concentration of a solute of interest present in the fresh groundwater end member (McCoy and Corbett, 2009; Knee and Paytan, 2011). These methods do not account for transformation of groundwater within the subterranean estuary or the saline component of submarine groundwater discharge. Since the results of this study suggest that saltwater provides labile organic carbon substrates as well as terminal electron acceptors that drive biogeochemical reactions (Chapter 2), saline SGD is a critical component both in terms of volume (Table 1-1) and by impacting the chemical composition of SGD. I therefore compare the magnitudes of combined fresh and saline SGD between sample sites to determine the likely impact of STE reactions on chemical fluxes.

Combined fresh and saline SGD fluxes (commonly referred to as total SGD) between Indian River Lagoon sites and the Yucatan are similar in magnitude, with estimates of Indian River Lagoon SGD at approximately $320 \text{ m}^3 \text{ km}^{-1} \text{ yr}^{-1}$ (Martin et al.

2007) while the Yucatan is estimated at approximately $112 \text{ m}^3 \text{ km}^{-1} \text{ yr}^{-1}$ (Null et al. 2014). While these SGD fluxes were calculated using different methods and the error may be high, they suggest that the widely distributed Indian River Lagoon system contributes equivalent or greater volumes of total SGD compared to the carbonate karst system of the Yucatan (Table 1-1). Because the concentrations of organic carbon, and likely other solutes, are higher from Indian River Lagoon than Yucatan STEs, overall SGD solute fluxes are likely to be considerably greater for Indian River Lagoon compared to Yucatan site, and may be related to the higher degree of biogeochemical alteration of fresh and marine SGD due to higher residence times in the freshwater-saltwater mixing zone and the lower water:rock ratio that provides solid phase organic carbon and mineral phases to drive reactions.

Impacts Due to Aquifer Solid Material

Because biogeochemical reactions may involve aquifer solid material, STE hydrogeology also exerts an influence on the chemical composition of SGD. For instance, organic carbon remineralization leads to CO_2 generation in both Yucatan (Chapter 3) and Indian River Lagoon (Chapter 4) sites. Increased acidity leads to the undersaturation and dissolution of CaCO_3 minerals in the Yucatan, but only in isolated locations of Indian River Lagoon, and SGD is a greater CO_2 source in part due to decreased buffering capacity of Indian River Lagoon pore waters. SGD from siliciclastic STEs may therefore be a greater source of CO_2 to surface waters than that from carbonate karst STEs, and may cause surface waters to become sources of CO_2 to the atmosphere. However, the extent of CaCO_3 buffering in karst STEs may be limited by low water residence time that may prohibit water from reaching thermodynamic

equilibrium with respect to CaCO_3 minerals, particularly when the CaCO_3 saturation state of groundwater approaches equilibrium and dissolution kinetics become slower.

Concluding Remarks

The results of this study allow several conclusions to be made regarding the role of SGD in coastal carbon cycling as a function of aquifer hydrogeology. Siliciclastic STEs are likely to contribute more solutes, including DOC, CDOM, and CO_2 to surface waters than carbonate karst STEs, given equivalent volumes of total SGD. Reduced buffering capacity of SGD in siliciclastic STEs results from a lower availability of CaCO_3 minerals, and SGD from these systems is more likely to increase CO_2 fluxes to surface water and to the atmosphere. In carbonate karst systems, buffering due to CaCO_3 dissolution may occur but could be limited by low reaction rates compared to the flow rate. Once delivered to surface water, a negative feedback for CO_2 concentrations may be induced due to SGD nutrient delivery that stimulates higher rates of primary productivity. In the Yucatan, this mechanism appears to be reduced due to retention of P within the aquifer when P sorbs to CaCO_3 mineral surfaces. While not examined here, nutrient retention is less likely to occur in Indian River Lagoon sediments due to lower CaCO_3 concentrations, though Fe oxide mineral precipitation could sorb remineralized P. However, previous studies suggest that most reduced Fe co-precipitates with sulfide to form iron sulfide minerals, which have limited sorption capacity for P (Roy, M. et al., 2010; Roy et al., 2013a)..

This study highlights that biogeochemical processing in STEs significantly impacts organic carbon (DOC and CDOM), remineralized carbon (CO_2 and CH_4) and nutrient concentrations in SGD, but that aquifer hydrogeology exerts an important control on the magnitude and type of reactions that may occur. These differences may

cause systematic variations in the composition of SGD between these two end member systems. The high variability in the concentrations and ranges of carbon-cycling reactions observed, as well as sensitivity to flow rate and end member composition, may preclude upscaling of these results to estimate large-scale impacts of SGD on coastal carbon cycling, although SGD may play a critical role in carbon budgets in individual study settings.

APPENDIX A
PARAFAC MODEL

Table A-1. Complete list of samples included in PARAFAC model. Site ID codes for Indian River Lagoon sites are: BRL (Banana River Lagoon), EGN (Eau Gallie North), and RWP (Riverwalk Park).

	Site ID	Sample date	Distance Offshore (m)	Sample Depth (m)	Salinity	pH	ORP	C1 (R.U.)	C2 (R.U.)	C3 (R.U.)	C4 (R.U.)	C5 (R.U.)
1	BRL	10-2014	6	0.2	2.76	6.84	-225	4.83	1.51	1.80	0.84	0.28
2	BRL	10-2014	6	0.6	1.43	6.89	-144	2.86	0.96	0.98	0.69	0.13
3	BRL	10-2014	6	1.2	1.46	6.91	-120	4.30	1.53	1.72	0.87	0.25
4	BRL	10-2014	6	1.5	1.47	6.92	-121	6.18	1.98	2.28	1.14	0.35
5	BRL	10-2014	6	1.8	1.48	6.93	-119	5.61	1.87	2.09	1.10	0.32
6	BRL	10-2014	6	2.1	1.51	6.97	-111	5.72	1.82	2.06	1.11	0.31
7	BRL	10-2014	6	0	23.85	7.61	-12	1.56	0.39	0.76	0.28	0.29
8	BRL	10-2014	1	0.1	5.83	6.28	-272	30.73	4.32	6.61	3.36	1.51
9	BRL	10-2014	1	0.2	8.38	6.28	-276	36.40	4.55	7.42	3.66	1.76
10	BRL	10-2014	1	0.3	9.87	6.30	-273	13.32	6.00	4.53	4.23	0.47
11	BRL	10-2014	1	0.6	11.85	6.27	-269	25.38	4.52	5.86	3.34	1.14
12	BRL	10-2014	1	1.0	7.91	6.28	-245	22.04	4.68	5.31	3.59	1.05
13	BRL	10-2014	1	1.0	6.72	6.31	-253	10.48	3.80	3.46	2.53	0.46
14	BRL	10-2014	11	0.2	1.85	6.92	-134	4.22	1.69	1.71	0.93	0.19
15	BRL	10-2014	11	0.6	1.41	6.94	-111	5.57	2.07	2.13	1.22	0.24
16	BRL	10-2014	11	1.0	1.42	6.94	-118	4.90	3.55	2.53	2.31	0.16
17	BRL	10-2014	11	1.5	1.40	6.94	-119	6.08	3.64	3.04	2.03	0.24
18	BRL	10-2014	11	1.8	1.39	6.94	-119	5.22	1.63	1.88	0.92	0.25
19	BRL	10-2014	11	2.1	1.41	7.00	-163	4.56	1.45	1.66	0.83	0.21
20	BRL	10-2014	11	2.1	1.40	6.97	-110	5.06	1.62	1.84	0.91	0.23
21	EGN	10-2014	0	0.15	5.45	6.63	6	0.43	0.14	0.26	0.07	0.06
22	EGN	10-2014	0	0.25	0.98	6.71	-4	0.22	0.09	0.15	0.04	0.02
23	EGN	10-2014	0	0.35	0.72	6.73	-29	0.22	0.09	0.15	0.04	0.02
24	EGN	10-2014	0	0.55	0.72	6.77	-51	0.27	0.10	0.17	0.05	0.03
25	EGN	10-2014	0	0.75	0.72	6.75	-28	0.24	0.09	0.15	0.04	0.02
26	EGN	10-2014	0	0.95	0.72	6.76	-40	0.24	0.09	0.16	0.04	0.02
27	EGN	10-2014	0	1.15	0.73	6.81	-39	0.22	0.08	0.14	0.04	0.02
28	EGN	10-2014	0	1.15	0.73	6.84	-25	0.22	0.09	0.15	0.03	0.02
29	EGN	10-2014	17.5	0.07	18.28	7.78	-216	1.61	0.37	0.81	0.24	0.23
30	EGN	10-2014	17.5	0.15	13.02	7.66	-335	1.62	0.38	0.80	0.24	0.22
31	EGN	10-2014	17.5	0.25	19.10	7.55	-244	1.56	0.37	0.78	0.23	0.21

Table A-1. Continued

	Site ID	Sample date	Distance Offshore (m)	Sample Depth (m)	Salinity	pH	ORP	C1 (R.U.)	C2 (R.U.)	C3 (R.U.)	C4 (R.U.)	C5 (R.U.)
32	EGN	10-2014	17.5	0.35	19.49	7.54	-271	1.49	0.36	0.75	0.21	0.20
33	EGN	10-2014	17.5	0.55	18.59	7.14	-259	1.35	0.37	0.74	0.23	0.19
34	EGN	10-2014	17.5	0.75	17.78	7.02	-294	1.04	0.36	0.58	0.19	0.13
35	EGN	10-2014	17.5	0.95	16.09	6.77	-171	0.98	0.36	0.54	0.18	0.10
36	EGN	10-2014	17.5	1.15	16.11	6.74	-84	0.94	0.35	0.52	0.17	0.10
37	EGN	10-2014	17.5	0	18.32	8.23	-32	1.64	0.38	0.82	0.25	0.24
38	EGN	10-2014	20	0.07	19.03	8.09	-195	1.57	0.37	0.80	0.23	0.25
39	EGN	10-2014	20	0.15	19.11	7.66	-264	1.58	0.38	0.79	0.23	0.24
40	EGN	10-2014	20	0.25	19.65	7.53	-298	1.50	0.37	0.76	0.22	0.22
41	EGN	10-2014	20	0.55	20.12	7.12	-288	1.24	0.35	0.69	0.22	0.18
42	EGN	10-2014	20	0.95	18.52	6.10	-219	1.04	0.40	0.63	0.22	0.14
43	EGN	10-2014	20	1.15	18.37	6.81	-179	1.00	0.40	0.60	0.22	0.12
44	EGN	10-2014	22.5	0.36	21.88	7.35	-304	1.35	0.35	0.70	0.20	0.20
45	EGN	10-2014	22.5	1.06	21.19	6.95	-272	1.09	0.37	0.64	0.23	0.15
46	EGN	10-2014	22.5	1.86	22.21	7.16	-287	1.25	0.41	0.65	0.26	0.13
47	EGN	10-2014	22.5	1.86	22.15	7.23	-221	1.23	0.39	0.62	0.25	0.12
48	EGN	10-2014	10	0.07	13.62	7.32	-212	1.76	0.43	0.79	0.27	0.21
49	EGN	10-2014	10	0.15	9.50	7.15	-198	1.17	0.34	0.59	0.18	0.15
50	EGN	10-2014	10	0.25	2.77	7.11	-137	0.71	0.27	0.42	0.11	0.09
51	EGN	10-2014	10	0.35	2.56	7.11	-144	0.82	0.29	0.46	0.13	0.11
52	EGN	10-2014	10	0.55	1.47	7.14	-95	0.64	0.25	0.38	0.10	0.08
53	EGN	10-2014	10	0.75	0.86	7.13	-99	0.46	0.17	0.27	0.07	0.06
54	EGN	10-2014	10	0.95	0.79	7.16	-77	0.63	0.25	0.38	0.11	0.08
55	EGN	10-2014	10	1.15	0.79	7.13	-39	0.69	0.28	0.43	0.11	0.09
56	EGN	10-2014	10	1.15	0.83	7.44	-57	0.45	0.17	0.27	0.07	0.06
57	EGN	10-2014	10	0	14.95	8.34	34	2.29	0.52	0.97	0.37	0.27
58	EGN	10-2014	15	0.07	15.88	7.90	-150	2.01	0.48	0.91	0.32	0.26
59	EGN	10-2014	15	0.25	13.24	7.19	-232	1.19	0.34	0.61	0.19	0.16
60	EGN	10-2014	15	0.35	12.64	7.14	-231	1.22	0.35	0.62	0.19	0.16
61	EGN	10-2014	15	0.55	13.30	7.16	-233	1.18	0.34	0.62	0.19	0.17
62	EGN	10-2014	15	0.75	10.69	7.06	-222	0.81	0.29	0.46	0.13	0.12
63	EGN	10-2014	15	0.95	5.47	6.99	-194	0.70	0.30	0.42	0.12	0.09
64	EGN	10-2014	15	1.15	1.29	6.94	-174	0.74	0.30	0.43	0.13	0.09
65	EGN	10-2014	15	1.15	6.12	6.94	-181	0.74	0.30	0.43	0.13	0.09
66	RWP	10-2014	0	0.6	22.73	7.03	-284	3.19	0.70	1.09	0.61	0.34
67	RWP	10-2014	0	1.5	10.95	6.60	-257	7.23	1.64	2.03	1.17	0.37

Table A-1. Continued

	Site ID	Sample date	Distance Offshore (m)	Sample Depth (m)	Salinity	pH	ORP	C1 (R.U.)	C2 (R.U.)	C3 (R.U.)	C4 (R.U.)	C5 (R.U.)
68	RWP	10-2014	0	1.5	11.29	6.60	-270	7.02	1.63	1.99	1.17	0.36
69	RWP	10-2014	5	0.1	25.00	7.16	-279	1.56	0.35	0.75	0.24	0.24
70	RWP	10-2014	5	0.2	25.05	7.17	-266	1.71	0.39	0.79	0.28	0.22
71	RWP	10-2014	5	0.3	22.63	6.75	-239	2.57	0.62	0.95	0.46	0.22
72	RWP	10-2014	5	0.6	22.87	6.69	-254	2.66	0.65	0.95	0.49	0.21
73	RWP	10-2014	5	1.0	7.58	6.78	-208	3.25	0.98	1.21	0.53	0.24
74	RWP	10-2014	5	1.5	0.53	6.89	-149	1.34	0.56	0.90	0.20	0.16
75	RWP	10-2014	5	2.0	0.36	6.95	-145	2.77	0.93	1.17	0.43	0.26
76	RWP	10-2014	5	0	24.41	8.29	-10	1.31	0.29	0.73	0.18	0.26
77	RWP	10-2014	10	0.6	15.43	6.62	-215	2.59	0.67	1.00	0.46	0.24
78	RWP	10-2014	10	1.0	0.77	6.89	-162	1.98	0.67	0.84	0.29	0.19
79	RWP	10-2014	10	1.5	0.41	7.01	-136	2.81	0.93	1.18	0.42	0.27
80	RWP	10-2014	10	2.0	0.36	7.01	-180	3.09	1.00	1.24	0.52	0.27
81	BRL	05-2015	1	0.2	5.51	6.23	-268	2.11	9.13	3.51	7.91	-0.16
82	BRL	05-2015	1	0.3	2.37	6.28	-271	19.26	9.31	5.69	7.07	0.53
83	BRL	05-2015	1	0.6	2.14	6.30	-261	17.60	8.90	4.86	8.39	0.43
84	BRL	05-2015	1	1.0	1.71	6.54	-78	12.85	5.24	4.12	3.80	0.45
85	BRL	05-2015	11	0.6	1.71	6.98		5.26	2.45	2.18	1.45	0.22
86	BRL	05-2015	11	0	22.95	8.21	-48	1.06	0.29	0.65	0.17	0.26
87	BRL	05-2015	21	0.2	16.69	7.01	-283	3.84	1.65	1.72	1.14	0.26
88	BRL	05-2015	21	1.0	6.44	6.27	-239	5.74	1.57	1.80	1.04	0.30
89	BRL	05-2015	21	1.5	1.67	6.92	-217	5.03	2.03	2.00	1.15	0.23
90	BRL	05-2015	21	1.8	1.56	6.91	-148	5.96	3.11	2.78	1.71	0.26
91	BRL	05-2015	11	0.2	2.15	6.95	-106	5.64	1.86	1.95	1.16	0.29
92	BRL	05-2015	11	1.5	1.65	6.97	-122	7.12	2.24	2.58	1.30	0.39
93	BRL	05-2015	11	2.1	1.63	7.02	-120	5.42	2.55	2.42	1.41	0.26
94	BRL	05-2015	21	0.6	10.86	6.77	-277	5.29	1.61	1.83	1.11	0.31
95	BRL	05-2015	21	2.5	1.55	6.90	-189	4.77	1.63	1.81	0.89	0.25
96	EGN	05-2015	0	1.15	0.96	6.92	-27	0.46	0.21	0.32	0.09	0.05
97	EGN	05-2015	17.5	0.15	22.63	7.43	-249	1.11	0.27	0.63	0.15	0.19
98	EGN	05-2015	17.5	0.35	21.75	7.25	-274	1.14	0.30	0.63	0.16	0.18
99	EGN	05-2015	17.5	0.55	18.19	7.05	-239	1.07	0.31	0.60	0.19	0.16
100	EGN	05-2015	17.5	0.95	12.29	6.84	-147	0.93	0.34	0.50	0.17	0.12
101	EGN	05-2015	17.5	1.15	12.67	6.82	-118	0.92	0.34	0.50	0.16	0.12
102	EGN	05-2015	20	0.07	22.33	7.71	-160	1.10	0.26	0.63	0.17	0.21
103	EGN	05-2015	20	0.25	22.29	7.35	-256	1.18	0.30	0.66	0.18	0.19

Table A-1. Continued

	Site ID	Sample date	Distance Offshore (m)	Sample Depth (m)	Salinity	pH	ORP	C1 (R.U.)	C2 (R.U.)	C3 (R.U.)	C4 (R.U.)	C5 (R.U.)
104	EGN	05-2015	20	0.55	21.68	7.11	-210	1.20	0.34	0.74	0.25	0.21
105	EGN	05-2015	20	0.95	19.73	6.74	-113	1.09	0.43	0.67	0.25	0.16
106	EGN	05-2015	20	1.15	19.56	6.78	-166	1.14	0.46	0.70	0.27	0.15
107	EGN	05-2015	22.5	0.36	22.25	7.37	-231	1.52	0.48	0.94	0.26	0.24
108	EGN	05-2015	22.5	1.06	23.33	6.93	-138	1.20	0.47	0.75	0.29	0.17
109	EGN	05-2015	22.5	1.86	23.36	7.29	-205	1.24	0.41	0.61	0.25	0.12
110	EGN	05-2015	22.5	1.86	23.40	7.16	-256	1.94	0.62	0.96	0.36	0.18
111	EGN	05-2015	22.5	0	22.93	7.79	-19	1.14	0.26	0.66	0.15	0.22
112	EGN	05-2015	20	0.15	22.42	7.43	-252	1.52	0.50	1.00	0.28	0.26
113	RWP	05-2015	0	0.6	21.49	6.90	-257	1.94	0.49	0.84	0.34	0.25
114	RWP	05-2015	0	1.0	2.18	6.76	-178	2.74	0.96	1.20	0.45	0.25
115	RWP	05-2015	0	1.5	0.70	6.83	-137	2.74	0.95	1.20	0.41	0.25
116	RWP	05-2015	0	2.0	0.56	6.95	-92	2.33	0.82	1.03	0.35	0.23
117	RWP	05-2015	10	0.2	10.18	6.73	-179	2.88	0.89	1.08	0.56	0.23
118	RWP	05-2015	10	0.6	0.90	6.91	-160	2.86	0.98	1.20	0.45	0.25
119	RWP	05-2015	10	1.0	0.36	7.01	-120	2.64	0.90	1.15	0.37	0.26
120	RWP	05-2015	10	1.5	0.42	7.22	-103	2.45	0.87	1.12	0.33	0.25
121	RWP	05-2015	20	0.2	13.52	6.77	-181	2.28	0.62	0.97	0.36	0.26
122	RWP	05-2015	20	0.6	1.11	6.84		2.49	0.87	1.14	0.33	0.26
123	RWP	05-2015	20	1.0	0.42	6.86		2.85	0.93	1.21	0.38	0.29
124	RWP	05-2015	20	1.5	0.37	6.87		2.66	0.89	1.17	0.35	0.27
125	RWP	05-2015	20	2.0	0.42	6.85	-166	2.60	0.85	1.11	0.35	0.26
126	RWP	05-2015	20	2.5	0.68	6.82		2.65	0.91	1.16	0.40	0.26
127	RWP	05-2015	20	2.5	0.67	6.94		2.69	0.91	1.18	0.38	0.26
128	RWP	05-2015	20	0	23.77	7.88	24	1.09	0.23	0.65	0.13	0.21
129	BRL	09-2015	1	0.2	5.08	6.14	-247	31.99	7.63	8.50	5.88	1.29
130	BRL	09-2015	1	0.3	3.03	6.11	-237	37.76	8.64	9.80	6.68	1.47
131	BRL	09-2015	1	0.6	3.65	6.04	-246	37.39	8.47	9.67	6.67	1.47
132	BRL	09-2015	1	1.0	6.59	6.74	-245	16.84	4.52	5.05	3.34	0.79
133	BRL	09-2015	1	1.0	7.92	6.27	-240	15.75	4.27	4.77	3.21	0.81
134	BRL	09-2015	11	0.2	1.78	6.88	-80	5.62	1.83	2.03	1.01	0.27
135	BRL	09-2015	11	0.6	1.61	6.90	-88	5.96	3.48	2.92	1.90	0.23
136	BRL	09-2015	11	1.5	1.63	6.90	-87	6.53	2.06	2.25	1.19	0.30
137	BRL	09-2015	11	2.1	1.65	6.90	-90	6.33	2.10	2.28	1.20	0.30
138	BRL	09-2015	11	0	20.66	7.86	-40	1.14	0.26	0.63	0.17	0.26
139	BRL	09-2015	21	0.2	4.90	6.86	-193	5.83	1.55	1.86	1.09	0.32

Table A-1. Continued

Site ID	Sample date	Distance Offshore (m)	Sample Depth (m)	Salinity	pH	ORP	C1 (R.U.)	C2 (R.U.)	C3 (R.U.)	C4 (R.U.)	C5 (R.U.)	
140	BRL	09-2015	21	0.6	5.83	6.74	-175	6.37	2.03	2.21	1.28	0.31
141	BRL	09-2015	21	0.9	2.92	6.76	-181	6.63	1.94	2.18	1.20	0.32
142	BRL	09-2015	21	1.5	1.65	6.89	-113	5.47	1.78	2.03	0.95	0.28
143	BRL	09-2015	21	2.0	1.63	6.88	-97	5.71	1.85	2.09	1.02	0.28
144	BRL	09-2015	21	2.5	1.94	7.08	-104	5.47	1.85	2.09	0.97	0.28
145	BRL	09-2015	45	0.2	12.82	7.18	-218	3.55	1.01	1.29	0.69	0.25
146	BRL	09-2015	45	0.6	9.81	7.01	-230	5.79	1.83	1.94	1.17	0.26
147	BRL	09-2015	45	1.2	2.42	6.92	-128	6.86	2.03	2.16	1.29	0.28
148	BRL	09-2015	45	1.5	2.30		-60	6.40	2.05	2.08	1.29	0.25
149	BRL	09-2015	45	1.8	2.36	7.03	-28	6.07	1.83	1.90	1.23	0.25
150	BRL	09-2015	45	2.1	2.64	7.02	-97	5.90	1.82	1.92	1.17	0.25
151	BRL	09-2015	45	2.1	2.68	7.03	-43	5.83	1.78	1.89	1.15	0.25
152	EGN	09-2015	0	0.15	0.48	6.18	108	0.21	0.07	0.14	0.03	0.03
153	EGN	09-2015	0	0.25	0.52	6.26	104	0.56	0.24	0.43	0.09	0.07
154	EGN	09-2015	0	0.55	0.65	6.72	0	0.80	0.34	0.57	0.14	0.09
155	EGN	09-2015	0	0.95	0.67	6.63	99	0.60	0.25	0.41	0.10	0.07
156	EGN	09-2015	0	1.15	0.66	6.51	100	0.37	0.15	0.27	0.06	0.05
157	EGN	09-2015	0	1.15	0.67	6.50	100	0.18	0.07	0.13	0.03	0.02
158	EGN	09-2015	17.5	0.15	19.07	7.19	-349	1.09	0.30	0.62	0.18	0.16
159	EGN	09-2015	17.5	0.35	18.63	7.25	-292	1.05	0.29	0.56	0.17	0.16
160	EGN	09-2015	17.5	0.55	16.65	7.33	-237	1.37	0.46	0.76	0.25	0.22
161	EGN	09-2015	17.5	0.95	15.32	6.75	-223	0.91	0.32	0.48	0.15	0.12
162	EGN	09-2015	17.5	1.15	15.41	6.68	-74	1.11	0.43	0.61	0.20	0.13
163	EGN	09-2015	20	0.07	17.27	7.83	-260	2.12	0.66	1.19	0.41	0.29
164	EGN	09-2015	20	0.15	17.98	7.55	-349	2.16	0.73	1.26	0.44	0.28
165	EGN	09-2015	20	0.25	19.14	7.48	-375	2.02	0.64	1.15	0.38	0.27
166	EGN	09-2015	20	0.55	20.11	7.21	-337	1.20	0.35	0.66	0.22	0.21
167	EGN	09-2015	20	0.95	19.53	6.81	-235	1.10	0.43	0.65	0.19	0.14
168	EGN	09-2015	20	1.15	19.41	6.80	-232	2.02	0.84	1.20	0.38	0.22
169	EGN	09-2015	20	1.15	19.49	6.82	-219	1.88	0.80	1.14	0.36	0.20
170	EGN	09-2015	22.5	0.66	20.77	7.43	-370	2.10	0.75	1.27	0.41	0.28
171	EGN	09-2015	22.5	0	18.79	8.06	-90	1.38	0.36	0.77	0.23	0.22
172	EGN	09-2015	22.5	1.06	23.46	6.97	-248	0.91	0.36	0.57	0.25	0.13
173	EGN	09-2015	22.5	1.86	22.89	7.34	-261	1.39	0.51	0.75	0.38	0.13
174	RWP	09-2015	0	0.6	6.65	6.63	-210	14.47	2.67	3.19	2.07	0.61
175	RWP	09-2015	0	1.0	0.73	6.83	-56	2.91	1.04	1.30	0.45	0.26

Table A1. Continued

	Site ID	Sample date	Distance Offshore (m)	Sample Depth (m)	Salinity	pH	ORP	C1 (R.U.)	C2 (R.U.)	C3 (R.U.)	C4 (R.U.)	C5 (R.U.)
176	RWP	09-2015	0	2.0	0.54	6.91	-72	2.39	0.88	1.11	0.35	0.24
177	RWP	09-2015	20	0.2	4.58	6.67	-128	3.36	1.01	1.34	0.55	0.35
178	RWP	09-2015	20	0.6	0.41	6.87	-90	2.72	0.97	1.24	0.37	0.28
179	RWP	09-2015	20	1.0	0.36	6.89	-63	2.55	0.92	1.18	0.35	0.27
180	RWP	09-2015	20	1.5	0.36	6.89	-91	2.71	0.97	1.23	0.38	0.28
181	RWP	09-2015	20	2.0	0.35	6.95	-93	2.71	0.95	1.21	0.38	0.27
182	RWP	09-2015	20	2.5	0.36	7.09	-118	3.09	1.09	1.38	0.43	0.29
183	RWP	09-2015	35	0.1	18.11	7.16	-225	1.99	0.48	0.91	0.30	0.27
184	RWP	09-2015	35	0.2	17.44	7.04	-220	2.22	0.58	0.96	0.35	0.25
185	RWP	09-2015	35	0.3	13.29	6.95	-225	2.83	0.79	1.12	0.47	0.26
186	RWP	09-2015	35	1.0	1.70	7.10	-186	4.07	1.33	1.57	0.67	0.30
187	RWP	09-2015	35	1.5	3.00	7.04	-158	3.79	1.20	1.49	0.57	0.29
188	RWP	09-2015	35	2.0	7.11	7.01	-164	4.56	1.32	1.62	0.74	0.29
189	RWP	09-2015	35	2.0	6.36	7.02	-148	4.42	1.30	1.61	0.72	0.29
190	RWP	09-2015	35	0	21.70	8.40	61	1.28	0.26	0.76	0.17	0.30
191	BRL	05-2016	1	0.2	6.13	6.10	-264	1.12	9.27	3.25	8.49	-0.22
192	BRL	05-2016	1	0.3	2.68	6.17	-265	-1.62	9.78	2.98	10.52	-0.32
193	BRL	05-2016	1	0.6	2.65	6.19	-255	-1.22	8.98	2.74	9.42	-0.29
194	BRL	05-2016	1	1.0	2.19	6.32	-262	32.50	4.39	6.32	3.61	1.36
195	BRL	05-2016	11	0.2	1.70	6.93	-101	5.56	5.42	3.70	3.22	0.16
196	BRL	05-2016	11	0.6	1.69	6.93	-100	4.83	2.13	2.00	1.22	0.22
197	BRL	05-2016	11	1.0	1.71	6.91	-103	7.05	2.85	2.78	1.65	0.33
198	BRL	05-2016	11	1.5	1.69	6.92	-105	5.96	2.83	2.61	1.61	0.26
199	BRL	05-2016	11	1.8	1.69	6.96	-87	9.20	3.04	3.54	1.59	0.49
200	BRL	05-2016	11	2.1	1.76	6.96	-92	4.74	1.89	1.90	1.08	0.23
201	BRL	05-2016	11	2.1	1.81	7.02	-100	4.57	1.68	1.78	0.93	0.21
202	BRL	05-2016	21	0.2	5.38	6.82	-258	3.88	1.87	1.75	1.15	0.28
203	BRL	05-2016	21	0.1	21.35	7.35	-234	3.59	1.74	2.00	1.25	0.43
204	BRL	05-2016	21	0.6	3.57	6.87	-233	6.18	5.14	3.66	3.19	0.19
205	BRL	05-2016	21	0.25	16.01	6.98	-224	5.06	3.01	2.17	2.59	0.22
206	BRL	05-2016	21	0.9	3.48	6.81	-226	4.34	6.90	3.90	4.58	0.03
207	BRL	05-2016	21	1.5	1.73	6.92	-141	4.42	1.95	1.84	1.11	0.20
208	BRL	05-2016	21	0.4	12.68	6.81	-225	4.36	3.06	2.17	2.12	0.13
209	BRL	05-2016	21	2.0	1.72	6.96	-145	3.64	1.62	1.51	0.90	0.16
210	BRL	05-2016	21	2.5	1.72	7.04	-131	4.24	2.03	1.96	1.01	0.21
211	BRL	05-2016	45	0.2	24.56	7.06	-298	1.32	0.40	0.59	0.29	0.14

Table A-1. Continued

Site ID	Sample date	Distance Offshore (m)	Sample Depth (m)	Salinity	pH	ORP	C1 (R.U.)	C2 (R.U.)	C3 (R.U.)	C4 (R.U.)	C5 (R.U.)	
212	BRL	05-2016	45	0.6	21.48	6.87	-286	2.36	0.81	0.93	0.60	0.17
213	BRL	05-2016	45	1.2	2.87	7.14	-133	5.40	3.43	2.63	2.15	0.17
214	BRL	05-2016	45	1.5	2.49	7.15	-74	3.28	1.25	1.26	0.72	0.14
215	BRL	05-2016	45	1.8	2.89	7.09	-117	4.52	2.14	1.92	1.24	0.17
216	BRL	05-2016	45	2.1	3.07	7.17	-51	5.39	2.46	2.30	1.39	0.21
217	BRL	05-2016	45	2.1	3.02	7.05	-86	4.56	2.00	1.92	1.07	0.19
218	BRL	05-2016	45	0	22.33	8.04	-20	1.52	0.60	1.15	0.34	0.38
219	EGN	05-2016	0	0.15	0.76	6.24	59	0.33	0.13	0.23	0.05	0.05
220	EGN	05-2016	0	0.25	0.97	6.42	34	0.27	0.11	0.18	0.04	0.03
221	EGN	05-2016	0	0.35	1.01	6.58	77	0.37	0.16	0.27	0.06	0.05
222	EGN	05-2016	0	0.75	1.11	6.93	59	0.33	0.12	0.21	0.06	0.03
223	EGN	05-2016	0	0.95	1.14	7.01	82	0.35	0.13	0.22	0.06	0.04
224	EGN	05-2016	0	1.15	1.09	6.88	36	0.37	0.15	0.24	0.06	0.04
225	EGN	05-2016	10	0.15	18.98	7.14	-190	1.15	0.39	0.68	0.21	0.19
226	EGN	05-2016	10	0.15	16.20	7.00	-158	0.64	0.20	0.38	0.11	0.09
227	EGN	05-2016	10	0.25	4.07	7.09	-139	1.51	0.67	0.99	0.27	0.17
228	EGN	05-2016	10	0.35	1.53	7.18	-23	0.93	0.39	0.60	0.15	0.11
229	EGN	05-2016	10	0.55	1.17	7.36	24	0.90	0.38	0.54	0.14	0.16
230	EGN	05-2016	10	0.75	2.59	7.15	-155	1.16	0.51	0.76	0.20	0.13
231	EGN	05-2016	10	0.95	0.90	7.00		0.87	0.38	0.57	0.14	0.10
232	EGN	05-2016	10	0.75	0.97	7.23	-35	0.76	0.31	0.47	0.12	0.11
233	EGN	05-2016	10	1.15	0.90	7.11	-70	0.85	0.36	0.55	0.14	0.09
234	EGN	05-2016	10	1.15	0.90		-73	0.95	0.41	0.62	0.16	0.11
235	EGN	05-2016	20	0.07	25.17	7.61	-105	1.32	0.43	0.84	0.26	0.22
236	EGN	05-2016	20	0.15	24.47	7.34	-219	1.18	0.38	0.73	0.23	0.20
237	EGN	05-2016	20	0.25	24.35	7.31	-250	1.45	0.51	0.90	0.29	0.21
238	EGN	05-2016	20	0.55	22.39	7.01	-247	1.64	0.64	1.08	0.36	0.23
239	EGN	05-2016	20	0.95	16.49	6.80	-132	2.40	1.15	1.53	0.54	0.26
240	EGN	05-2016	20	1.15	16.01	6.82	-91	2.17	0.99	1.36	0.46	0.23
241	EGN	05-2016	22.5	0.36	25.03	7.36	-238	1.45	0.50	0.87	0.29	0.20
242	EGN	05-2016	22.5	0.36	24.13	7.33	-261	1.18	0.29	0.60	0.17	0.18
243	EGN	05-2016	22.5	1.06	23.23	6.91	-157	1.08	0.45	0.71	0.27	0.16
244	EGN	05-2016	22.5	1.86	22.52	7.37	-218	1.56	0.47	0.83	0.32	0.17
245	EGN	05-2016	5	0.1	8.33	6.99	-164	1.73	0.67	1.08	0.33	0.25
246	EGN	05-2016	5	0.2	1.23	7.15	-52	0.56	0.20	0.33	0.08	0.10
247	EGN	05-2016	5	0.4	1.02	7.17	-8	0.63	0.23	0.37	0.09	0.10

Table A-1. Continued

	Site ID	Sample date	Distance Offshore (m)	Sample Depth (m)	Salinity	pH	ORP	C1 (R.U.)	C2 (R.U.)	C3 (R.U.)	C4 (R.U.)	C5 (R.U.)
248	EGN	05-2016	5	0.6	1.09	7.28	-11	0.93	0.34	0.53	0.14	0.17
249	EGN	05-2016	5	0.8	1.63	7.31	-37	0.91	0.33	0.55	0.14	0.11
250	EGN	05-2016	5	0	23.80	7.46	29	1.25	0.37	0.75	0.22	0.20
251	RWP	05-2016	0	0.2	24.93	7.31	-228	2.26	0.87	1.31	0.56	0.34
252	RWP	05-2016	0	0.25				2.08	0.52	0.90	0.36	0.27
253	RWP	05-2016	0	0.6				3.87	1.66	1.77	0.80	0.32
254	RWP	05-2016	0	0.8				3.05	1.39	1.52	0.56	0.43
255	RWP	05-2016	10	0.6	9.05	6.82	-228	3.52	1.18	1.39	0.64	0.31
256	RWP	05-2016	10	0.2	24.10	7.37	-226	1.46	0.34	0.76	0.21	0.23
257	RWP	05-2016	10	1.0	0.45	7.03	-140	3.26	1.17	1.42	0.51	0.30
258	RWP	05-2016	10	1.5	0.40	7.10	-137	3.11	1.11	1.39	0.47	0.30
259	RWP	05-2016	10	0.4	23.92	7.32	-208	1.37	0.32	0.66	0.20	0.29
260	RWP	05-2016	10	2.0	0.36	7.16	-97	3.01	1.08	1.36	0.44	0.29
261	RWP	05-2016	10	0.6	24.08	7.42	-216	1.46	0.35	0.69	0.23	0.25
262	RWP	05-2016	10	0.8	8.14	6.95	-218	3.64	1.14	1.30	0.72	0.32
263	RWP	05-2016	20	0.2	11.29	6.81	-170	2.42	0.74	1.03	0.40	0.28
264	RWP	05-2016	20	0.1	24.44	7.35	-222	1.32	0.32	0.65	0.18	0.31
265	RWP	05-2016	20	0.6	0.50	7.12	-119	2.27	0.84	1.07	0.30	0.25
266	RWP	05-2016	20	1.0	0.40	7.00	-120	2.49	0.89	1.13	0.34	0.26
267	RWP	05-2016	20	1.5	0.39	7.00	-131	1.83	0.68	0.87	0.26	0.21
268	RWP	05-2016	20	0.4	14.67	6.99	-205	2.23	0.65	0.94	0.35	0.28
269	RWP	05-2016	20	2.0	4.00	7.12	-122	2.67	0.96	1.21	0.37	0.26
270	RWP	05-2016	20	2.5	0.36	7.11	-127	2.41	0.87	1.11	0.33	0.25
271	RWP	05-2016	35	0.1	24.36	7.19	-257	1.32	0.32	0.70	0.20	0.20
272	RWP	05-2016	35	0.2	24.36	7.24	-239	1.53	0.52	0.96	0.30	0.24
273	RWP	05-2016	35	0.3	24.26	7.22	-240	1.25	0.40	0.76	0.24	0.20
274	RWP	05-2016	35	1.0	2.23	7.06	-131	3.68	1.74	1.80	0.78	0.30
275	RWP	05-2016	35	1.5	1.77	7.08	-172	3.41	1.18	1.44	0.53	0.27
276	RWP	05-2016	35	2.0	5.56	6.96	-207	3.23	1.24	1.32	0.69	0.20
277	RWP	05-2016	35	0	24.37	7.53	-25	1.17	0.25	0.67	0.15	0.23
278	Mangroves	04-2014		1.1				16.94	3.15	4.01	1.56	0.34
279	Mangroves	04-2014		0				7.45	1.43	2.07	0.79	0.24
280	Gorgos spring	09-2014			20.29	7.39	-158	0.83	0.36	0.41	0.19	0.07
281	Gorgos spring	09-2014			20.21	7.05	-130	0.98	0.41	0.47	0.22	0.09
282	Gorgos spring	09-2014			19.91	7.12	-224	0.93	0.38	0.44	0.22	0.08
283	Gorgos spring	09-2014			19.97	7.15	-221	0.81	0.33	0.38	0.19	0.07

Table A-1. Continued

Site ID	Sample date	Distance Offshore (m)	Sample Depth (m)	Salinity	pH	ORP	C1 (R.U.)	C2 (R.U.)	C3 (R.U.)	C4 (R.U.)	C5 (R.U.)
284	Gorgos spring	09-2014		19.17	7.13	-227	1.20	0.50	0.57	0.28	0.10
285	Hol Kokol spring	09-2014		9.88	7.29	-188	1.85	0.74	0.84	0.38	0.12
286	Hol Kokol spring	09-2014		9.77	7.21	-205	1.44	0.57	0.67	0.28	0.09
287	Lagoon SW	09-2014		32.74	8.08	83	0.04	0.01	0.02	0.01	0.02
288	Laja spring	09-2014		21.33	7.14	-208	0.84	0.34	0.41	0.18	0.06
289	Pargos spring	09-2014		22.07	7.26	-49	0.68	0.28	0.33	0.16	0.06
290	Pargos spring	09-2014		21.89	7.16	-181	0.75	0.31	0.36	0.17	0.07
291	Pargos spring	09-2014		21.84	7.16	-192	0.74	0.30	0.35	0.17	0.06
292	Pargos spring	09-2014		22.38	7.21	-174	0.81	0.35	0.40	0.19	0.07
293	Pargos spring	09-2014		24.58	7.36	-26	0.56	0.23	0.26	0.13	0.04
294	Pargos spring	09-2014		32.68	8.05	-71	0.08	0.03	0.04	0.02	0.02
295	Pargos spring	09-2014		26.64	7.38	-3	0.48	0.19	0.23	0.11	0.04
296	Pargos spring	09-2014		32.87	8.01	88	0.04	0.02	0.02	0.01	0.02
297	Pargos spring	09-2014		24.62	7.43	21	0.55	0.23	0.27	0.13	0.04
298	Pargos spring	09-2014		32.77	7.87	57	0.04	0.02	0.03	0.01	0.02
299	Pargos spring	09-2014		32.81	8.08	83	0.03	0.01	0.02	0.01	0.01
300	Pargos spring	09-2014					0.06	0.03	0.04	0.02	0.01
301	UNAM well	09-2014	18	5.63	7.13	-240	1.62	0.70	0.82	0.34	0.10
302	UNAM well	09-2014	26	13.38	7.14	-221	1.26	0.52	0.61	0.28	0.07
303	UNAM well	09-2014	35	29.44	7.32	-230	0.23	0.09	0.12	0.05	0.02
304	UNAM well	09-2014	40	31.04	7.29	-198	0.16	0.07	0.10	0.04	0.02
305	Cenote C7B	09-2014	20	0.67	7.20	-83	0.15	0.08	0.11	0.03	0.02
306	Cenote C7B	09-2014	28	0.68	7.10	-159	0.06	0.03	0.04	0.01	0.01
307	Cenote C7B	09-2014	29	0.67	7.38	-229	0.16	0.08	0.12	0.03	0.02
308	Cenote C7B	09-2014	30	1.50	7.21	-302	0.20	0.10	0.14	0.04	0.05
309	Cenote C7B	09-2014	31	5.14	6.48	-313	0.48	0.18	0.40	0.15	0.16
310	Cenote C7B	09-2014	32	9.42	6.36	-306	1.13	0.37	0.77	0.26	0.39
311	Cenote CKH	09-2014	30	0.76	7.04	-72	0.15	0.08	0.11	0.03	0.03
312	Cenote CKH	09-2014	31	0.76	7.02	-99	0.11	0.06	0.08	0.02	0.03
313	Cenote CKH	09-2014	32	0.75	7.00	-94	0.16	0.08	0.12	0.03	0.03
314	Cenote CKH	09-2014	33	0.75	6.98	-119	0.16	0.08	0.12	0.03	0.03
315	Cenote CKH	09-2014	34	0.75	6.92	-152	0.12	0.06	0.09	0.02	0.02
316	Cenote CTC	09-2014	1	0.27	7.04	-101	1.59	0.57	0.64	0.34	0.09
317	Cenote CZ	09-2014	2	0.70	7.11	-98	0.20	0.09	0.13	0.04	0.02
318	Cenote CZ	09-2014	35	1.34	6.97	-247	0.19	0.09	0.14	0.04	0.02
319	Cenote CZ	09-2014	38	2.96	6.93	-270	0.43	0.19	0.27	0.10	0.08

Table A-1. Continued

	Site ID	Sample date	Distance Offshore (m)	Sample Depth (m)	Salinity	pH	ORP	C1 (R.U.)	C2 (R.U.)	C3 (R.U.)	C4 (R.U.)	C5 (R.U.)
320	Cenote CZ	09-2014		40	2.97	6.90	-258	0.25	0.10	0.17	0.07	0.05
321	Cenote Muj	09-2014		1	0.29	7.79	53	0.28	0.10	0.20	0.05	0.17
322	Cenote Muj	09-2014		5	0.57	7.18	26	0.29	0.12	0.21	0.06	0.10

APPENDIX B
YUCATAN WATER CHEMISTRY DATA

Table B-1. Water chemistry input parameters for geochemical modeling in PHREEQc

Sample type	Site ID	Salinity	Temp. (°C)	HS- (uM)	Cl (mM)	SO ₄ (mM)	Na (mM)	K (mM)	Mg (mM)	Ca (mM)	DIC (mM)	NH ₄ (µM)	PO ₄ (uM)
Cenote	Cenote Siete Bocas- 20 m	0.7	25.1	37.1	6.2	0.3	5.5	0.1	1.2	3.0	7.4	0.5	0.09
Cenote	Cenote Kin Ha- 20 m	0.7	24.7	19.4	6.6	0.4	5.9	0.1	1.4	3.2	8.0	0.6	0.10
Cenote	Cenote Zapote - 2m	0.7	26.3	21.4	6.6	0.4	5.8	0.1	1.4	3.1	7.8	1.3	0.10
Spring	Gorgos spring	20.3	30	21.4	354.6	17.9	301.6	10.3	33.0	8.2	4.0	99.3	0.47
Spring	Gorgos spring	20.2	28.8	41.0	356.7	18.0	290.4	6.5	31.7	8.1	4.1	85.2	0.32
Spring	Gorgos spring	19.9	29.2	53.7	330.6	16.7	284.3	6.3	31.2	7.7	4.0	102.2	0.41
Spring	Gorgos spring	20.0	29.2	37.1	361.8	18.3	321.4	6.8	35.4	8.3	4.0	85.9	0.22
Spring	Gorgos spring	19.2	28.9	39.0	351.2	17.8	281.4	3.2	30.7	7.8	4.3	108.6	0.53
Spring	Hol Kokol spring	9.9	28.8	24.3	164.9	8.2	143.1	0.0	15.5	5.1	4.7	43.6	0.77
Spring	Hol Kokol spring	9.8	28.7	37.1	181.4	9.1	143.5	3.2	15.5	5.1	4.3	46.0	0.54
Spring	Laja spring	21.3	28.7	61.6	369.4	18.7	314.2	6.2	34.2	8.5	3.6	80.4	0.48
Spring	Pargos spring	26.6	30.1	27.3	438.3	22.3	373.1	7.8	41.2	9.1	3.2	58.0	0.43
Spring	Pargos spring	32.9	30.1	38.0			516.4	10.9	57.8	10.9	2.0	8.4	0.07
Spring	Pargos spring	24.6	29.7	40.0	432.1	22.0	366.2	10.2	40.3	8.6	2.1	36.0	0.84
Spring	Pargos spring	32.8	30.1	29.2	579.7	29.5	486.7	0.0	54.7	10.3	3.2	3.7	0.01
Spring	Pargos spring	22.1	29	39.0	387.8	19.7	322.5	6.9	35.4	8.5	3.7	54.1	0.49
Spring	Pargos spring	21.8	29.4	29.2	377.1	19.1	316.4	6.9	34.8	8.4	3.7	72.6	1.11
Spring	Pargos spring	22.4	29.8	22.4	392.5	19.9	320.0	7.0	35.3	8.3	3.6	54.2	0.73
Spring	Pargos spring	24.6	30.2	21.4	435.6	22.1	372.4	7.9	41.2	9.1	3.2	42.8	0.44
Spring	Pargos spring	32.8	30.1	33.1	577.6	29.4	485.4	8.6	54.3	10.3	2.0	2.9	0.13
Spring	Pargos spring	24.6	30.2	43.9	406.4	20.7	405.4	7.0	44.9	9.1	3.6	54.9	0.38
Spring	Pargos spring	32.7	29.3	28.2	566.3	28.8	478.7	10.4	53.5	10.3	2.1	10.2	0.75
Well	UNAM - 18 m	5.6	32	33.1	509.2	24.0	85.3	0.8	9.5	4.2	5.9	75.5	0.44
Lagoon	Lagoon surface water	32.7	30.1	26.3	583.1	29.6	476.3	9.9	57.5	11.5	2.1	2.1	0.04

APPENDIX C
INDIAN RIVER LAGOON WATER CHEMISTRY DATA

Table C-1. Water chemistry input parameters for geochemical modeling in PHREEQc.

Piezometer	Depth (m)	SAL (PSU)	T (°C)	pH	Cl (mM)	SO ₄ (mM)	Na (mM)	K (mM)	Mg (mM)	Ca (mM)	DIC (mM)
BRL 1	0.2	6.13	26.9	6.1	118.05	5.44	96.62	1.99	10.68	7.33	8.50
BRL 1	0.3	2.68	26.3	6.17	49.34	1.75	40.50	0.85	4.55	5.93	9.82
BRL 1	0.6	2.65	25.6	6.19	38.42	1.10	37.00	1.14	4.82	3.76	10.90
BRL 1	1	2.19	25	6.32	31.30	0.96	22.84	0.73	2.69	5.38	9.56
BRL 11	0.2	1.7	27.4	6.93	64.75	3.41	56.00	1.19	5.93	6.77	4.87
BRL 11	0.6	1.69	27	6.93	23.41	1.36	17.41	0.49	2.17	4.51	5.42
BRL 11	1	1.71	25.8	6.91	24.07	1.36	17.42	0.50	2.18	4.51	5.44
BRL 11	1.5	1.69	26.3	6.92	23.52	1.35	17.14	0.49	2.15	4.51	5.39
BRL 11	1.8	1.69	25.3	6.96	23.66	1.33	17.26	0.52	2.17	4.57	5.28
BRL 11	2.1	1.76	25.6	6.96	24.27	1.27	17.39	0.51	2.13	4.65	5.43
BRL 11	2.1	1.81	25.8	7.02	24.27	1.29	17.49	0.53	2.14	4.68	5.38
BRL 21	0.2	5.38	27.5	6.82	206.34	10.56	172.34	3.62	19.27	9.07	4.12
BRL 21	0.6	3.57	27.1	6.87	125.65	6.63	108.67	2.42	11.49	9.77	4.88
BRL 21	0.9	3.48	26.2	6.81	101.02	5.26	82.34	1.84	9.38	6.51	5.08
BRL 21	1.5	1.73	26	6.92	49.70	2.43	20.20	0.70	2.36	4.84	5.56
BRL 21	2	1.72	25.4	6.96	24.39	1.24	17.64	0.64	2.13	4.52	5.47
BRL 21	2.5	1.72	25.2	7.04	23.78	1.25	17.08	0.61	2.06	4.38	5.31
BRL 45	0.2	24.56	27	7.06	359.84	18.23	305.79	6.56	34.58	7.92	3.45
BRL 45	0.6	21.48	26.7	6.87	338.32	17.38	287.22	6.07	32.50	8.17	3.80
BRL 45	1.2	2.87	26	7.14	77.95	4.07	68.10	1.98	7.73	3.13	4.37
BRL 45	0.5	2.49	25.9	7.15	34.56	1.86	28.12	0.98	4.11	2.82	4.52
BRL 45	1.8	2.89	25.1	7.09	43.30	2.28	34.54	1.19	4.63	3.55	4.59
BRL 45	2.1	3.07	25.3	7.17	45.57	2.40	36.28	1.20	4.72	3.74	4.61
BRL 45	2.1	3.02	28.4	7.05	45.80	2.40	28.96	0.62	3.45	5.51	4.62
BRL 45	0	22.33	27.7	8.04	360.45	18.25	307.48	6.71	34.61	7.05	1.90
EGN 0	0.15	0.76	26.9	6.24	9.23	0.65	4.63	0.13	2.22	1.94	3.57
EGN 0	0.25	0.97	27	6.42	11.95	0.80	5.80	0.13	2.86	2.73	1.14
EGN 0	0.35	1.01	27.1	6.58	12.63	0.83	6.19	0.13	3.08	2.98	4.88
EGN 0	0.75	1.11	27.4	6.93	13.47	0.88	6.88	0.13	3.12	3.80	5.33
EGN 0	0.95	1.14	27.6	7.01	13.45	0.88	6.86	0.13	3.14	3.79	5.42
EGN 0	1.15	1.09	27.4	6.88	13.39	0.87	6.78	0.13	3.29	3.61	5.52

Table C-1. Continued

Piezometer	Depth (m)	SAL (PSU)	T (°C)	pH	Cl (mM)	SO ₄ (mM)	Na (mM)	K (mM)	Mg (mM)	Ca (mM)	DIC (mM)
EGN 10	0.25	4.07	26.8	7.09	51.15	3.15	66.87	1.33	8.34	4.85	4.27
EGN 10	0.75	2.59	27.1	7.15	18.89	1.47	14.17	0.28	2.45	3.61	4.69
EGN 10	0.95	0.9	27	7	10.44	1.03	7.10	0.09	1.71	3.55	4.81
EGN 10	1.15	0.9	26.8	7.11	10.46	1.04	7.03	0.18	1.70	3.56	4.77
EGN 10	1.15	0.9	26.8	--	10.42	1.03	7.08	0.09	1.70	3.56	4.80
EGN 10	0	23.8	27.7	7.46	386.24	19.67	328.73	7.07	36.89	7.47	1.99
EGN 20	0.07	25.17	30.2	7.61	400.62	20.42	342.40	7.22	38.63	7.75	1.99
EGN 20	0.15	24.47	29.1	7.34	397.13	20.23	340.75	7.31	38.21	7.82	2.14
EGN 20	0.25	24.35	28	7.31	392.99	20.00	335.27	7.17	37.60	7.86	2.70
EGN 20	0.55	22.39	27.6	7.01	343.21	17.46	294.24	6.18	32.71	7.49	3.40
EGN 20	0.95	16.49	27.7	6.8	248.68	12.92	214.94	4.56	22.79	6.05	4.21
EGN 20	1.15	16.01	26.9	6.82	253.16	13.38	217.74	4.60	24.42	6.40	4.27
EGN 22.5	0.36	24.13	27.4	7.33	397.49	20.08	341.75	7.18	38.64	7.97	2.56
EGN 22.5	0.36	25.03	27.9	7.36	400.21	20.32	340.37	7.33	38.24	7.96	2.64
EGN 22.5	1.06	23.23	27.2	6.91	369.72	18.36	314.18	6.72	36.28	8.35	3.60
EGN 22.5	1.56	22.52	26.3	7.37	356.80	17.69	301.53	6.42	34.22	7.62	3.85
RWP 10	0.6	9.05	27.3	6.82	76.55	3.69	75.31	1.61	8.73	4.79	5.32
RWP 10	1	0.45	26.7	7.03	3.19	0.04	2.66	0.13	0.89	2.63	6.91
RWP 10	1.5	0.4	26.4	7.1	2.15	0.01	1.56	0.08	0.62	2.77	6.82
RWP 10	2	0.36	25.7	7.16	1.60	0.00	1.07	0.04	0.21	3.11	6.76
RWP 20	0.2	11.29	27.9	6.81	203.26	10.19	172.15	3.79	18.57	7.52	4.41
RWP 20	0.6	0.5	27.1	7.12	4.48	0.13	3.50	0.10	0.31	3.44	6.73
RWP 20	1	0.4	26.6	7	1.84	0.01	1.31	0.08	0.18	3.14	6.81
RWP 20	1.5	0.39	25.6	7	1.81	0.01	1.31	0.07	0.18	3.14	6.81
RWP 20	2	4	25.4	7.12	1.87	0.02	1.58	0.04	0.15	3.07	6.84
RWP 20	2.5	0.36	24.6	7.11	1.50	0.01	1.19	0.04	0.19	3.04	6.82
RWP 35	0.1	24.36	27.2	7.19	381.87	19.19	328.36	7.09	36.91	7.71	2.70
RWP 35	0.2	24.36	27.1	7.24	382.07	19.26	327.15	7.05	36.78	7.67	2.60
RWP 35	0.3	24.26	27	7.22	383.22	19.32	326.72	7.04	36.73	7.65	2.54
RWP 35	0.6	20	26.5	7.06	274.81	13.61	236.97	5.25	26.57	6.36	3.92
RWP 35	1	2.23	25.9	7.06	31.29	1.19	22.70	0.63	3.57	2.99	6.78
RWP 35	1.5	1.77	26.5	7.08	35.88	1.76	33.36	0.56	3.75	4.58	6.93
RWP 35	2	5.56	24.9	6.96	81.40	4.35	72.72	1.29	8.64	5.00	6.69
RWP 35	2	5.53	25.2	7.02	82.02	4.38	67.34	1.20	7.96	4.85	6.68
RWP 35	0	24.37	27.6	7.53	383.39	19.42	328.77	7.03	36.84	7.56	2.03

LIST OF REFERENCES

- Abril G. and Borges A. V. (2004) Carbon Dioxide and Methane Emissions from Estuaries. In *Greenhouse Gas Emissions: Fluxes and Processes, Hydroelectric Reservoirs and Natural Environments* (eds. A. Tremblay, L. Varfalvy, C. Roehm, and M. Garneau). Environmental Science Series, Springer, Berlin. pp. 187–207.
- Anderson R. F. and Schiff S. L. (1987) Alkalinity Generation and the Fate of Sulfur in Lake Sediments. *Can. J. Fish. Aquat. Sci.* **44**, 188–193.
- Arndt S., Jorgenson B. B., LaRowe D. E., Middelburg J. J., Pancost R. D. and Regnier P. (2013) Quantifying the degradation of organic matter in marine sediments: A review and synthesis. *Earth-Science Reviews* **123**, 53–86.
- Back W. and Hanshaw B. (1970) Comparison of chemical hydrogeology of the carbonate peninsulas of Florida and Yucatan. *Journal of Hydrology* **10**, 330–368.
- Baker A., Inverarity R., Charlton M. and Richmond S. (2003) Detecting river pollution using fluorescence spectrophotometry: Case studies from the Ouseburn, NE England. *Environmental Pollution* **124**, 57–70.
- Baker A. and Spencer R. G. M. (2004) Characterization of dissolved organic matter from source to sea using fluorescence and absorbance spectroscopy. *The Science of the total environment* **333**, 217–32.
- Bastviken D., Cole J., Pace M. and Tranvik L. (2004) Methane emissions from lakes: Dependence of lake characteristics, two regional assessments, and a global estimate. *Global Biogeochemical Cycles* **18**, 1–12.
- Beck A. J., Tsukamoto Y., Tovar-Sanchez A., Huerta-Diaz M., Bokuniewicz H. J. and Sañudo-Wilhelmy S. A. (2007) Importance of geochemical transformations in determining submarine groundwater discharge-derived trace metal and nutrient fluxes. *Applied Geochemistry* **22**, 477–490.
- Beddows P., Smart P. L., Whitaker F. F. and Smith S. L. (2007) Decoupled fresh-saline groundwater circulation of a coastal carbonate aquifer: Spatial patterns of temperature and specific electrical conductivity. *Journal of Hydrology* **346**, 18–32.
- Berner R. A. (1980) *Early Diagenesis: A Theoretical Approach.*, Princeton University Press.
- Berner R. A., Scott M. R. and Thomlinson C. (1970) Carbonate alkalinity in the pore waters of anoxic marine sediments. *Limnology and Oceanography*, 544–549.
- Blanchon P., Eisenhauer A., Fietzke J. and Liebtrau V. (2009) Rapid sea-level rise and reef back-stepping at the close of the last interglacial highstand. *Nature* **458**, 881–884.

- Blomqvist S., Gunnars A. and Elmgren R. (2004) Why the limiting nutrient differs between temperate coastal seas and freshwater lakes: A matter of salt. *Limnology and Oceanography* **49**, 2236–2241.
- Blough N. V. and Del Vecchio R. (2002) Chromophoric DOM in the Coastal Environment. In *Biogeochemistry of Marine Dissolved Organic Matter* (eds. D. A. Hansell and C. A. Carlson). Elsevier Science. pp. 509–546.
- Borges A. V., Champenois W., Gypens N., Delille B. and Harlay J. (2016) Massive marine methane emissions from near-shore shallow coastal areas. *Scientific Reports* **6**, 27908
- Brooks H. K. (1961) The submarine spring off Crescent Beach, Florida. *Quarterly Journal of the Florida Academy of Sciences* **24**, 122–134.
- Brown A. L., Martin J. B., Sreaton E. J., Ezell J. E., Spellman P. and Gulley J. (2014) Bank storage in karst aquifers: The impact of temporary intrusion of river water on carbonate dissolution and trace metal mobility. *Chemical Geology* **385**, 56–69.
- Bugna G. C., Chanton J. P., Cable J. E., Burnett W. C. and Cable P. H. (1996) The importance of groundwater discharge to the methane budgets of nearshore and continental shelf waters of the northeastern Gulf of Mexico. *Geochimica et Cosmochimica Acta* **60**, 4735–4746.
- Burnett W. C., Aggarwal P. K., Aureli a, Bokuniewicz H., Cable J. E., Charette M. a, Kontar E., Krupa S., Kulkarni K. M., Loveless a, Moore W. S., Oberdorfer J. a, Oliveira J., Ozyurt N., Povinec P., Privitera a M. G., Rajar R., Ramessur R. T., Scholten J., Stieglitz T., Taniguchi M. and Turner J. V (2006) Quantifying submarine groundwater discharge in the coastal zone via multiple methods. *The Science of the total environment* **367**, 498–543.
- Cai W.J. (2011) Estuarine and coastal ocean carbon paradox: CO₂ sinks or sites of terrestrial carbon incineration? *Annual Review of Marine Science* **3**, 123–45.
- Cai W.J., Wang Y., Krest J. and Moore W. S. (2003) The geochemistry of dissolved inorganic carbon in a surficial groundwater aquifer in North Inlet, South Carolina, and the Carbon fluxes to the coastal ocean. *Geochimica et Cosmochimica Acta* **67**, 631–637.
- Caraco N. F., Cole J. J. and Likens G. E. (1989) Evidence for sulphate-controlled phosphorus release from sediments of aquatic systems. *Nature* **31**, 316–318.
- Carruthers T. J. B., van Tussenbroek B. I. and Dennison W. C. (2005) Influence of submarine springs and wastewater on nutrient dynamics of Caribbean seagrass meadows. *Estuarine, Coastal and Shelf Science* **64**, 191–199.

- Del Castillo C. E. (2005) Remote Sensing of Organic Matter in Coastal Waters. In *Remote Sensing of Coastal Aquatic Environments: Technologies, Techniques and Applications* (eds. R. L. Miller, C. E. Del Castillo, and B. A. McKee). Springer, Dordrecht, The Netherlands.
- Cawley K. M., Ding Y., Fourqurean J. and Jaff R. (2012) Characterising the sources and fate of dissolved organic matter in Shark Bay, Australia: A preliminary study using optical properties and stable carbon isotopes. *Marine and Freshwater Research* **63**, 1098–1107.
- Chambers, R.M. and Odum, W.E. (1990) Porewater Oxidation, Dissolved Phosphate and the Iron Curtain: Iron-Phosphorus Relations in Tidal Freshwater Marshes. *Biogeochemistry* **10**, 37-52.
- Chapelle F. H., Shen Y., Strom E. W. and Benner R. (2016) The removal kinetics of dissolved organic matter and the optical clarity of groundwater. *Hydrogeology Journal* **24**, 1413–1422.
- Chen C. A. and Wang S. (1999) Carbon, alkalinity and nutrient budgets on the East China Sea continental Shelf. *Journal of Geophysical Research* **104**, 20,675-20,686.
- Corbett D., Chanton J., Burnett W., Dillon K., Rutkowski C. and Fourqurean J. (1999) Patterns of groundwater discharge into Florida Bay. *Limnology and Oceanography* **44**, 1045–1055.
- Coronado C., Candela J., Iglesias-Prieto R., Sheinbaum J., López M. and Ocampo-Torres F. J. (2007) On the circulation in the Puerto Morelos fringing reef lagoon. *Coral Reefs* **26**, 149–163.
- Davison W. and Woof C. (1990) The Dynamics of Alkalinity Generation by an Anoxic Sediment Exposed to Acid Water. *Water Resources* **24**, 1537–1543.
- DeJonge V. N. and Villerius L. a. (1989) Possible role of carbonate dissolution in estuarine phosphate dynamics. *Limnology and Oceanography* **34**, 332–340.
- Dorsett A., Cherrier J., Martin J. B. and Cable J. E. (2011) Assessing hydrologic and biogeochemical controls on pore-water dissolved inorganic carbon cycling in a subterranean estuary: A ¹⁴C and ¹³C mass balance approach. *Marine Chemistry* **127**, 76–89.
- Dulaiova H., Camilli R., Henderson P. B. and Charette M. A. (2010) Coupled radon, methane and nitrate sensors for large-scale assessment of groundwater discharge and non-point source pollution to coastal waters. **101**, 553–563.
- Egleston E. S., Sabine C. L. and Morel M. M. (2010) Revelle revisited : Buffer factors that quantify the response of ocean chemistry to changes in DIC and alkalinity. *Global Biogeochemical Cycles* **24**, 1–9.

- Engel A. S., Porter M. L., Stern L. A., Quinlan S. and Bennett P. C. (2004) Bacterial diversity and ecosystem function of filamentous microbial mats from aphotic (cave) sulfidic springs dominated by chemolithoautotrophic “Epsilonproteobacteria.” *FEMS Microbiology Ecology* **51**, 31–53.
- Fleury P., Bakalowicz M. and de Marsily G. (2007) Submarine springs and coastal karst aquifers: A review. *Journal of Hydrology* **339**, 79–92.
- Froelich P. N., Klinkhammer G. P., Bender M. L., Luedtke G. R., Heath D. P. D., Cullen D., Hammond B. and Hartman V. (1979) Early oxidation of organic matter in pelagic sediments of the Eastern equatorial Atlantic: suboxic diagenesis. *Geochimica et Cosmochimica Acta* **43**, 1075–1090.
- Gonneea M. E. and Charette M. A. (2014) Hydrologic controls on nutrient cycling in an unconfined coastal aquifer. *Environmental Science and Technology* **48**, 14178–14185.
- Gonneea M. E., Charette M. a., Liu Q., Herrera-Silveira J. a. and Morales-Ojeda S. M. (2014) Trace element geochemistry of groundwater in a karst subterranean estuary (Yucatan Peninsula, Mexico). *Geochimica et Cosmochimica Acta* **132**, 31–49.
- González-Herrera R., Sánchez-y-Pinto I. and Gamboa-Vargas J. (2002) Groundwater-flow modeling in the Yucatan karstic aquifer, Mexico. *Hydrogeology Journal* **10**, 539–552.
- Gulley J. D., Martin J. B. and Brown A. (2016) Organic carbon inputs, common ions and degassing: rethinking mixing dissolution in coastal eogenetic carbonate aquifers. *Earth Surface Processes and Landforms* **41**, 2098–2110.
- Gulley J. D., Martin J. B., Moore P. J., Brown A., Spellman P. D. and Ezell J. (2015) Heterogeneous distributions of CO₂ may be more important for dissolution and karstification in coastal eogenetic limestone than mixing dissolution. *Earth Surface Processes and Landforms* **40**, 1057–1071.
- Gulley J., Martin J. B., Sreaton E. J. and Moore P. J. (2011) River reversals into karst springs : A model for cave enlargement in eogenetic karst aquifers. *GSA Bulletin* **123**, 457–467.
- Gulley J., Martin J. and Moore P. (2014) Vadose CO₂ gas drives dissolution at water tables in eogenetic karst aquifers more than mixing dissolution. *Earth Surface Processes and Landforms* **39**, 1833–1846.
- Guo W., Stedmon C. A., Han Y., Wu F., Yu X. and Hu M. (2007) The conservative and non-conservative behavior of chromophoric dissolved organic matter in Chinese estuarine waters. *Marine Chemistry* **107**, 357–366.
- Hach (2013) Sulfide, Methylene Blue Method. In *DR/890 Colorimeter Procedures Manual* pp. 571–574.

- Hanshaw B. B. and Back W. (1980) Chemical mass-wasting of the northern Yucatan Peninsula by groundwater dissolution. *Geology* **8**, 222.
- Hernández-Terrones L., Rebolledo-Vieyra M., Merino-Ibarra M., Soto M., Le-Cossec A. and Monroy-Ríos E. (2011) Groundwater pollution in a karstic region (NE Yucatan): Baseline nutrient content and flux to coastal ecosystems. *Water, Air, and Soil Pollution* **218**, 517–528.
- Holloway J. M. and Dahlgren R. A. (2002) Nitrogen in rock: Occurrences and biogeochemical implications. *Global Biogeochemical Cycles* **16**, 65-1-65–17.
- Hopkinson C. S., Buffam I., Hobbie J., Vallino J., Perdue M., Eversmeyer B., Prah F., Covert J., Hodson R., Moran M. a, Smith E., Baross J., Crump B., Findlay S. and Foreman K. (1998) Terrestrial inputs of organic matter to coastal ecosystems: An intercomparison of chemical characteristics and bioavailability. *Biogeochemistry* **43**, 221–234.
- Hu C., Muller-Karger F. E. and Swarzenski P. W. (2006) Hurricanes, submarine groundwater discharge, and Florida's red tides. *Geophysical Research Letters* **33**, L11601.
- Jankowska H., Matciak M. and Nowacki J. (1994) Salinity variations as an effect of groundwater seepage through the seabed (Puck Bay, Poland). *Oceanologia* **36**, 33–46.
- Jannash H. (1995) Microbial Interactions with Hydrothermal Fluids. In *Seafloor Hydrothermal Systems: Physical, Chemical, Biological, and Geological Interactions* (eds. S. E. Humphris, R. A. Zierenberg, L. S. Mullineaux, and R. E. Thomson). American Geophysical Union, Washington, D.C. pp. 273–296.
- Jensen H. S., McGlathery K. J., Marino R. and Howarth R. W. (1998) Forms and availability of sediment phosphorus in carbonate sand of Bermuda seagrass beds. *Limnology and Oceanography* **43**, 799–810.
- Johannesson K. H., Chevis D. a., Burdige D. J., Cable J. E., Martin J. B. and Roy M. (2011) Submarine groundwater discharge is an important net source of light and middle REEs to coastal waters of the Indian River Lagoon, Florida, USA. *Geochimica et Cosmochimica Acta* **75**, 825–843.
- Khadka M. B., Martin J. B. and Jin J. (2014) Transport of dissolved carbon and CO₂ degassing from a river system in a mixed silicate and carbonate catchment. *Journal of Hydrology* **513**, 391–402.
- Kim G. and Swarzenski P. W. (2010) Submarine Groundwater Discharge (SGD) and Associated Nutrient Fluxes to the Coastal Ocean. In *Carbon and Nutrient Fluxes in Continental Margins* (ed. K.-K. et al. Liu). Springer-Verlag Berlin Heidelberg. pp. 529–538.

- Knee K. L. and Paytan A. (2011) *Submarine Groundwater Discharge: A Source of Nutrients, Metals, and Pollutants to the Coastal Ocean*. eds. E. Wolansky and D. S. McLusky, Waltham: Academic Press.
- Koch M. S., Benz R. E. and Rudnick D. T. (2001) Solid-phase phosphorus pools in highly organic carbonate sediments of northeastern Florida Bay. *Estuarine Coastal and Shelf Science* **52**, 279–291.
- Kothawala D. N., von Wachenfeldt E., Koehler B. and Tranvik L. J. (2012) Selective loss and preservation of lake water dissolved organic matter fluorescence during long-term dark incubations. *Science of the Total Environment* **433**, 238–246.
- Kroeger K. D. and Charette M. a. (2008) Nitrogen biogeochemistry of submarine groundwater discharge. *Limnology and Oceanography* **53**, 1025–1039.
- Kroeger K. D., Swarzenski P. W., Greenwood W. J. and Reich C. (2007) Submarine groundwater discharge to Tampa Bay : Nutrient fluxes and biogeochemistry of the coastal aquifer. *Marine Chemistry* **104**, 85–97.
- Kuivila K. M. and Murray J. W. (1984) Organic matter diagenesis in freshwater sediments : The alkalinity and total CO₂ balance and methane production in the sediments of Lake Washington. *Limnology and Oceanography* **29**, 1218–1230.
- Kwon E. Y., Guebuem K., Primeau F., Moore W. S., Cho H. M., DeVries T., Sarmiento J. L., Charette M. A. and Cho Y. K. (2014) Global estimate of submarine groundwater discharge based on an observationally constrained radium isotope model. *Geophysical Research Letters* **41**, 1–7.
- Lambert M. J. and Burnett W. C. (2003) Submarine Groundwater Discharge Estimates at a Florida Coastal Site Based on Continuous Radon Measurements. *Biogeochemistry* **66**, 55–73.
- Langmuir D. (1997) *Aqueous Environmental Geochemistry*., Prentice-Hall, Inc., Upper Saddle River, NJ.
- Lapointe B. E., Littler M. M. and Littler D. S. (1992) Nutrient Availability to Marine Macroalgae in Siliciclastic versus Carbonate-Rich Coastal Waters. *Estuaries* **15**, 75–82.
- Lapworth D. J., Goody D. C., Butcher a. S. and Morris B. L. (2008) Tracing groundwater flow and sources of organic carbon in sandstone aquifers using fluorescence properties of dissolved organic matter (DOM). *Applied Geochemistry* **23**, 3384–3390.
- Leader J. W., Dunne E. J. and Reddy K. R. (2007) Phosphorus sorbing materials: sorption dynamics and physicochemical characteristics. *Journal of Environment Quality* **37**, 174–181.

- Lecher A. L., Kessler J., Sparrow K., Kodovska F. G., Dimova N., Murray J., Tulaczyk S. and Paytan A. (2015) Methane transport through submarine groundwater discharge to the North Pacific and Arctic Ocean at two Alaskan sites. *Limnology and Oceanography* **61**, S344–S355.
- Lee R. W. (1999) Oxidation of sulfide by *Spartina alterniflora* roots. *Limnology and Oceanography* **44**, 1155–1159.
- Lide D. R. and Frederikse H. P. . eds. (1995) *CRC Handbook of Chemistry and Physics*. 76th ed., CRC Press, Inc., Boca Raton, FL.
- Linkhorst A., Dittmar T. and Waska H. (2017) Molecular Fractionation of Dissolved Organic Matter in a Shallow Subterranean Estuary: The Role of the Iron Curtain. *Environmental Science and Technology* **51**, 1312–1320.
- Liu Q., Charette M. A., Breier C. F., Henderson P. B., Mccorkle C., Martin W. and Dai M. (2017) Carbonate system biogeochemistry in a subterranean estuary-Waquoit Bay, USA. *Geochimica et Cosmochimica Acta* **203**, 422-439.
- Liu Q., Dai M., Chen W., Huh C. -a., Wang G., Li Q. and Charette M. a. (2012) How significant is submarine groundwater discharge and its associated dissolved inorganic carbon in a river-dominated shelf system? *Biogeosciences* **9**, 1777–1795.
- Lovley D. R. and Chapelle F. H. (1995) Deep subsurface microbial processes. *Reviews of Geophysics* **33**, 365–381.
- Lyons D. A., Arvanitidis C., Blight A. J., Chatzinikolaou E., Guy-Haim T., Kotta J., Orav-Kotta H., Queirós A. M., Rilov G., Somerfield P. J. and Crowe T. P. (2014) Macroalgal blooms alter community structure and primary productivity in marine ecosystems. *Global Change Biology* **20**, 2712–2724.
- Mahieu K., De Visscher A., Vanrolleghem P. A. and Van Cleemput O. (2008) Modelling of stable isotope fractionation by methane oxidation and diffusion in landfill cover soils. *Waste Management* **28**, 1535–1542.
- Malowany K., Stix J., Van Pelt A. and Lucic G. (2015) H₂S interference on CO₂ isotopic measurements using a Picarro G1101-i cavity ring-down spectrometer. *Atmospheric Measurement Techniques Discussions* **8**, 5651–5675.
- Markager S., Stedmon C. A. and Søndergaard M. (2011) Seasonal dynamics and conservative mixing of dissolved organic matter in the temperate eutrophic estuary Horsens Fjord. *Estuarine, Coastal and Shelf Science* **92**, 376–388.
- Martin J. B., Hartl K. M., Corbett D. R., Swarzenski P. W. and Cable J. E. (2003) A Multi-Level Pore-Water Sampler for Permeable Sediments. *Journal of Sedimentary Research* **73**, 128–132.

- Martin J. B., Cable J. E., Jaeger J., Hartl K. and Smith C. G. (2006) Thermal and chemical evidence for rapid water exchange across the sediment-water interface by bioirrigation in the Indian River Lagoon, Florida. *Limnology and Oceanography* **51**, 1332–1341.
- Martin J. B., Cable J. E., Smith C., Roy M. and Cherrier J. (2007) Magnitudes of submarine groundwater discharge from marine and terrestrial sources: Indian River Lagoon, Florida. *Water Resources Research* **43**.
- McCollum T. and Shock E. (1997) Geochemical constraints on chemolithoautotrophic metabolism by microorganisms in seafloor hydrothermal systems. *Geochimica et Cosmochimica Acta* **61**, 4375–4391.
- McCoy C. a and Corbett D. R. (2009) Review of submarine groundwater discharge (SGD) in coastal zones of the Southeast and Gulf Coast regions of the United States with management implications. *Journal of environmental management* **90**, 644–51.
- McGowan K. T. and Martin J. B. (2007) Chemical composition of mangrove-generated brines in Bishop Harbor, Florida: Interactions with submarine groundwater discharge. *Marine Chemistry* **104**, 58–68.
- Megonigal J. P., Hines M. E. and Visscher P. T. (2005) Anaerobic Metabolism: Linkages to Trace Gases and Aerobic Processes. In *Biogeochemistry Vol. 8 Treatise on Geochemistry* (ed. W. H. Schlesinger). Elsevier, Pergamon, Oxford. pp. 317–424.
- Metcalf C. D., Beddows P. a., Bouchot G. G., Metcalfe T. L., Li H. and Van Lavieren H. (2011) Contaminants in the coastal karst aquifer system along the Caribbean coast of the Yucatan Peninsula, Mexico. *Environmental Pollution* **159**, 991–997.
- Michael H. a, Mulligan A. E. and Harvey C. F. (2005) Seasonal oscillations in water exchange between aquifers and the coastal ocean. *Nature* **436**, 1145–1148.
- Mitterer R. M. (2010) Methanogenesis and sulfate reduction in marine sediments: A new model. *Earth and Planetary Science Letters* **295**, 358–366.
- Moore W. S. (1999) The subterranean estuary: A reaction zone of ground water and sea water. *Marine Chemistry* **65**, 111–125.
- Morse J. W. and Arvidson R. S. (2002) The dissolution kinetics of major sedimentary carbonate minerals. *Earth-Science Reviews* **58**, 51–84.
- Murphy K. R., Hambly A., Singh S., Henderson R. K., Baker A., Stuetz R. and Khan S. J. (2011) Organic Matter Fluorescence in Municipal Water Recycling Schemes : Toward a Unified PARAFAC Model. *Environmental Science and Technology* **45**, 2909–2916.

- Murphy K. R., Stedmon C. A., Graeber D. and Bro R. (2013) Fluorescence spectroscopy and multi-way techniques. PARAFAC. *Analytical Methods* **5**, 6557.
- Mutchler T., Dunton K. H., Townsend-Small A., Fredriksen S. and Rasser M. K. (2007) Isotopic and elemental indicators of nutrient sources and status of coastal habitats in the Caribbean Sea, Yucatan Peninsula, Mexico. *Estuarine, Coastal and Shelf Science* **74**, 449–457.
- Null K. A., Knee K. L., Crook E. D., de Sieyes N. R., Rebolledo-Vieyra M., Hernández-Terrones L. and Paytan A. (2014) Composition and fluxes of submarine groundwater along the Caribbean coast of the Yucatan Peninsula. *Continental Shelf Research* **77**, 38–50.
- Ohno T. (2002) Fluorescence inner-filtering correction for determining the humification index of dissolved organic matter. *Environmental Science & Technology* **36**, 742–746.
- Parkhurst D. (1995) User's guide to PHREEQC - A computer program for speciation, reaction-path, advective-transport, and inverse geochemical calculations. *U.S. Geological Survey Water-Resources Investigations Report* **95-4227**, 143.
- Parkhurst L. (1997) Geochemical mole-balance modeling with uncertain data. *Water Resources Research* **33**, 1957–1970.
- Parra S. M., Mariño-tapia I., Enriquez C. and Valle-levinson A. (2014) Variations in turbulent kinetic energy at a point source submarine groundwater discharge in a reef lagoon. *Ocean Dynamics* **64**, 1601–1614.
- Parra S. M., Valle-Levinson A., Mario-Tapia I. and Enriquez C. (2015) Salt intrusion at a submarine spring in a fringing reef lagoon. *Journal of Geophysical Research C: Oceans* **120**, 2736–2750.
- Paytan A. and McLaughlin K. (2007) The oceanic phosphorus cycle. *Chemical Reviews* **107**, 563–576.
- Perry E., Velazquez-Oliman G. and Socki R. A. (2003) Hydrogeology of the Yucatán Peninsula. In *The Lowland Maya: Three Millennia at the Human–Wildland Interface* (eds. A. Gomez-Pompa, M. F. Allen, S. L. Fedick, and J. J. Jimenez-Osornio). CRC Press, Inc. pp. 115–138.
- Plummer L. N. (1975) Mixing of sea water with calcium carbonate ground water. In *Quantitative Studies in the Geological Sciences: Geological Society of America Memoir 142* (ed. E. H. T. Whitten). pp. 219–236.
- Preuss I., Knoblauch C., Gebert J. and Pfeiffer E. M. (2013) Improved quantification of microbial CH₄ oxidation efficiency in arctic wetland soils using carbon isotope fractionation. *Biogeosciences* **10**, 2539–2552.

- Price R. M. and Herman J. S. (1991) Geochemical investigations of salt-water intrusion into a coastal carbonate aquifer: Mallorca, Spain. *Geological Society of America Bulletin* **103**, 1270–1279.
- Price R. M., Jolicoeur J. L. and Stalker J. C. (2008) Geochemistry of Phosphorus in a Carbonate Aquifer Affected by Seawater Intrusion. *20th Salt Water Intrusion Meeting Naples, FL June 23-27, 2008*, 213–216.
- Price R. M., Savabi M. R., Jolicoeur J. L. and Roy S. (2010) Adsorption and desorption of phosphate on limestone in experiments simulating seawater intrusion. *Applied Geochemistry* **25**, 1085–1091.
- Redfield A. C. (1934) On The Proportions of Organic Derivations in Sea Water and Their Relation to The Composition of Plankton. *James Johnstone Memorial Volume*, 177–192.
- Roy, M., Martin J. B., Cable J. E., Smith C. G. and Cherrier J. (2010) Iron cycling in the seepage face of a subterranean estuary (Indian River Lagoon, Florida). *Geochimica et Cosmochimica Acta* **74**, 5560–5573.
- Roy M., Rouxel O., Martin J. B. and Cable J. E. (2012) Iron isotope fractionation in a sulfide-bearing subterranean estuary and its potential influence on oceanic Fe isotope flux. *Chemical Geology* **300–301**, 133–142.
- Roy M., Martin J. B., Cable J. E. and Smith C. G. (2013a) Variations of iron flux and organic carbon remineralization in a subterranean estuary caused by inter-annual variations in recharge. *Geochimica et Cosmochimica Acta* **103**, 301–315.
- Roy M., Martin J. B., Cable J. E. and Smith C. G. (2013b) Variations of iron flux and organic carbon remineralization in a subterranean estuary caused by inter-annual variations in recharge. *Geochimica et Cosmochimica Acta* **103**, 301–315.
- Ruttenberg K. C. and Berner R. a. (1993) Authigenic apatite formation and burial in sediments from non-upwelling, continental margin environments. *Geochimica et Cosmochimica Acta* **57**, 991–1007.
- Sabine C. L., Feely R. a, Gruber N., Key R. M., Lee K., Bullister J. L., Wanninkhof R., Wong C. S., Wallace D. W. R., Tilbrook B., Millero F. J., Peng T.-H., Kozyr A., Ono T. and Rios A. F. (2004) The oceanic sink for anthropogenic CO₂. *Science* **305**, 367–371.
- Sadat-noori M., Maher D. T. and Santos I. R. (2016) Groundwater Discharge as a Source of Dissolved Carbon and Greenhouse Gases in a Subtropical Estuary. *Estuaries and Coasts* **39**, 639–656.
- Sanders C. J., Santos I. R., Barcellos R. and Silva Filho E. V. (2012) Elevated concentrations of dissolved Ba, Fe and Mn in a mangrove subterranean estuary: Consequence of sea level rise? *Continental Shelf Research* **43**, 86–94.

- Sanford W. E. and Konikow L. (1989) Porosity development in coastal carbonate aquifers. *Geology* **17**, 249–252.
- Santoro A. (2010) Microbial nitrogen cycling at the saltwater–freshwater interface. *Hydrogeology Journal* **18**, 187–202.
- Sarmiento J. L. and Gruber N. (2006) *Ocean Biogeochemical Dynamics.*, Princeton University Press.
- Sayles F.L. and Mangelsdorf P.C. (1977) The equilibrium of clay minerals with sea water: exchange reactions. *Geochimica et Cosmochimica Acta* **41**, 950–960.
- Schmitter-Soto J. J., Comín F.A., Escobar-Briones E., Herrera-Silveira J., Alcocer J., Suárez-Morales E., Elías-Gutiérrez M., Díaz-Arce V., Marín L. E. and Steinich B. (2002) Hydrogeochemical and biological characteristics of cenotes in the Yucatan Peninsula (SE Mexico). *Hydrobiologia* **467**, 215–228.
- Schutte C. A., Wilson A. M., Evans T., Moore W. S. and Joye S. B. (2016) Methanotrophy controls groundwater methane export from a barrier island. *Geochimica et Cosmochimica Acta* **179**, 242–256.
- Schwarzenbach R. P., Gschwend P. M. and Imboden D. M. (2003) *Environmental Organic Chemistry*. 2nd Ed., John Wiley & Sons, Ltd., Hoboken, New Jersey.
- Scott T. (1988) The lithostratigraphy of the Hawthorn Group (Miocene of Florida). *Florida Geological Survey Bulletin* **59**, 147 pp.
- Short F. T., Dennison W. C. and Capone D. G. (1990) Phosphorus-limited growth of the tropical seagrass *Syringodium filiforme* in carbonate sediments. *Marine Ecology Progress Series* **62**, 169–174.
- Slomp C. P. and Van Cappellen P. (2004) Nutrient inputs to the coastal ocean through submarine groundwater discharge: controls and potential impact. *Journal of Hydrology* **295**, 64–86.
- Smart P. L., Dawans J. M. and Whitaker F. (1988) Carbonate dissolution in a modern mixing zone. *Nature* **335**, 811–813.
- Smith C. G., Cable J. E., Martin J. B. and Roy M. (2008) Evaluating the source and seasonality of submarine groundwater discharge using a radon-222 pore water transport model. *Earth and Planetary Science Letters* **273**, 312–322.
- Smith S. V, Valdes D., David L., Merino M. and Buddemeier R. W. (1999) Quantifying Groundwater Flow Using Water Budgets and Multiple Conservative Tracers, 1–8.

- Spencer R. G. M., Ahad J. M. E., Baker A., Cowie G. L., Ganeshram R., Upstill-Goddard R. C. and Uher G. (2007) The estuarine mixing behaviour of peatland derived dissolved organic carbon and its relationship to chromophoric dissolved organic matter in two North Sea estuaries (U.K.). *Estuarine, Coastal and Shelf Science* **74**, 131–144.
- Spiteri C., Slomp C. P., Charette M. A., Tuncay K. and Meile C. (2008a) Flow and nutrient dynamics in a subterranean estuary (Waquoit Bay, MA, USA): Field data and reactive transport modeling. *Geochimica et Cosmochimica Acta* **72**, 3398–3412.
- Spiteri C., Slomp C. P., Tuncay K. and Meile C. (2008b) Modeling biogeochemical processes in subterranean estuaries: Effect of flow dynamics and redox conditions on submarine groundwater discharge of nutrients. *Water Resources Research* **44**, W02430.
- Stookey L. L. (1970) Ferrozine- a new spectrophotometric reagent for iron. *Analytical Chemistry* **42**, 779–781.
- Stumm W. and Morgan J. J. (1996) *Aquatic Chemistry*. 3rd Ed., John Wiley & Sons, Ltd., New York.
- Suryaputra I. G. N. A., Santos I. R., Huettel M., Burnett W. C. and Dittmar T. (2015) Non-conservative behavior of fluorescent dissolved organic matter (FDOM) within a subterranean estuary. *Continental Shelf Research* **110**, 183–190.
- Swarzenski P. W., Reich C. D., Spechler R. M., Kindinger J. L. and Moore W. S. (2001) Using multiple geochemical tracers to characterize the hydrogeology of the submarine spring off Crescent Beach, Florida. *Chemical Geology* **179**, 187–202.
- Szymczycha B., Maciejewska A., Szczepanska A. and Pempkowiak J. (2013) The submarine groundwater discharge as a carbon source to the Baltic Sea. *Biogeosciences Discussions* **10**, 2069–2091.
- Szymczycha B., Vogler S. and Pempkowiak J. (2012) Nutrient fluxes via submarine groundwater discharge to the Bay of Puck, southern Baltic Sea. *Science of the Total Environment* **438**, 86–93.
- The MathWorks I. MATLAB and Statistics Toolbox Release 2015a.
- Thomas H., Schiettecatte L., Suykens K. and Kon Y. J. M. (2009) Enhanced ocean carbon storage from anaerobic alkalinity generation in coastal sediments. , 267–274.
- Toggweiler R. J. (1999) An ultimate limiting nutrient. *Nature* **400**, 151–152.
- Tyrrell T. (1999) The relative influences of nitrogen and phosphorus on oceanic primary production. *Nature* **400**, 525–531.

- Valle-Levinson A., Mariño-Tapia I., Enriquez C. and Waterhouse A. F. (2011) Tidal variability of salinity and velocity fields related to intense point-source submarine groundwater discharges into the coastal ocean. *Limnology and Oceanography* **56**, 1213–1224.
- Verruijt A. (1968) A note on the Ghyben-Herzberg Formula. *Bulletin of the International Association of Scientific Hydrology* **13**, 43–46.
- Visscher A., de Pourcq I. and Chanton J. (2004) Isotope fractionation effects by diffusion and methane oxidation in landfill cover soils. *Journal of Geophysical Research Atmospheres* **109**, 1–8.
- Vodacek A., Blough N. V., Degrandpre M. D., Peltzer E. T. and Nelson R. K. (1997) Seasonal variation of CDOM and DOC in the Middle Atlantic Bight: Terrestrial inputs and photooxidation. *Limnology and Oceanography* **42**, 674–686.
- Walker S. A., Amon R. M. W., Stedmon C., Duan S. and Louchouart P. (2009) The use of PARAFAC modeling to trace terrestrial dissolved organic matter and fingerprint water masses in coastal Canadian Arctic surface waters. *Journal of Geophysical Research: Biogeosciences* **114**, 1–12.
- Weston N. B., Vile M. a., Neubauer S. C. and Velinsky D. J. (2011) Accelerated microbial organic matter mineralization following salt-water intrusion into tidal freshwater marsh soils. *Biogeochemistry* **102**, 135–151.
- Whelan T., Van Tussenbroek B. I. and Barba Santos M. G. (2011) Changes in trace metals in *Thalassia testudinum* after hurricane impacts. *Marine Pollution Bulletin* **62**, 2797–2802.
- Whiticar M. J. (1999) Carbon and hydrogen isotope systematics of bacterial formation and oxidation of methane. *Chemical Geology* **161**, 291-314.
- Whiticar M. J. and Schoell M. (1986) Biogenic methane formation in marine and freshwater environments: CO₂ reduction vs. acetate fermentation- Isotope evidence. *Geochimica et Cosmochimica Acta* **50**, 693–709.
- Windom H. L., Moore W. S., Niencheski F. H. and Jahnke R. A. (2006) Submarine groundwater discharge: A large, previously unrecognized source of dissolved iron to the South Atlantic Ocean. *Marine Chemistry* **102**, 252–266.
- Yamashita Y., Scinto L. J., Maie N. and Jaffé R. (2010) Dissolved Organic Matter Characteristics Across a Subtropical Wetland's Landscape: Application of Optical Properties in the Assessment of Environmental Dynamics. *Ecosystems* **13**, 1006–1019.

- Yang L., Chen C. T. A., Hong H., Chang Y. C. and Lui H. K. (2015) Mixing behavior and bioavailability of dissolved organic matter in two contrasting subterranean estuaries as revealed by fluorescence spectroscopy and parallel factor analysis. *Estuarine, Coastal and Shelf Science* **166**, 161–169.
- Young C., Martin J. B., Branyon J., Pain A., Valle-Levinson A., Mariño-Tapia I. and Vieyra M. R. (2017) Effects of short-term variations in sea level on dissolved oxygen in a coastal karst aquifer, Quintana Roo, Mexico. *Limnology and Oceanography*.
- Zimmermann C. F., Montgomery J. R. and Carlson P. R. (1985) Variability of Dissolved Reactive Phosphate Flux Rates in Nearshore Estuarine Sediments: Effects of Groundwater Flow. *Estuaries* **8**, 228.

BIOGRAPHICAL SKETCH

Andrea Joy Pain is from St. Paul Minnesota. She received her Bachelor of Arts from Wesleyan University in earth & environmental sciences in 2008, where she began studying the biogeochemistry of bioluminescent bays in Vieques, Puerto Rico. After her undergraduate she spent two years teaching English on the French Caribbean island of Guadeloupe. She then pursued a Master of Science and graduated from ETH Zurich 2012, with a focus in biogeochemistry and pollutant dynamics. She began her doctoral studies at the University of Florida in 2013.